8-25-2017

Experimental Investigation on the Effects of Free Stream Turbulence and Fuel Type on Structure and Blowoff Characteristics of Turbulent Premixed Bluff-body Stabilized Flames

Bikram Roy Chowdhury
University of Connecticut - Storrs, bikram.jumech@gmail.com

Experimental Investigation on the Effects of Free Stream Turbulence and Fuel Type on Structure and Blowoff Characteristics of Turbulent Premixed Bluff-body Stabilized Flames

Bikram Roy Chowdhury, PhD

University of Connecticut, 2017

An experimental investigation on the effect of different levels of turbulence intensity and properties of the fuel/air mixture on the structure and characteristics of lean flames stabilized on an axisymmetric bluff body is described in this thesis. Simultaneous imaging of hydroxyl (OH) and formaldehyde (CH_2O) by planar laser induced fluorescence and particle image velocimetry (PIV) were used to study the interaction between the flame and the flow field. CH_2O fluorescence and the pixel-by-pixel multiplication of OH and CH_2O fluorescence signals were utilized to mark preheat and heat release regions respectively. In addition, high-speed chemiluminescence imaging was performed to understand the time resolved characteristics of the flame.

The first part of the thesis focuses on the characteristics of stably burning lean methane/-, propane/- and ethylene/air flames when subjected to low (4 %), moderate (14 %) and intense (24 and 30%) levels of free stream turbulence. The flame front structure was observed to be strongly dependent on the free stream turbulence level of the incoming fuel/air mixture as well on the properties of the fuel/air mixture. Formation of cusps and unburnt mixture fingers were observed as the turbulence intensity was increased from 4 to 14 % but, the heat release region remained continuous. Under intense turbulence conditions, methane/- and ethylene/air (ϕ = 0.85) flames exhibited localized extinctions along the flame sheet and flamelet merging events which created

isolated pockets of reactants in the flame envelope. In addition to these features, propane/- and ethylene/air (ϕ=0.655) flames exhibited the occurrence of flame fragmentation events and the general shape of these flames were observed to intermittently switch from a symmetric (varicose) to asymmetric (sinuous) mode. Several properties were measured to characterize the effects of turbulence – flame interaction which includes the average preheat and reaction zone thicknesses, strain rates and curvature along the flame front, burning fraction, flame brush thickness, flame surface density, area ratio and turbulent flame speed.

The next part of the thesis focuses on blowoff dynamics of lean methane/-, propane/- and ethylene/air flames for mean velocities of 5, 10 and 15 m/s and subjected to free stream turbulence levels from 4 to 30%. Apart from the propane/air flames at an apporach velcoity of 5 m/s and turbulence intensity of 30 %, increasing turbulence intensity was found to reduce the flame stability. The blowoff equivalence ratios of propane/air flames was observed to be higher than methane/- and ethylene/air flames. As blowoff was approached, the flame front and shear layer vortices entangled inducing high local strain rates on the flame front that exceed the extinction strain rate resulting in significant breaks along the reaction zone. At conditions near blowoff, significant increase in the frequency of breaks along the reaction zone was observed for low and moderate turbulence conditions. For the higher turbulence conditions, fragmentation of the flame along with the presence of sinuous wakes was observed which aided in the penetration of reactants into the recirculation zone. Velocity vectors near the flame holes indicate the penetration of the reactants into the recirculation zone. Mostly similar sequence of events was observed for methane/-, propane/- and ethylene/air flames near blowoff. Several properties were

measured to characterize the near blowoff flames which include the strain rate and curvature statistics along the flame front, burning fraction, asymmetric index and the average duration of the blowoff event. Based on the observation from the experiments, turbulent flame speed was attributed to be the primary factor in governing the blowoff equivalence ratio. This point of view was examined by comparing the mean strain rate of methane/- and ethylene/air flames at the equivalence ratio corresponding to near blowoff for propane/air flames.

Experimental Investigation on the Effects of Free Stream Turbulence and Fuel Type on Structure and Blowoff Characteristics of Turbulent Premixed Bluff-body Stabilized Flames

Bikram Roy Chowdhury

B.E., Jadavpur University, 2012

A Dissertation

Submitted in Partial Fulfillment of the

Requirements for the Degree of

Doctor of Philosophy

at the

University of Connecticut

2017

APPROVAL PAGE

Doctor of Philosophy Dissertation

Experimental Investigation on the Effects of Free Stream Turbulence and Fuel Type on Structure and Blowoff Characteristics of Turbulent Premixed Bluff-body Stabilized Flames

Presented by

Bikram Roy Chowdhury, B.E.

Major Advisor _____
Baki M. Cetegen

Associate Advisor _____
Michael W. Renfro

Associate Advisor _____
Chih-Jen Sung

Associate Advisor _____
Tianfeng Lu

Associate Advisor _____
Xinyu Zhao

University of Connecticut
2017

Acknowledgements

I wish to express my deepest gratitude to my advisor Prof. Baki M. Cetegen for his advice, guidance and continuous support that have made this dissertation possible. It has been a privilege to work under the mentorship of such an accomplished academician. I would like to thank Prof. Michael Renfro and Prof. Jackie Sung for generously loaning several key pieces of lab equipment, without which I would not be able to produce most of the results that make up this dissertation. Sincere and heartfelt thanks to my associate advisors Prof. Michael W. Renfro, Prof. Jackie Sung, Prof. Tianfeng Lu and Prof. Xinyu Zhao for valuable insights and advices on numerous occasions from which I have immensely benefitted.

I would like to acknowledge General Electric for the financial support through the General Electric Graduate fellowship which has helped in the conduct of this research. I would like to thank senior engineer Mr. Thomas Mealy for his help with experimental design and machining. Heartfelt thanks to Steve White for providing me the computation resources and attending to the software issues immediately. I would like to thank the administrative staff at the department, Tina Barry, Kelly Tyler, Laurie Hockla, and Elizabeth Dracobly, who made sure all the paperwork, was taken care of and I get the research supplies on time.

I express my sincere thanks all members of the Cetegen group, both past and present, Dr. Jason, George, James, Kyle, Rishi and Cory for their help with this accomplishment. I would like to thank members of the Renfro lab, Steve and Dr. Kathryn for their help. I would also like to thank members of the Sung group, Dr.Brady, Xiao, Jason and Roger for helping me in operating their lab equipments. I am also thankful to Bifen and Park for helping me with the numerical simulations.

I express my sincere thanks to Prof. Dipak Dey and Mrs. Rita Dey for their wisdom, support and advice throughout my graduate school. I would like to thank my friends, Dr. Goutham, Dr. Pradeep, Anwesha, Arindom, Raj, Koyel, Sudipta, Snehasis, Biswanath, Arijit, Dr. Rajat, Dr.Amrita, Dr. Chanchal, Poulomi, Aritra, Shilpa and Tithi for their continuous support and motivation during my graduate school.

I would like to thank Jyoti for all of her advice, patience and love. Her endless motivation and support has kept me inspired and ultimately paved the way for completion of my research work. Thanks for putting up with me at my worst and pushing me to my best.

The most important of all, I thank my parents, Mr. Gautam Roy Chowdhury and Mrs. Nibedita Roy Chowdhury and my brother Preetam Roy Chowdhury for being a source of constant moral courage and inspiration. Their love and continuous support has kept me motivated through all my academic endeavors. I would also like to thank my relatives for their love, support and continuous motivation.

Table of Contents

List of Tables

List of Figures

CHAPTER ONE

1. Introduction

Introduction

Turbulent premixed combustion has been an important subject of research in the last several decades owing to its practical applications in gas turbines, spark ignition engines and lean premixed and pre-vaporized combustors. To make the modern power generation and propulsion devices more compact, mixing is strongly enhanced by operating these devices under highly turbulent conditions. Flame stabilization schemes that have been widely used in practical combustors mainly involve bluff body or swirl stabilization, or a combination of both. The turbulent flow conditions arise from both high-speed turbulent inlet flow (free stream turbulence) and the turbulence generated by the flame stabilization scheme in a combustor.

Stricter regulations on acceptable emission levels from combustion technology are being put in place, and as a result innovative technologies must be developed to meet these new emission standards. To achieve this task, focus in combustion engineering has shifted towards developing combustion technologies that utilize lean, premixed combustion [1]. Premixed operating conditions allow for better control of combustor temperature and reduce NO_x emissions, however premixed combustion schemes can result in stability issues within the combustor. Flame blowoff is a critical issue that can arise when a combustor is operated in lean premixed mode. Also, the growing global energy demand is motivating the gas turbine industry to seek fuel-flexible combustors capable of burning a variety of fuels to increase energy supply stability and security. As a result, a thorough understanding of premixed combustion behavior and lean limit phenomena must be achieved before utilization in practical engineering systems.

In addition to the interest from an experimental perspective, the state-of-the-art combustion simulations have begun to capture many of the salient features of premixed flames to the point that experimental data obtained from canonical flame configurations can be utilized to test these predictive capabilities [2]. The accuracy of the models relies on their ability to properly simulate the underlying physics of the associated combustion process. Therefore, fundamental insights on turbulence–flame interactions and variation of the various statistical flame parameters under highly turbulent conditions are useful for model development and validation and ultimately for use of computational tools for design of turbulent combustion systems.

In this dissertation, results from an in-depth experimental study and analysis of the experimental results of the effect of different levels of free stream turbulence and properties of the fuel/air mixture on stabilization dynamics of lean premixed bluff body stabilized flame are presented. The flame – flow interaction has been studied experimentally using advanced optical diagnostic techniques including, high-speed chemiluminescence imaging, time-resolved particle image velocimetry (PIV), and simultaneous imaging of hydroxyl (OH) and formaldehyde (CH_2O) by planar laser induced fluorescence and particle image velocimetry. The employed diagnostics allowed for visualization of flame structure, flame location, and flame-flow field interactions.

The remainder of this chapter will include a brief review of past research on turbulent premixed flames (1.1) and current state of understanding of the blowoff dynamics of bluff-body stabilized flames (1.2).

1.1 Turbulent Premixed Flame Studies

To investigate the effect of turbulence on premixed flames, experimental studies have been performed on different flame geometries which are classified in the "Envelope" category (Bunsen-type flames), "Oblique" category (V-shaped flames), "Unattached" category (low swirl or counterflow flames) and propagating flame kernels [1]. Effects of turbulence in modifying the flame front structure have been demonstrated and summarized in the review papers of Driscoll [2], Clavin [3] and Lipatnikov and Chomiak [4]. Most of the flame structure imaging experiments done prior to 2009 did not exceed turbulence Reynolds numbers of about 2000 [2–7]. Localized extinction of the flame surface had been observed by Dunn *et al.* [8] for a series of flames studied in a Piloted Premixed Jet Burner by simultaneous line measurement of major species and temperature by the Raman – Rayleigh technique. Recently highly-piloted premixed jet flames under intense turbulence (up to 46 % turbulence intensity and turbulence Reynolds numbers up to 100,000) have been studied by Driscoll and his coworkers [9–11]. They have found that flame structure is significantly altered under intense turbulence with significant broadening of the preheat zone. Based on the experimental investigation at these highly turbulent conditions, they reported that the local flame structure did not agree with the predictions of the Borghi regime diagram [12]. A modified regime diagram for turbulent premixed flames have been presented by Skiba *et al.* [13] wherein the Klimov-Williams criterion has been replaced by a metric that relates the turbulent diffusivity to molecular diffusivity within the preheat zone.

Several studies have focused on the characteristics of planar V-shaped flames subject to different levels of free stream turbulence [5,14–22]. Experimental results of Kheirkhah and Gülder [14,15], Goix *et al.* [17] showed that for low turbulence intensity (~ 4-6 %), the flame front is weakly wrinkled and can be somewhat represented by two straight flame fronts. For moderate

turbulence intensity (~10 %), the flame front topology has been shown to depend on the distance from the flame holder. Flame segments near the bluff body featured weak wrinkles, similar to the low turbulence intensity conditions while the flame segments in the downstream region showed stronger corrugations. For higher turbulence intensities (~ 17 %), strong levels of wrinkling along with formation of cusps, mushroom shaped-structures, localized quenching and pockets of reactants have been reported using laser tomography technique by Kheirkhah *et al.* [15]. The flame brush thickness is an important parameter which represents the approximate distance over which a flame front exists. Measurements by Kheirkhah and Gülder [14,15] and Namazian *et al.* [19] have shown that the brush thickness is strongly dependent on the vertical distance away from the flame holder, mean (U_m) and root mean square (u') of the streamwise velocity at the burner exit, integral length scale of the flow field (l_o) and the fuel-air equivalence ratio(ϕ). Lipatnikov and Chomiak [4] have showed that at locations near the flame holder, the brush thickness is linearly correlated with turbulence intensity (u'/U_m) and distance from the flame holder (y), and is given by $\delta_t \approx yu'/U_m$ while in the downstream region it is proportional to the square root of vertical distance (y), turbulence intensity (u'/U_m) as well as the integral length scale, $\delta_t \approx \sqrt{2l_o yu'/U_m}$. These analytical expressions however, do not include the dependency on equivalence ratio which is in contrast to the experimental results in [14,15,19] and it has been argued to be the incapability of turbulent diffusion theory for predicting the effect of ϕ on the flame front dynamics [4].

Flame surface density is an important parameter which has been used to relate the turbulent burning velocity to flamelet structure. Variation of flame surface density (FSD) for V-shaped flames has been investigated in several past studies [5,18,20,21]. In all of these works, two dimensional estimates of flame surface denisty has been computed. Variation of FSD with mean

progress variable $\bar{c}$ has been reported to feature a parabolic-like disribution skewed towards a $\bar{c}$ greater than 0.5, which has been attributed to the formation of cusps [5]. Using the flame brush thickness and flame surface density estimates, Sattler *et al.* [22] computed the area ratio (A_T/A_L) and showed that it has an increasing trend with increasing turbulence. A_T and A_L represent the surface area of wrinkled, turbulent flame and unwrinkled, laminar flame respectively. However, a difference in growth rate of this parameter was reported for the different flames they had studied, which could not be explained solely by changes in the normalized velocity fluctuations of the flow, $u'/S_{L,O}$. $S_{L,O}$ represents the unstretched, laminar burning velocity of the corresponding premixed fuel/air mixture.

1.2 Bluff – body flame stabilization

Stabilization of premixed flames in high velocity flows has been an important subject of combustion research over the past several decades. The main reason for this has been the wide range of applications in aero propulsion and power generation applications. Practical applications include flame stabilization in afterburners of military aircraft engines, gas turbine combustors and industrial furnaces. This subject includes rich culmination of different branches of physical sciences involving combustion chemistry, flame-turbulence interaction, shear flows and hydrodynamic stability theory. Flame stabilization using a bluff-body flame holder is achieved by formation of a localized low velocity recirculation zone that is created by sudden flow divergence. Continuous ignition of the incoming mixture takes place in the shear layers bounding this recirculation zone containing hot products and results in a stable, anchored flame [23]. In the seminal works of Zukoski and Marble [23,24], Williams *et al.*. [25] and Longwell [26], blowoff criteria were established for flame holding in uniformly homogenized premixed gases, and the effects of different bluff-body geometries on flame holding were identified. The issue of

lean blowoff limits for different combustible mixtures, variable temperature and pressure, blockage ratio and the effect of fuel droplet vaporization and mixing have been considered in the works of Plee and Mellor [27], Rao and Lefebvre [28], Rizk and Lefebvre [29]. In addition to these experimental efforts, a series of models have been developed based on the competing time scales related to fluid dynamics in the vicinity of recirculating flow, chemical reaction or ignition time scales as well as the turbulent diffusion of heat and mass between the reactants and products. There have been also attempts to correlate flame blowoff data collected from many studies in the literature utilizing different correlation parameters [30] with limited success. In such efforts difficulty arises from lack of knowledge of detailed experimental conditions for each study and many different configurations and fuels utilized in them. Scatter in these data correlations is typically very large.

To explain the lean blowoff phenomena, various phenomenological theories have been proposed which primarily rely on the competition between a chemical time scale for the mixture and a characteristic fluid mechanical time scale near the recirculation zone. Longwell [26] viewed the recirculation zone as a well-stirred reactor and suggested that blowoff occurs when the rate of entrainment of fresh reactants and the rate of its consumption is not balanced. An alternate view was proposed by Zukoski and Marble [23,24] based on a critical time τ_{cr} required for ignition of the fresh stream i.e. $\tau_{cr} = L_{RZ}/V_{B.O}$, where L_{RZ} is the streamwise length of the recirculation zone and $V_{B.O}$ is the measured blowoff velocity and blowoff occurs when the chemical ignition time exceeds the critical time. Yamaguchi *et al.* [31] has proposed a flamelet based description of local extinction by excessive stretch, followed by influx of cold reactants from the downstream end of the recirculation zone which may lower the temperature of the recirculation zone below a critical level required to sustain a flame.

More recently, the flame structure near blowoff has been studied by employing time resolved imaging. Significant contributions have been made by Kiel *et al.* [32], Nair and Lieuwen [33,34], Chaudhuri *et al.* [35,36] and Tuttle *et al.* [37,38] towards the understanding of the mechanism of blowoff process for lean premixed flames. They found that the flame front moves into the high vorticity region as blowoff is approached, resulting in localized extinctions along the shear layer due to excessively high strain rates. This is followed by the recession of the flame into the recirculation zone with complete extinction occurring when the re-ignition of flame segments bounding the shear layers is no longer possible. However, these works have been limited to low free stream turbulence levels corresponding to a maximum turbulence Reynolds number of a few hundred. In these experiments, premixed flames were anchored on bluff bodies having small blockage ratios (~ 6-7 %), producing flames that lie in the wrinkled and corrugated flamelet regimes of the turbulent flame regime diagram.

The blowoff processes of short axisymmetric flames supported on bluff bodies with larger blockage ratio (~ 51 %) have been studied recently by Dawson *et al.* [39] and Kariuki *et al.* [40–42]. Heat release images obtained in Ref. [41,42] show that at conditions approaching blowoff, localized extinctions occur along the shear layer, followed by reduction in flame height and entrainment of reactants from the top of the recirculation zone. The flames studied in Ref. [39–42] were also stabilized in approach flows with low free stream turbulence levels. These flames were typically in the thin reaction zone regime and the high velocity fluctuations were generated owing to large blockage ratio flame holders. Limited research has been done in studying the phenomena of flame extinction of the bluff-body stabilized flames under high turbulence Reynolds number conditions. Ballal and Lefebvre [43] investigated the effect of free stream turbulence on the extinction limits of lean, premixed flames with the focus on developing

relevant correlations for predicting the blowoff equivalence ratio. To the best of our knowledge, this is the only work in the literature where the turbulence intensities in the approach flow were varied up to 15%.

To investigate the effect of fuel properties on blowoff, the primary approach has been to obtain the blowoff equivalence ratio and obtain empirical correlations for blowoff for different fuels. Extensive experiments have been performed at Air Force Research Laboratory by Huelskamp *et al.* [44] using methane, propane and jet fuels. Similar approach has been followed in the review paper of Shanbhogue *et al.* [30]. All of these works eventually formulated correlations based on Damköhler number theory which relates characteristic flow residence time and chemical timescales. Scatter in these data correlations is typically very large.

1.3 Summary

Flame stabilization is governed by the turbulence levels of the incoming flow as well as on the properties of the fuel air mixtures. In practical devices, combustion occurs under highly turbulent conditions where both the velocity fluctuation (u') as well as integral length scale of the flow (l_o) are large. Based on the review of the literature, it is realized that the previous studies for stably burning V-shaped flames were limited to free stream turbulence intensity of ~17% and integral length scales of the flow were much smaller than those present in practical combustors. In the experimental works done to study the blowoff dynamics of bluff body stabilized flames, the free stream turbulence intensities were limited to 6-7%. Thus, the goal of the research conducted in this thesis was to examine the effects of free stream turbulence levels and fuel type on bluff body premixed flame stabilization at turbulence intensities approaching 30% and turbulence Reynolds number up to 4300.

1.4 Outline of the Thesis

In this dissertation, an experimental investigation is described of the response of lean, bluff body stabilized flames when subjected to varying levels of turbulence intensities as well as on the properties of different fuel/air mixtures. Experiments have provided data which could serve as input for model validation in computational studies investigating bluff-body stabilized, turbulent premixed flames at conditions away from and near flame blowoff.

Chapter 2 describes the experimental setup and the various diagnostic techniques employed in this study. The characteristics of the non-reacting flow field obtained by hot wire anemometry and high-speed particle image velocimetry are included. In Chapter 3, characteristics of stably burning lean methane/-, propane/- and ethylene/air flames subjected to low (4 %), moderate (14 %) and intense (24 and 30%) levels of turbulence are presented. Chapter 4 presents the results from the study of the effect of different levels of free stream turbulence on the blowoff dynamics of lean propane/air flames. In Chapter 5 the results of blowoff dynamics for methane/- and ethylene/air flames are presented and the effect of fuel/air mixture properties on lean extinction limits are discussed. Chapter 6 summarizes the understanding reached from the current study and main findings.

CHAPTER TWO

2. Experimental Methodology

This chapter outlines the experimental setup, measurement techniques and the experimental conditions tested in the present study.

2.1 Experimental Setup

The layout of the experimental setup is shown in Fig. 2.1. A conical brass burner with an exit diameter of 40 mm and 3.2:1 nozzle diameter contraction ratio was used. A disk-shaped bluff-body with a diameter of 10 mm (shown in the inset of Fig. 2.1) was concentrically fitted at the burner exit using a rod of 6 mm diameter. The air flow was supplied by a twin-screw air compressor (Gardner-Denver, Model ECHQHE) with a maximum mass flow rate capacity of 0.1 kg/s. The compressor discharge air was first dried by a refrigeration dryer (Hankinson Model 80200) and then metered by a bank of critical flow orifices to obtain the desired air mass flow rate or nozzle exit velocity. Fuel-air mixture was prepared in a mixing chamber containing a series of baffles and perforated plates and fed into the burner upstream of the contraction section.

The fuel flow rate was metered by using a set of mass flow controllers which were interfaced to a DAQ board (NI Model PCI-MIO-16E-1) and the data acquisition computer. Instrument-grade propane and chemically pure grade of methane and ethylene (supplied by CT Airgas) were used as fuels.

The free stream turbulence intensity levels of the incoming fuel-air mixture were varied stepwise from 4 to 30% by employing a combination of perforated plates, slotted plates, side impinging jets and mesh screens. The schematic of the turbulence generating arrangement, mounted at the exit of the burner is shown in Fig. 2.2.

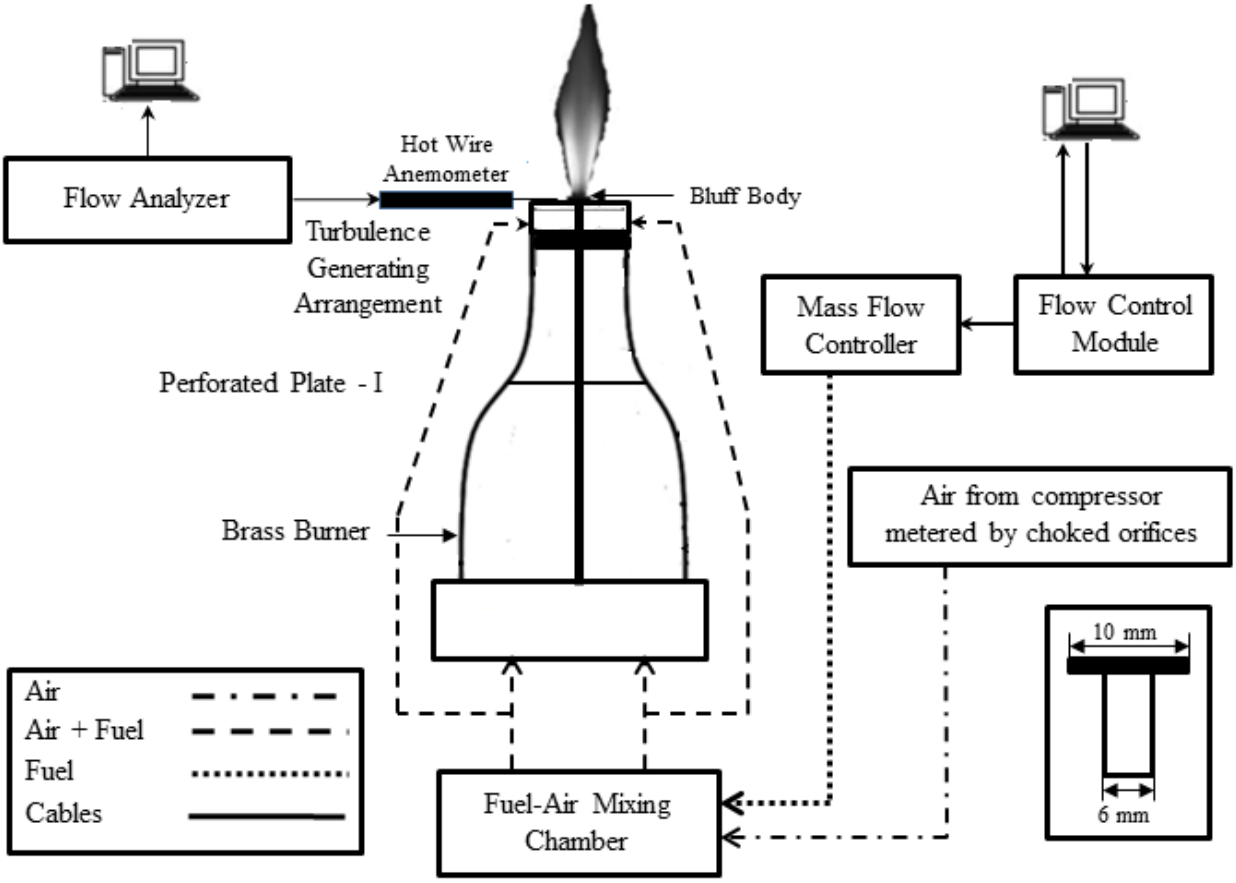

Fig. 2.1. Layout of the experimental setup

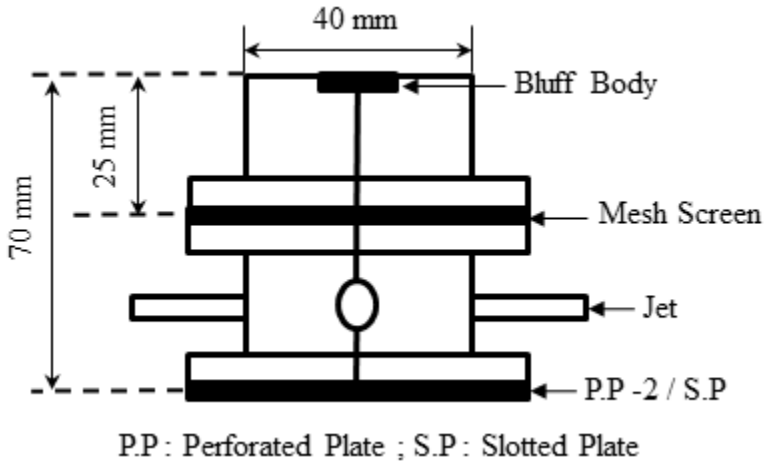

Fig. 2.2. Schematics of the turbulence generating arrangement

A fine mesh screen of 1 mm opening was placed 25 mm upstream of the bluff body, for all the cases to break large scale eddies and produce more uniform turbulence characteristics at the burner exit. Low turbulence intensity of ~ 4% was generated by placing a perforated plate (P.P - 1) 130 mm upstream of the bluff body. This perforated plate (P.P - 1) had a hole diameter of 6 mm and a pitch distance of 10.2 mm between the centers of the neighboring holes. This resulted in a blockage ratio of approximately 60%. For moderate turbulent intensity level of ~ 14%, another perforated plate (P.P - 2) having a hole diameter of 5 mm and pitch of 8 mm was placed 70 mm upstream of the bluff body. Slotted plates of different widths and having blockage ratios of 67% and 78% were placed 70 mm upstream of the bluff body replacing P.P - 2 to produce higher turbulence intensities of 24 and 30% respectively. In addition, four radially symmetric opposed jets were employed normal to the main flow direction between the slotted plate and mesh screen for the 24 and 30% turbulence intensity conditions. The jets were supplied with the same premixed fuel-air mixture drawn from the mixing chamber at about 10 % of the main flow. The jets contribute to the breakup of the large eddies shed by the slotted plates as well as enhancing the turbulence in the flow.

2.2 Diagnostic Techniques

In the following section, the various measurement techniques which have been employed for the current study are discussed.

2.2.1. Hot Wire Anemometry

The turbulent flow field was characterized by using hot wire anemometry. The velocity measurements were taken with a calibrated single sensor, hot film anemometer probe (TSI, Inc. Model 1210-20) and a high frequency response anemometer (TSI, Inc. IFA 100) in the plane of

the bluff body along the radial direction. The probe was mounted on a micrometer stage for radial traversing. The probe was operated at a sampling frequency (f_s) of 80 kHz and the raw data was low pass filtered at $f_a = f_s/2 = 40$ kHz to prevent aliasing. Measurements at each location were taken for 18 seconds. The integral turbulent length scales (l_o) for different conditions were determined by processing the hot film data. The turbulent length scales were determined by the approach similar to that of Coppola and Gomez [45] in which the turbulent power density spectra were fit into a correlation expression. The one-dimensional power spectrum in the frequency domain, E{f}, was estimated using the Welch method [46]. The integral length scale was determined by optimally fitting the integral region of the power spectrum with the Von Karman's turbulence spectrum [47].

$$\frac{U_m E\{f\}}{l_o u'^2} = 4\left[1 + \left(\frac{8\pi f l_o}{3U_m}\right)^2\right]^{-5/6} \quad (1)$$

where U_m is the mean velocity, f is the frequency, l_o is the integral length scale and u'^2 is the velocity variance.

2.2.2. CH emission measurements for estimation of blowoff equivalence ratio*

The blowoff condition was approached by gradual reduction of the equivalence ratio by ramping down the fuel flow rate. For determining the blowoff equivalence ratio, chemiluminescence signal from CH^* emission was collected using a Photomultiplier-tube (Ealing Electro Optics, Model S20 UV), fitted with a narrow pass filter at λ = 430 ±10 nm. The PMT measurements were carried out at a sampling frequency of 50 kHz. The PMT view field was masked to view a downstream distance of 20 mm from the tip of the bluff-body. As the fuel flow rate was ramped down, the decrease of fuel flow rate was recorded simultaneously with the PMT signal and the flame blowoff point was determined when the PMT signal dropped abruptly. This entire process

was automated and controlled by the LabView software interface. The sensitivity of the measured blowoff equivalence ratio to time delays associated with the response of flow controllers and flow convection time lag from flow controller to the burner exit was determined and different ramp rates were employed to investigate these effects. It was found that a rate of mixture equivalence ratio decrease of $d\phi/dt=0.005\ s^{-1}$ provided consistent blowoff results. Therefore, it was ensured that the ramp down rate of the fuel flow and system response delays did not bias the blowoff equivalence ratio.

2.2.3. High Speed Chemiluminescence Imaging

High speed chemiluminescence imaging was conducted using a Photron Fastcam SA5 high speed camera. The camera was focused using a 35 mm, f/1.4 Nikkor lens in combination with a +4 macro lens attachment. The macro lens allowed no UV light to pass through, therefore no OH* signal was detected by the camera. Tests were performed with a CH bandpass filter centered at 430nm +/-10nm. There were no significant differences observed in the chemiluminescence signal when the filter was used; this suggested that most of the chemiluminescence acquired without the filter was CH*. Because the bandpass filter allowed for only 40% transmissivity, the acquisition of the final chemiluminescence images were done so without the use of any filter. To visualize the dynamics of the stably burning flames, the camera was operated at 5 kHz. The frame rate of the camera was lowered to 1 kHz for near blowoff flames to allow for better signal-to-noise ratio.

In a turbulent reacting flow, such as the one presented here, having time resolved information is necessary for studying flame stability. High speed chemiluminescence allows for a more affordable option for obtaining time resolved information on flame stabilization, as opposed to diagnostic techniques such as high speed PLIF systems.

2.2.4. High Speed Particle Image Velocimetry

High-speed PIV measurements were conducted at 5 kHz for measurement of the velocity field. The system consisted of a Nd:YLF diode laser (Litron, Model LDY304-PIV) providing about 10 mJ/pulse. Using a combination of lenses, the beam was focused into a sheet of approximately 0.3 mm thick and was aligned with the bluff body center. The Mie scattering images were captured by a high speed CMOS camera (Vision Research Phantom Model v710) having a resolution of 1008 x 696 pixels. An f/4, Nikkor 105 mm lens was attached to the camera to focus on the laser sheet. The field of view was 56 x 39 mm (2 mm above the plane of the bluff body to prevent laser scatter), providing a resolution of 0.056 mm per pixel. A target plate with 1 mm diameter dots spaced 4 mm apart was placed along the center of the bluff body in alignment with the laser sheet, for proper calibration of the Mie scattering images. The timing of the PIV system was controlled by Dynamic Studio v.3.41 software. Based on the mean velocity of the flow, the time between laser pulses was varied to ensure that the particles in the flow traveled roughly one quarter width of the interrogation window. Micron sized silicone oil droplets generated by a set of nebulizers, were used for seeding the flow. The silicone oil (polydimethylsiloxane) had a viscosity of 50 centistokes and a density of 970 kg/m^3.

LaVision DaVis 7.2 software was used to process the Mie scattering images to obtain vector fields. Multi-pass cross-correlation algorithm starting with a 64 x 64 interrogation window size and reducing to a final interrogation window size of 16 x 16 with 50% overlap was used. The spacing between the velocity vectors was 0.448 mm.

The integral length scales computed from the hot wire anemometer data was verified by using the velocity field information from the high-speed PIV measurements. The integral length scale was estimated from the relation,

$$l_O = \int_0^{h^*} R_{uu}(x, y, h)dh \quad (2)$$

where x and y are the horizontal and vertical positions of the point at which the integral lengths were computed, h is the spacing between the velocity vectors in the streamwise direction and h* is the vertical extent at which the autocorrelation of the axial velocity (R_{uu}) first attains zero. The autocorrelation was obtained by using the following relation,

$$R_{uu}(x, y, h) = \frac{\overline{[u(x,y)-\overline{u(x,y)}][u(x,y+h)-\overline{u(x,y+h)}]}}{\overline{[u(x,y)-\overline{u(x,y)}]^2}} \quad (3)$$

where the over-bar symbol represent ensemble averaging.

The integral length scales computed from the PIV data were found to be within 8% of those obtained from the hot film data.

2.2.5. Simultaneous PIV and PLIF imaging of OH and CH_2O

To locate the heat release region as well as to study the flame-flow interactions, simultaneous PLIF imaging of OH and CH_2O and particle image velocimetry (PIV) was performed. Two regions of interest were selected – Near the bluff body (spanning from 2 to 21 mm above the bluff body, 40 x 19 mm) and far from the bluff body (spanning from 21 to 40 mm above the bluff body, 56 x 19 mm), as shown in Fig. 2.3. The horizontal span of the region of interest far from the bluff body had to be increased to 56 mm owing to widening of the flame for the intense turbulent conditions at downstream locations. 600 images sets were obtained for each test condition.

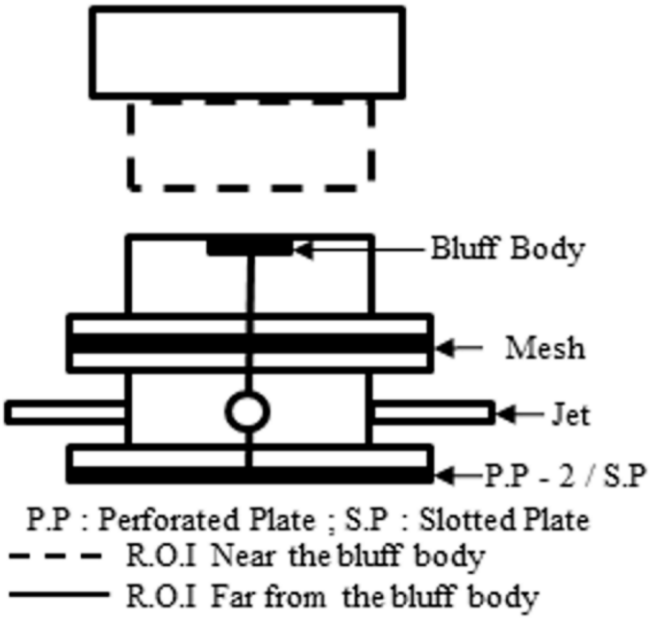

Fig. 2.3. Domains of investigation using simultaneous PLIF imaging of OH and CH_2O and PIV

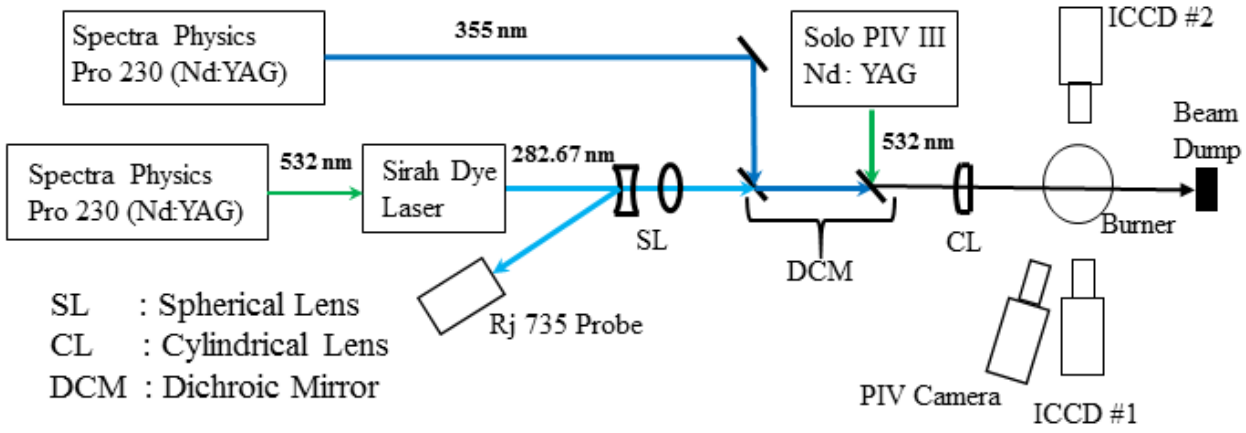

Fig. 2.4.Schematics of the laser diagnostics setup

The schematics of the laser diagnostics setup is shown in Fig. 2.4. The OH PLIF system consisted of a frequency doubled, Nd:YAG laser (Spectra Physics PRO 230) pumping a Rhodamine 590 containing dye laser (Sirah Precision Dye Laser). The generated laser beam

tuned near 566 nm was passed through a doubling crystal to create a beam at a wavelength of 282.67 nm, centered on the $Q_1(5)$ ro-vibrational transition in the $A^2\Sigma^+ \leftarrow X^2\Pi$ (1,0) band of OH. The shot-to-shot variation in beam energy was recorded by using Rj– 7620 Energy Ratiometer coupled with RjP – 735 Pyroelectric probe. The probe was aligned along the direction of backscatter of 282.67 nm beam from the lens system (SL) which was used for collimating the beam. Fluorescence signal was collected using an image intensified PI-Max CCD camera having 1024 x 1024 pixel resolution and coupled with a Nikkor 105-mm UV-lens fitted with Semrock Bright Line filter (FF01-320/40-25) which has a central wavelength of 320 nm and a width of ~ 40 nm. A gate width of 250 ns was used. The pixel resolution of the OH PLIF images for the field of view near and far from the bluff body was 39 x 39 μm and 55 x 55 μm respectively.

The CH_2O PLIF imaging was carried out using the third harmonics of a Spectra Physics Pro-230 Nd:YAG laser operating at 355 nm with pulse energies of approximately 300 mJ. The 355 nm beam was used to excite the A-X $4^1_0(15, 5)$ transition of CH_2O. The shot-to-shot variation of the 355 nm beam was monitored using a photodiode during image acquisition. The CH_2O fluorescence signal was collected using a PI-Max II intensified camera having a 1024 x 256 pixel resolution. The intensified camera was focused using a Nikon 105-mm lens fitted with Omega Optical Inc. (450DF70D) filter that has greater than 60% transmission for wavelengths between 425 and 485 nm and near zero transmission outside of the 410-490 nm range. The intensifier gate width was set at 200 ns. The CH_2O PLIF images had a pixel resolution 75 x 75 μm.

The PIV system consisted of a dual-cavity 50 mJ/pulse Nd:YAG laser (New Wave Solo PIV III), a frame-straddling 1024 x 1280 CCD camera (Flow Master 3S) and DaVis 7.2 post-processing software. Alumina particles ~1μm in diameter were used to seed the flow. The pixel resolutions were 0.039 mm and 0.0546 mm for the near and far field of view, respectively. The time

between laser pulses was varied based on the mean flow velocity, which ensured that the particles in the flow traveled roughly one-quarter width of the interrogation window. The PIV camera was equipped with a Nikon 200-mm focal length lens fitted with a 532 +/- 1 nm bandpass filter (Andover 532FS02-50). The Mie scattering images were processed by using the LaVision DaVis 7.2 software package. A multi-pass cross correlation algorithm was used starting with an interrogation window size of 128 x 128 pixels and finally reducing to an interrogation window of 16 x 16 pixels with 50% overlap. The spacing between the velocity vectors was 0.3125 mm and 0.4375 mm for the near and far field of view, respectively.

The three beams were combined using two dichroic mirrors as shown in Fig. 2.4. A laser sheet was created by expanding the beams using a combination of cylindrical lenses having focal lengths of 300 mm and -200 mm while a cylindrical lens of 500 mm was used to focus the sheet as it passed through the region of interrogation. The laser sheet was aligned along the center plane of the bluff-body. The laser sheet had a constant height of 20 mm along the region of interest and was formed 2 mm above the bluff-body to prevent laser light scatter from it. The sheet thicknesses of the OH and CH_2O beam were approximately 150 μm and 200 μm respectively. The thickness of each laser sheet was measured by the scanning knife-edge technique. This was accomplished by placing a knife edge (a razor blade) normal to the laser sheet and traversing across it so that the beam was blocked progressively by the movement of the knife edge. The power of the transmitted laser beam was measured by a power meter while the knife edge was traversed. The derivative of the power versus distance curve is the mean sheet intensity profile. The thickness of the laser sheet was defined as twice the distance from the center of the beam to where the light intensity dropped to $1/e^2$ of its maximum value.

The timing of the laser pulses and image acquisition by the three cameras was managed by using two delay generators (Stanford DG535). The OH PLIF laser pulse was delayed from the CH_2O laser pulse by 400 ns to prevent crosstalk between the PLIF measurements. The PLIF laser pulses were temporally centered between the two PIV laser pulses. Beam profiles were evaluated by passing the OH and CH_2O laser sheets through a cuvette filled with ethanol and imaging the corresponding fluorescence.

2.3 PLIF Image Analysis

For alignment of the CH_2O PLIF, OH PLIF, and PIV images a transparent calibration plate with a grid pattern was placed at the measurement plane, defined by the laser sheet and imaged simultaneously by the three cameras. Identical reference points were selected on the plate. LaVision DaVis 7.2 was used to perform calibration for each camera using the calibration plate image and the selected reference points. After calibration, OH PLIF data was interpolated onto a grid matching the resolution to that of CH_2O grid. Then to obtain the heat release rate from the OH and CH_2O PLIF images, a number of corrections were made on the grid corrected fluorescence images. First, the PLIF images were corrected for background noise by subtracting a background image taken in the absence of the flame. Secondly, the images were corrected for beam profile variations. To perform the corrections for beam profile variation, first the instantaneous images of the fluorescence signals from the ethanol filled cuvette were calibrated as described above. The fluorescence images corresponding to the OH PLIF laser sheet were interpolated onto a grid matching the resolution to that of CH_2O grid and then the averaged beam profiles were evaluated. This was followed by dividing the instantaneous OH and CH_2O PLIF images by the corresponding average beam profiles. The OH PLIF images were then corrected for shot-to-shot power variation based on the measurements from the energy meter. To enhance

the signal-to- noise ratio of the PLIF images, filtering was performed using a 3 x 3 median filter. Following these corrections, pixel-by-pixel multiplication of the OH and CH_2O image was performed.

Proper contour of the heat release zone was then identified from the product image by applying a local thresholding technique as demonstrated by Temme *et al.* [9]. First, a global threshold was generated based on the standard deviation of the product image signals. Then, all the pixels with intensity count greater than twice the calculated standard deviation above the minimum signal were set to one and the rest were set to zero. From the newly binarized image, a skeleton was formed. Each pixel in the product image was then compared with the intensity count of the nearest pixel on the skeleton. This process was repeated twice, using the image of the previous step as an input. In this way, local thresholding technique was applied to obtain the heat release region. The global threshold value was varied from one-half to four times of the standard deviation of the final image to ensure that the results presented were independent of the image processing technique and no significant differences in the thickness of preheat and reaction zones were observed.

Using the properly thresholded overlap region of OH and CH_2O PLIF images, the average preheat and reaction zone thicknesses for each image were determined. For reaction zone thickness calculation, the distance between each pixel on the skeleton and the nearest pixel on the edge of the heat release region was determined. As the skeleton lies along the center of the heat release zone, the calculated distance was multiplied by a factor of two. Then average reaction zone thickness for the image was estimated by summing up these distances over the whole skeleton and dividing it by the length of the skeleton. To obtain the preheat zone thickness, first the reaction zone was excluded from the CH_2O PLIF image. Then the image was

thresholded at 30% of its local maximum as this location corresponds to approximately 500K temperature location in laminar flame simulations as has been used by others. Subsequently, the skeleton was determined and the average preheat zone thickness was estimated in a similar manner as described above for the reaction zone thickness.

Prior to application of this diagnostics in turbulent flames, measurements of preheat and reaction zone thicknesses were performed for a laminar Bunsen burner flame. Measurements were performed for lean methane/air and propane/air flames at ϕ=0.85 and ethylene/air flames at ϕ=0.655. Experiments could not be performed for laminar ethylene/air flames at ϕ=0.85 owing to flashback issues. A sample image of the instantaneous OH and CH_2O PLIF image for a laminar propane/air flame at ϕ= 0.85 is shown in Fig. 2.5. The OH filled region is shown in red while the border of the thin, continuous overlap region of OH and CH_2O is shown by the thick blue lines. The raw images have been processed in an identical manner as described above.

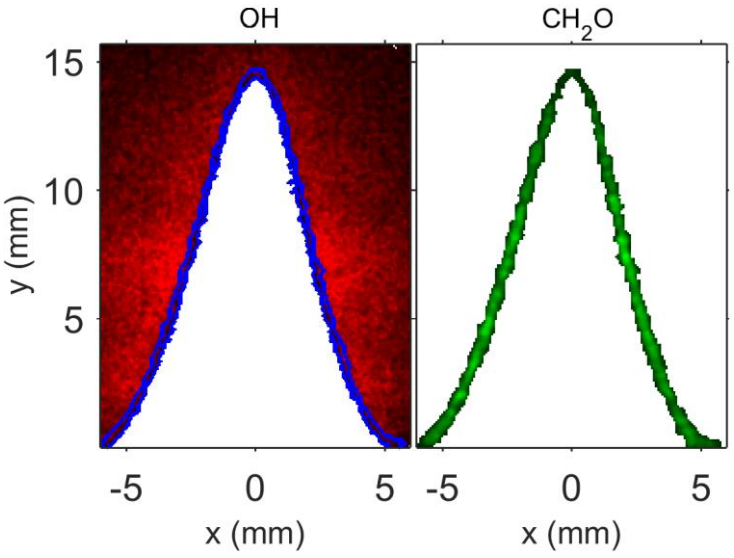

Fig. 2.5. Instantaneous OH and CH_2O PLIF image for a premixed propane/air laminar flame.

For comparison, preheat and reaction zone thicknesses were computed for a planar flame from the PREMIX [48] simulation using the USC Mech II mechanism of Wang *et al.* [49]. Profiles for temperature, heat release, formaldehyde and overlap of formaldehyde and OH are shown in Fig. 2.6 for propane/air flames at ϕ=0.85. The reaction zone thickness is defined as the width of the CH_2O-OH overlap layer at 50% of its maximum value. The preheat zone thickness is defined as the width of the CH_2O signal from where it exceeds 30 % of the maximum value on the reactant side to the leading edge of the reaction zone. Similar to Ref. [9], the leading edge of the preheat zone was selected at the location where the temperature is 550 K which corresponds to 30 % of the CH_2O signal according to the CHEMKIN simulation.

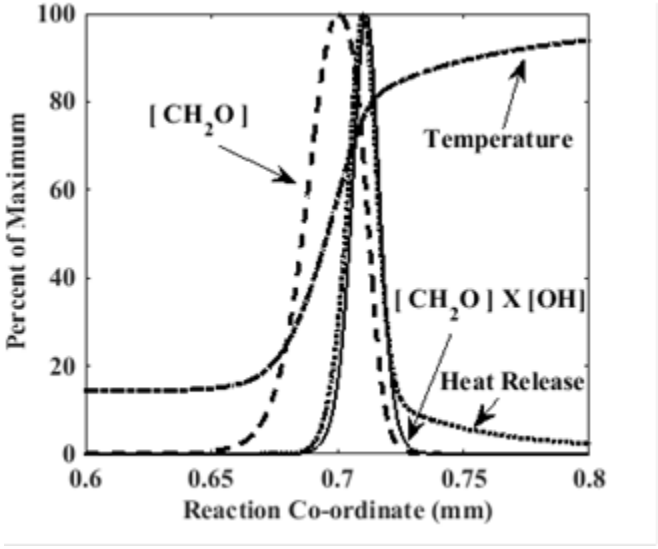

Fig. 2.6. CHEMKIN laminar flame computations showing the formaldehyde region, overlap of formaldehyde and OH along with the heat release region and temperature.

The preheat zone and reaction thicknesses obtained from the numerical simulation and experiments are summarized in Table 2.1 and Table 2.2, respectively. For all the cases, the experimentally estimated preheat zone thicknesses are observed to be about 1.1 – 1.16 times thicker than those computed for a planar flame while the reaction zone thicknesses are about 1.3

– 1.4 times thicker than the numerically simulated value. Possible reasons for this discrepancy are: (1) limited image resolution (2) finite laser sheet thickness (3) difference between the actual laminar flame configuration and the ideal condition simulated in CHEMKIN. Similar discrepancies were also been reported by Skiba *et al.* [10] and Zhou *et al.* [50]. Based on the observation for lean methane/- and propane/air flames at ϕ=0.85 and ethylene/air flames at ϕ=0.655, it can be safely assumed that experimentally estimated preheat and reaction zone thickness for laminar ethylene/air flames at ϕ=0.85 would have shown a similar trend.

Table 2.1. Comparison of preheat zone thickness obtained from numerical simulation and experiments

Fuel	Equivalence Ratio	PREMIX (mm)	Experiment (mm)
Methane	0.85	0.270	0.304
Propane	0.85	0.226	0.262
Ethylene	0.655	0.216	0.238

Table 2.2. Comparison of reaction zone thickness obtained from numerical simulation and experiments

Fuel	Equivalence Ratio	PREMIX (mm)	Experiment (mm)
Methane	0.85	0.148	0.198
Propane	0.85	0.130	0.183
Ethylene	0.655	0.161	0.209

2.4 Non-reacting flow field

The properties of the inlet flow employed for different experiments presented in this study are tabulated in Table 2.3. Three mean velocities of 5, 10 and 15 m/s were examined in the experiments. This corresponds to global flow Reynolds numbers of 3220, 6440 and 9660, respectively based on the bluff body diameter. For each mean streamwise exit velocity, turbulence intensities of 4, 14, 24 and 30% were studied, except for the lowest mean velocity of 5 m/s where the intense turbulent condition (T.I ~ 30%) could not be examined owing to flashback issues. The turbulence Reynolds number was computed using the root mean square of axial velocity fluctuations (u') and integral length scale (l_o) determined from the hot wire anemometer data as $Re_T = u'.l_o/\nu$ where ν is the kinematic viscosity of air. The integral length scales computed from the PIV at mid-span between the burner inner wall and the rod supporting

the bluff body in the radial plane for the different conditions are included in Table 2.3. These values are observed to be within 8 % of those estimated by using the hot wire anemometer.

Characteristics of the mean and RMS of the streamwise velocity was obtained by processing the data from hot wire anemometry. The variation of the mean axial velocity in the plane of the bluff body is shown in Fig. 2.7. The results are normalized by the mean bulk flow velocity (U_m) of the corresponding condition. These measurements were made in the absence of the bluff body between the burner inner wall and the stem supporting the bluff body along the radius. The locations of the measurement were at a spacing of 1 mm. As the turbulence intensity is increased stepwise from 4 to 30%, the mean velocity profile is observed to change progressively from a nearly parabolic to a top hat profile. The variation of the root mean square of axial velocity fluctuations is shown in Fig. 2.8. These results were normalized by the local mean velocity measured at the corresponding location. The turbulence intensity is observed to be nearly uniform except a slight increase near the boundaries of the burner rim and the rod supporting the bluff body.

Table 2.3. Properties of the tested experimental conditions[#]

U_m (m/s)	$U_{C.P}$ (m/s)	$\frac{u'}{U_{C.P}}$	Integral scale, l_O (mm) (H.W.A)	Integral scale, l_O (mm) (P.I.V)	Re_T
5	5.5	0.04	3.1	3.16	44
5	5.3	0.15	8.1	8.34	436
5	5.3	0.25	12.9	13.55	1222
10	10.9	0.04	2.8	2.93	79
10	10.3	0.14	7.8	8.19	783
10	10.8	0.24	12.6	12.61	2182
10	10.3	0.3	13.3	13.84	2898
15	15.8	0.05	2.62	2.87	138
15	15.2	0.16	7.42	7.82	1261
15	15.8	0.26	12.2	12.87	3433
15	15.2	0.3	13.1	13.93	4280

U_m is the mean velocity which is spatially averaged over the burner exit. $U_{C.P}$ and u' were measured at midspan between the burner rim inner wall and the rod holding the bluff body, which is 8.5 mm from the rim wall.

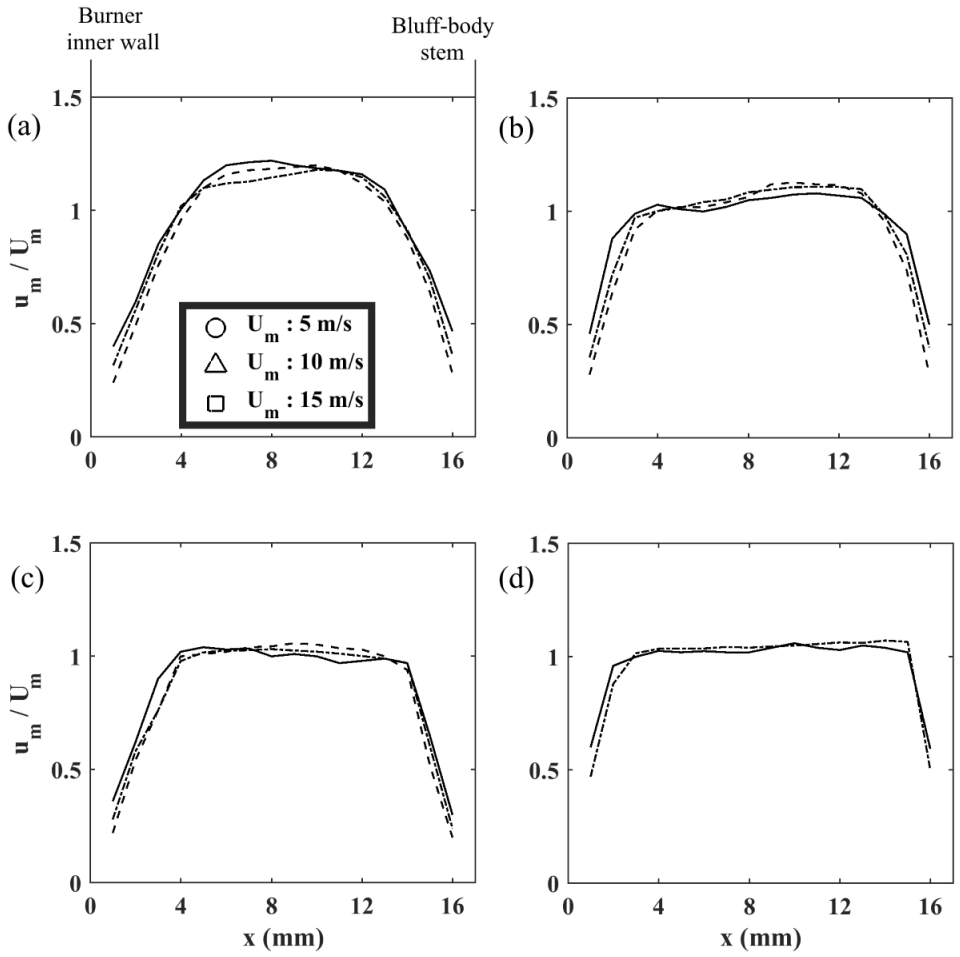

Fig. 2.7. Variation of the mean streamwise velocity for the different conditions corresponding to turbulent intensities of (a) 4 % (b) 14 % (c) 24% and (d) 30 %. u_m is the local mean velocity at a specific location while U_m is the mean velocity which is spatially averaged over the burner exit.

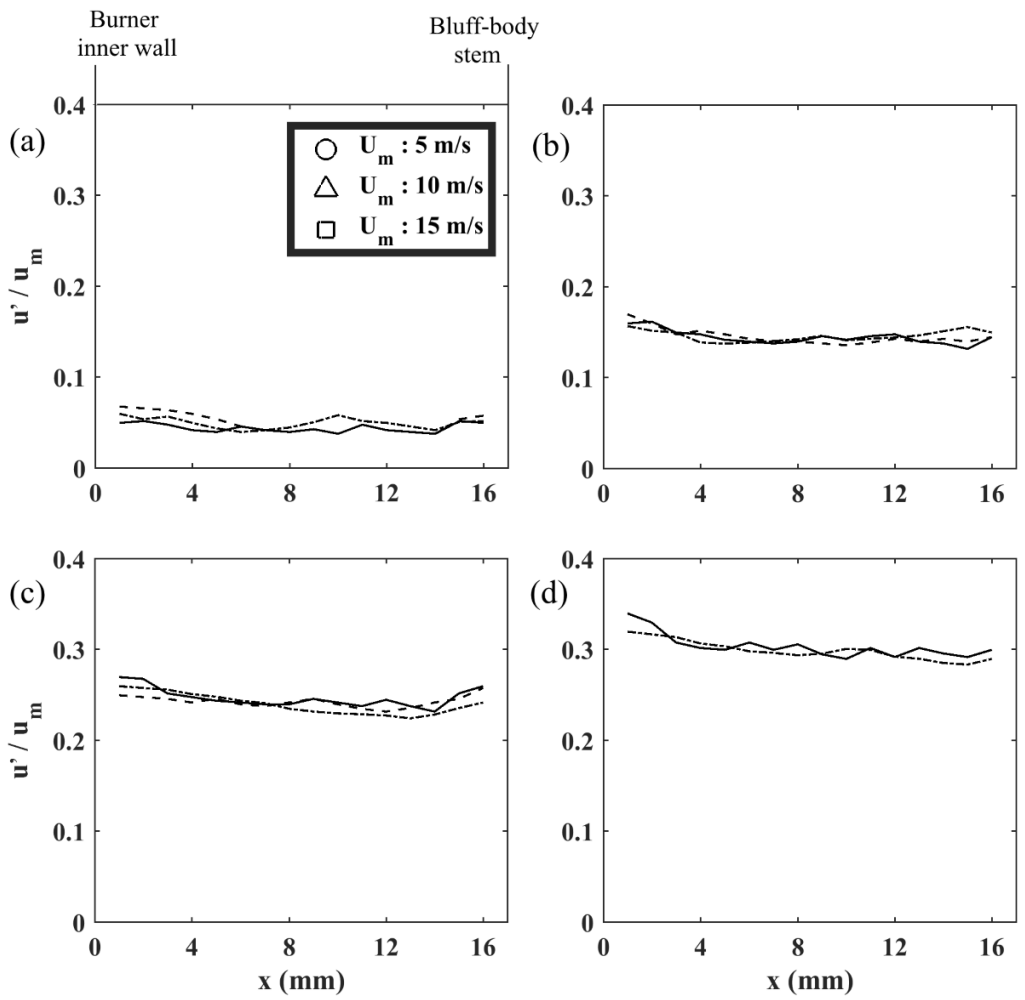

Fig. 2.8. Variation of the fluctuating component of the streamwise velocity for the different conditions corresponding to turbulent intensities of (a) 4 % (b) 14 % (c) 24% and (d) 30 %. u_m is the local mean velocity at a specific location.

From the velocity measurements obtained from the high speed PIV, spatial variation of the turbulent intensity was estimated, as shown in Fig. 2.9. As expected, turbulence intensity decays downstream of the bluff body for all the flow conditions. For the low and moderate turbulent conditions, the turbulent intensity at a distance of four times the bluff body diameter was observed to reduce to about 78% of the value at the exit of the burner while for the intense turbulent conditions (24 and 30%) it reduced to about 83%. The additions of impinging jets for

the intense turbulent conditions prevent a steeper decay of turbulence intensity in the streamwise direction.

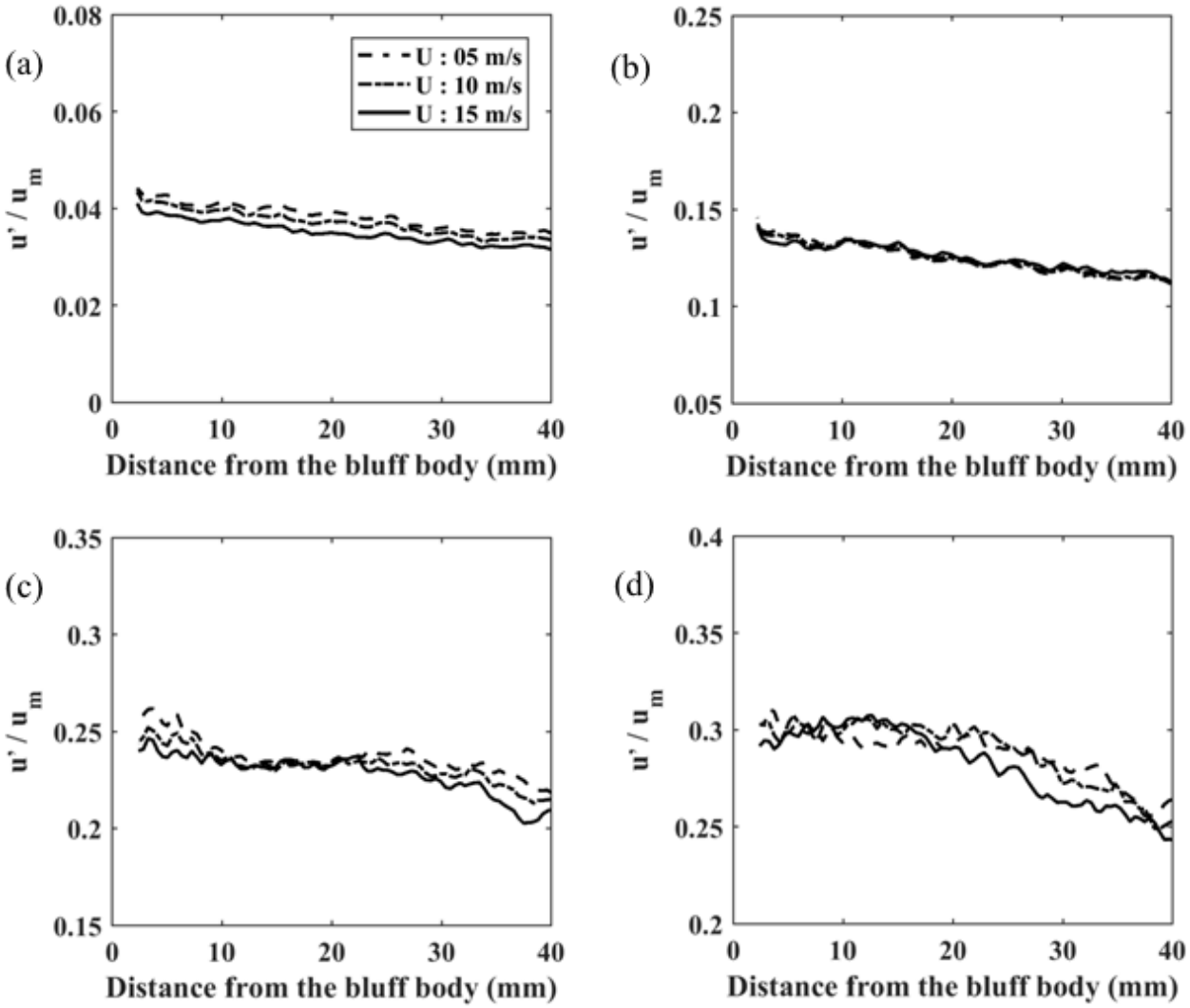

Fig. 2.9. Variation of turbulence intensity along the streamwise direction for (a) T.I : 4% (b) T.I : 14 % (c) T.I : 24% and (d) 30 %

CHAPTER THREE

3. Effects of fuel properties and free stream turbulence on characteristics of bluff-body stabilized flames

Introduction

Characteristics of turbulent premixed flames are strongly influenced by the free stream turbulence levels as well as the properties of the incoming fuel-air mixture. In this chapter, results are presented for the characteristics of lean methane/-, propane/- and ethylene/air flames subjected to different levels of turbulent intensities. Selection of these three fuels was based on the differing fuel properties and their representation of practical fuels and fuel components. Methane is the simplest hydrocarbon with high hydrogen content and Lewis number less than unity and is commonly used for power generation in land-based gas turbines. Lewis number less than unity flames have been shown to behave differently when subjected to hydrodynamic strain relative to those having Lewis number greater than unity [51]. Propane is the simplest fuel that represents hydrocarbons with Lewis number greater than unity and is commonly employed in practical applications. Experiments have been performed using propane/air mixture in the present setup at low free stream turbulence levels in the past by Chaudhuri *et al.* [35,52] and therefore, to understand the effect of higher levels of free stream turbulence on similar flames, propane was selected as a fuel. Ethylene has a faster chemistry than methane and propane and is an important component in the oxidation chemical mechanism of complex hydrocarbons [53,54]. Measurements of average preheat and reaction zone thicknesses, strain rate, burning fraction, curvature, flame brush thickness, flame surface density, area ratio and turbulent flame speed have been obtained for a range of experimental test conditions. In this chapter, first the

experimental conditions and the fuel properties at the studied conditions are presented followed by a discussion of the results and a summary of the important conclusions.

3.1 Experimental Conditions

The experimental conditions employed are tabulated in Table 3.1. Two mean velocities of 10 and 15 m/s were examined which corresponds to global flow Reynolds numbers of 6440 and 9660, respectively based on the bluff body diameter. For each mean streamwise exit velocity, turbulence intensities of 4, 14, 24 and 30% were studied. Lean premixed mixtures of methane/-, propane/- and ethylene/air at an equivalence ratio of 0.85 were used. In addition, ethylene/air flames at an equivalence ratio of 0.655 have also been studied, except for the mean velocity of 15 m/s where the intense turbulent condition (T.I ~ 30%) could not be examined owing to blowoff issues. Ethylene/air flames at an equivalence ratio of 0.655 were studied since its laminar flame speed is similar to that of propane at ϕ=0.85. The flames analyzed in the experiments correspond to the regimes of wrinkled flames, corrugated flames and thin reaction zone in Borghi's regime diagram [12], as shown in Fig.3.1. For normalization unstrained laminar flame speed and thickness values were computed using the PREMIX code [48] and the mechanism of Wang *et al.* [49]. The unstretched laminar flame thickness (δ_f) is defined as the temperature difference across a laminar flame divided by the maximum temperature gradient. Lewis numbers were computed using the database of transport properties of the mechanism of Wang *et al.* [49].

Table 3.1.Properties of the tested experimental conditions#

Fuel	U_m (m/s)	$\frac{u'}{U_{C.P}}$	Integral scale, l_O (mm)	$\frac{u'}{S_{L,O}}$	$\frac{l_{O,HWA}}{\delta_f}$	Re_T	Le
Methane (ϕ : 0.85)	10	0.04	2.8	1.5	5.9	79	0.964
	10	0.14	7.8	4.7	16.3	783	
	10	0.24	12.6	8.1	26.3	2182	
	10	0.30	13.3	9.7	27.7	2898	
	15	0.05	2.62	2.2	5.5	138	
	15	0.16	7.42	7.2	15.5	1261	
	15	0.26	12.2	12.9	25.5	3433	
	15	0.30	13.1	14.3	27.3	4280	
Propane (ϕ : 0.85)	10	0.04	2.8	1.4	7.2	79	1.875
	10	0.14	7.8	4.2	20.1	783	
	10	0.24	12.6	7.3	32.3	2182	
	10	0.30	13.3	8.7	34.1	2898	
	15	0.05	2.62	1.9	6.8	138	
	15	0.16	7.42	6.4	19.1	1261	
	15	0.26	12.2	11.6	31.3	3433	
	15	0.30	13.1	12.8	33.6	4280	
Ethylene (ϕ : .655)	10	0.04	2.8	1.4	6.7	79	1.348
	10	0.14	7.8	4.3	18.7	783	
	10	0.24	12.6	7.4	30.2	2182	
	10	0.30	13.3	8.8	31.9	2898	
	15	0.05	2.62	1.9	6.3	138	
	15	0.16	7.42	6.5	17.8	1261	
	15	0.26	12.2	11.7	29.3	3433	
Ethylene (ϕ : 0.85)	10	0.04	2.8	0.9	9.1	79	1.336
	10	0.14	7.8	2.7	25.5	783	
	10	0.24	12.6	4.6	41.1	2182	
	10	0.30	13.3	5.5	43.4	2898	
	15	0.05	2.62	1.2	8.5	138	
	15	0.16	7.42	4.1	24.2	1261	
	15	0.26	12.2	7.2	39.8	3433	
	15	0.30	13.1	8.1	42.7	4280	

U_m is the mean velocity which is spatially averaged over the burner exit. $U_{C.P}$ and u' were measured at midspan between the burner rim inner wall and the rod holding the bluff body, which is 8.5 mm from the rim wall. $S_{L,O}$ is the unstretched laminar flame speed of the corresponding fuel/air mixture.

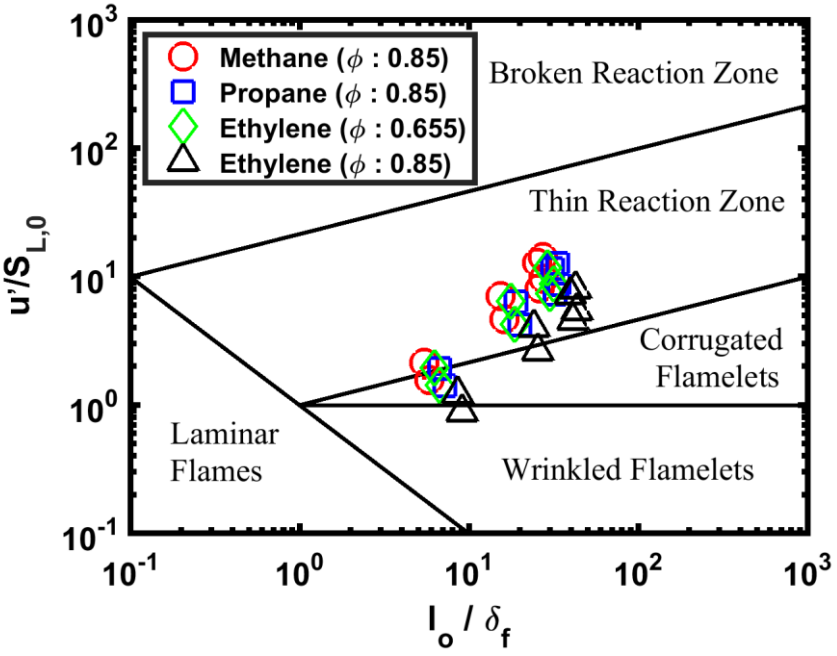

Fig.3.1. Experimental conditions overlaid on the premixed combustion regime diagram

3.2 Results and Discussions

3.2.1. Flame Front Topology

The flame front topology is strongly dependent on the free stream turbulent intensity of the incoming mixture. The results are discussed in the following three subsections for Low (~ 4%), Moderate (~ 14 %) and Intense (~ 30 %) turbulence intensities. Sample instantaneous images for these conditions are presented in three columns – (i) CH_2O PLIF image (ii) OH PLIF image with thick blue lines bordering the proper overlap region of OH and CH_2O representing the heat release region and (iii) Borders of the heat release region superimposed on vorticity contours / velocity field by using thick black lines.

Low turbulence intensity: Instantaneous images of the low turbulence intensity condition corresponding to the different fuel/air mixtures are shown in Fig. 3.2. The edge of the OH PLIF signal delineates the boundary between the burnt and unburnt gases, and therefore tentatively

marks the flame front. The recirculating region behind the bluff body is filled with hot combustion products as indicated by the presence of OH. The CH_2O PLIF signal is observed on the unburnt side adjacent to the flame front, where preheated reactants are expected. A continuous region of overlap of CH_2O and OH, qualitatively marking the heat release region, exists at this low turbulence condition for all fuel/air mixtures. These flames lie in the wrinkled and corrugated flamelet regime in the regime diagram shown in Fig.3.1 and exhibit a typical laminar flamelet structure. For all the conditions, the flame front envelopes the high vorticity regions of the shear layer bounding the hot products region and is observed to be smoothly wrinkled due to the convecting Kelvin Helmholtz vortices, as shown in Fig. 3.2 a – d. As expected from the laminar flame simulations, the ethylene flame stabilized at ϕ=0.85 is observed to be wider relative to methane and propane flames due to higher flame speed and the preheat region marked by the CH_2O PLIF signal is observed to be thinner.

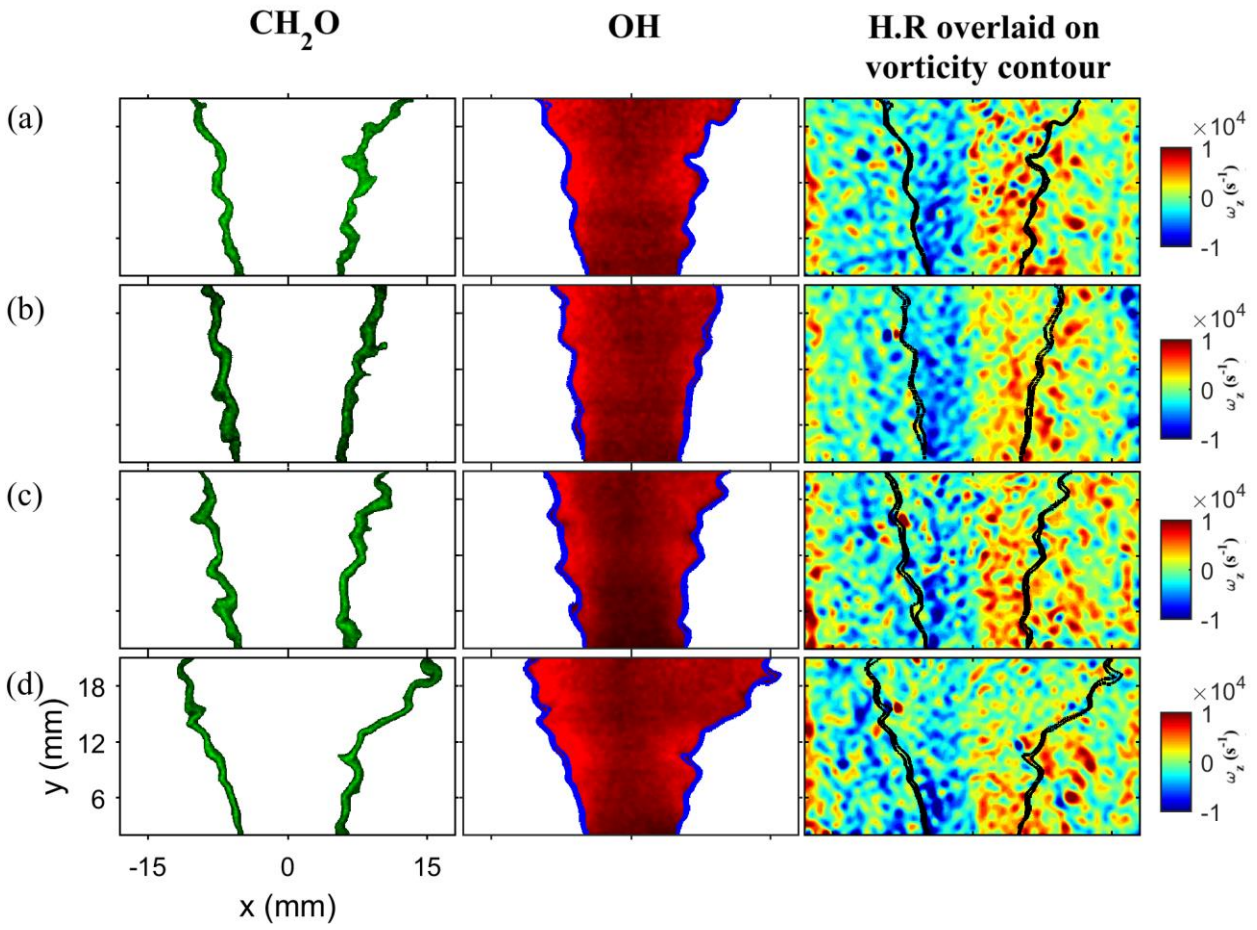

Fig. 3.2. Instantaneous images of CH_2O PLIF, OH PLIF and heat release region overlaid on the vorticity contours for the low turbulence (4%) condition corresponding to (a) Methane (b) Propane (c) Ethylene (ϕ=0.655) and (d) Ethylene (ϕ=0.85).

Moderate turbulence intensity: Instantaneous images corresponding to moderate turbulence intensity condition for the different fuel/air mixtures are shown in Fig.3.3. Increasing the free stream turbulence intensity from 4 to 14% affects the flame front topology as can be seen by comparison of these images in Fig. 3.2. The wrinkling of the flame front increases for all the cases with pronounced formation of cusps, which are flame segments with negative and large values of curvature. From the PLIF images, long elongated fingers filled with preheated reactants, shown by the presence of CH_2O in Fig.3.3 a-d are observed to protrude into the hot

products region. The occurrence of these structures has been reported in experimental studies of low swirling flames by Cheng *et al.* [55]; Shepherd and Cheng [56], Bunsen type flames by Chen *et al.* [57], Buschmann *et al.* [6] and others. The physical mechanism which controls the growth of these elongated ligaments has been recently studied by Lipatnikov *et al.* [58] using DNS. Their analysis indicate that acceleration of unburned gas due to local pressure gradient induced by heat release in surrounding flamelets can produce unburned mixture fingers which penetrate into the combustion products. From the 600 images of each case, the propensity of formation of these unburned mixture fingers was found to be higher for the ethylene flames at ϕ=0.85 relative to methane/- and propane/air mixture compositions. Stronger wrinkling and formation of these flame front structures can result in increasing the flame surface area, turbulent burning velocity and mean flame brush thickness relative to the low turbulence intensity condition. For all the investigated cases at this turbulence condition, the PLIF images of OH and CH_2O show mostly continuous heat release regions and thereby, exhibiting a typical "flamelet" like structure.

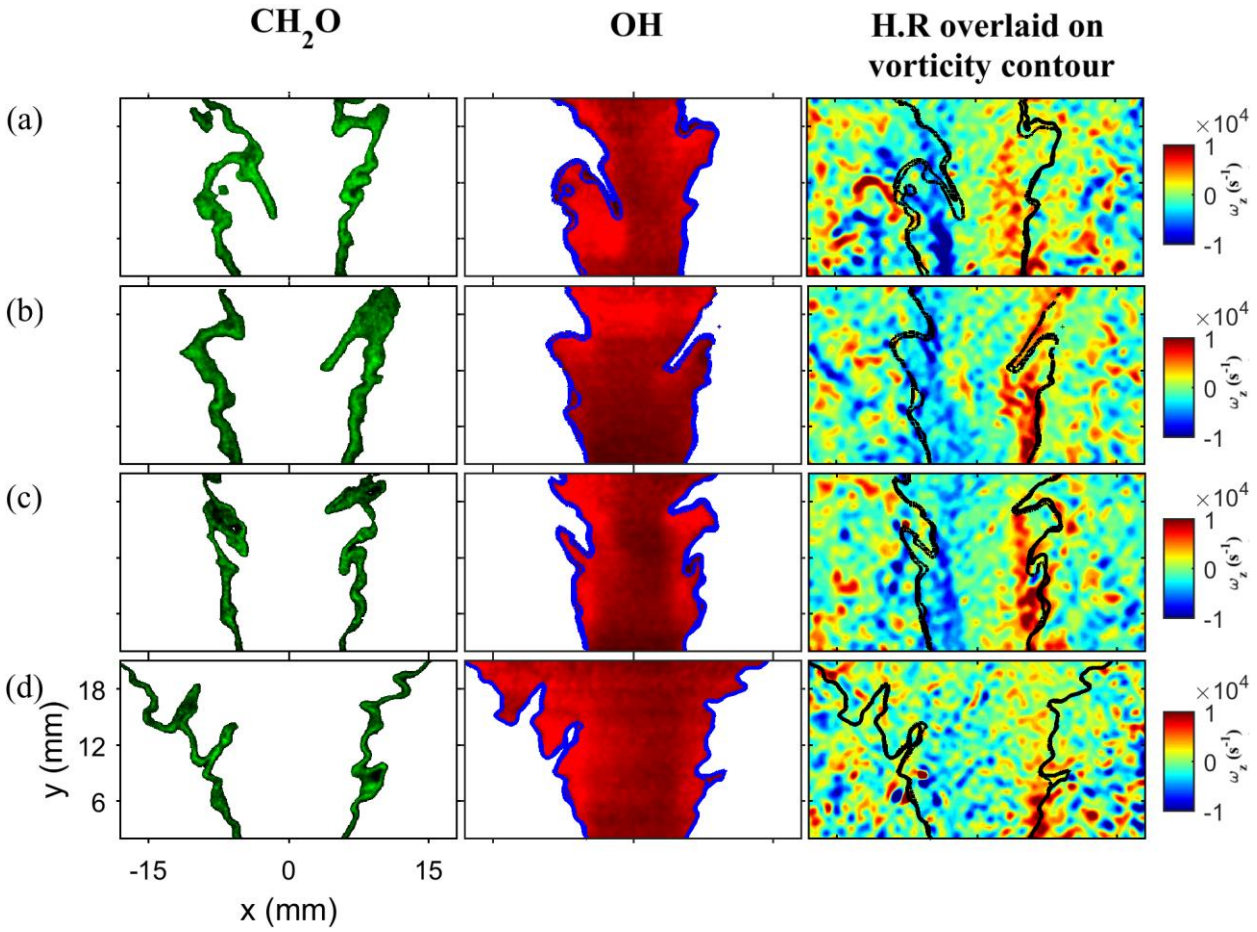

Fig.3.3. Instantaneous images of CH_2O PLIF, OH PLIF and heat release region overlaid on the vorticity contours for moderate turbulence (14%) condition corresponding to (a) Methane (b) Propane (c) Ethylene (ϕ=0.655) and (d) Ethylene (ϕ=0.85).

High turbulence intensity: Significant wrinkling and distortion of the flame front occurs as the turbulence intensity is increased to 30 %. Analysis of the instantaneous PLIF images suggests that the flame front features certain characteristics as shown in Fig.3.4 - Fig.3.7. Similar characteristics were observed for the flames stabilized at mean velocities of 10 and 15 m/s. Qualitative study of these characteristics is of importance as it can provide physical insights into the variation of the various statistical parameters discussed later in this chapter. Details of the different flame front characteristics are provided below:

(i) Flamelet Merging: Under highly turbulent conditions, flamelet merging is a common phenomenon which involves the propagation of flame front structures towards one another. Fig.3.4 a-d offer evidence that merging of flamelets does occur for all the studied fuel/air mixtures at the intense turbulent condition, but the rate of merging cannot be quantified with the present diagnostics. First, long fingers of wrinkled flame surfaces are created due to penetration of preheated reactants into combustion products. Then as the flame fronts propagate towards one another, they form a neck region that burns through to create a pocket. This is seen in the boxed regions in Fig.3.4 a-d where a "neck" appears to have been formed with two reactive flame fronts marked by the overlap of OH and CH_2O propagating towards each other with only a thin layer of preheated reactants between them. Flamelet merging can result in destruction of flame surface area and thus, reduction in local burning rate. Similar phenomenon have been reported by Filatyev *at al.* [59] and has been attributed as the primary reason for the observation of bending behavior in the variation of turbulent flame speed. The images of the neck region shown in Fig.3.4 are similar to time resolved images of flamelet merging reported by Osborne *et al.* [60] (Fig. 16).

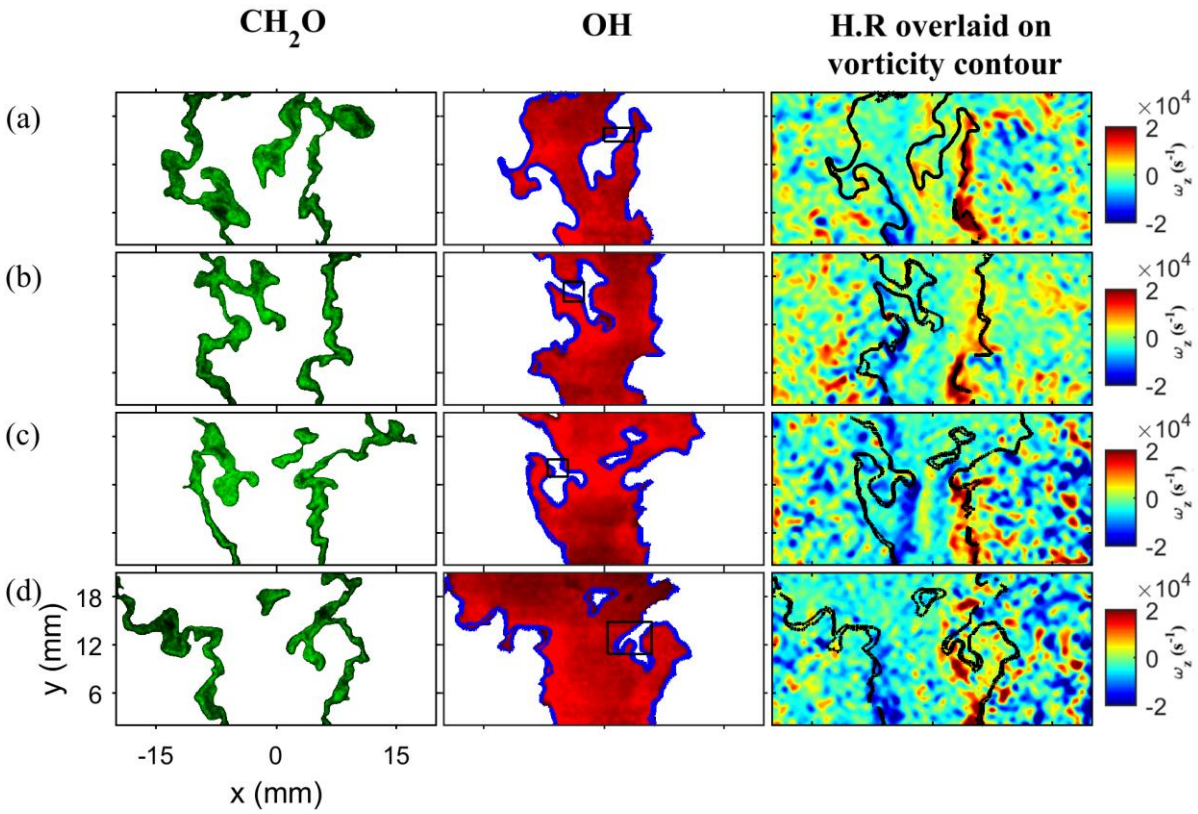

Fig.3.4. Instantaneous images of CH_2O PLIF, OH PLIF and heat release region overlaid on the vorticity contours for high turbulence condition (30 %) corresponding to mean velocity of 10 m/s showing the occurrence of flamelet merging and localized extinctions for flames corresponding to (a) Methane (b) Propane (c) Ethylene (ϕ=0.655) and (d) Ethylene (ϕ=0.85).

(ii) *Localized extinctions:* At the intense turbulent condition, large-scale eddies with stronger vortical strengths are observed to interact with the flame front. This can induce higher hydrodynamic strain locally on the flame front which can lead to localized quenching along the flame sheet where the local strain rate exceeds the extinction strain rate, κ_{ext}. This is clearly seen to occur for all the cases, as shown in Fig.3.4 a- d where breaks are observed along the overlap region of OH and CH_2O. From the PLIF images obtained for the different fuel/air mixtures, higher propensity of localized extinctions along the flame sheets are

observed for the lean propane/air flames at ϕ=0.85 and ethylene/air flames at ϕ=0.655 relative to methane/- and ethylene/air flames at ϕ=0.85 and will be discussed quantitatively in terms of burning fraction later in the chapter. The occurrence of localized extinctions result in decrease of the flame surface area and consequently the local consumption rate.

(iii) *Pocket formation:* At the highly turbulent conditions, pockets of preheated reactants are observed in the regions downstream of the bluff body which is usually filled with hot combustion products under low and moderate turbulent intensity conditions. Fig.3.5a –d shows multiple islands of CH_2O with thin overlap regions with OH indicating the occurrence of heat release along the boundaries. Pocket formation can occur due to flamelet merging events and localized extinctions along the flame sheet. The formation of holes along the flame sheet can provide a channel for penetration of fresh reactants into the regions occupied by the hot combustion products. This provides a possibility for the transfer of mass and energy between the incoming cold reactants and the products resulting in formation of islands of preheated reactant regions, marked by the presence of CH_2O signal. For all the fuel/air mixture conditions, fewer images with pockets were observed for turbulent intensity condition of 24% and no such images were observed at the low and moderate turbulence levels.

In an additional experiment, flame front topology was studied by using time resolved mie scattering images. Micron sized silicone oil droplets generated by a set of nebulizers, were used for seeding the flow. Analysis of these images illustrated the formation of pockets by flamelet merging phenomenon. However, as the simultaneous PLIF/PIV diagnostic was not time resolved and limited to two dimensional plane, the exact mechanism responsible for the

observation of islands of CH_2O in the OH filled regions and localized extinctions along the flame sheet cannot be identified with certainty as such features can also arise due to flame motion into and out of the two-dimensional plane.

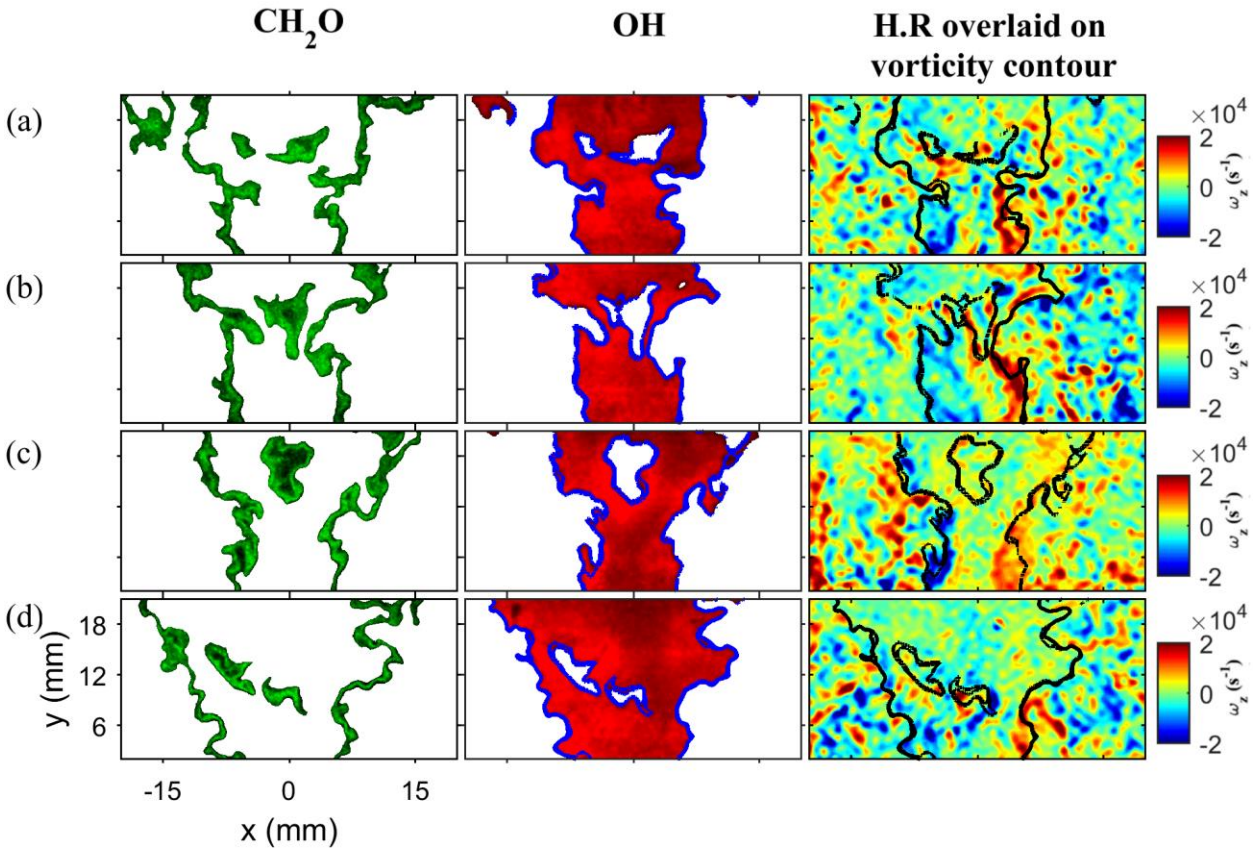

Fig.3.5. Instantaneous images of CH_2O PLIF, OH PLIF and heat release region overlaid on the vorticity contours for high turbulence condition (30 %) corresponding to mean velocity of 10 m/s showing the occurrence of pockets of preheated gases for flames corresponding to (a) Methane (b) Propane (c) Ethylene (ϕ=0.655) and (d) Ethylene (ϕ=0.85).

(iv) *Fragmentation of the flame segments:* Siginificant localized extinctions along the shear layer and/or flame pinching events can lead to fragmentation of the flame. Such an event of disintegration of the flame into multiple segments is observed only for lean propane/- and

ethylene/air flames at ϕ=0.655, as shown in Fig.3.6. The instantaneous recirculation zone represented by the contour of U_y = 0 is shown by the red lines on the velocity field data in Fig.3.6 and the heat release regions are overlaid on the velocity field. It is observed that for both the cases, the main flame segment has fragmented primarily into two sections with the bottom segment retreating to the tip of the recirculation zone and remaining attached to the bluff body while the other flame segment is observed in the downstream region with thin reaction layers surrounding it. There may be two likely scenarios leading to this type of flame topology. (1) significant localized extinction along the outer flame envelope through which the reactants enter all the way to the central part of the flame and heat-up of the reactive mixture there (formaldehyde signal region) and/or (2) flame pinching events resulting in fragmentation of the flame occurring in the central part of the flame. The exact mechanism for the occurrence of this phenomenon is still speculative and is a subject of active research.

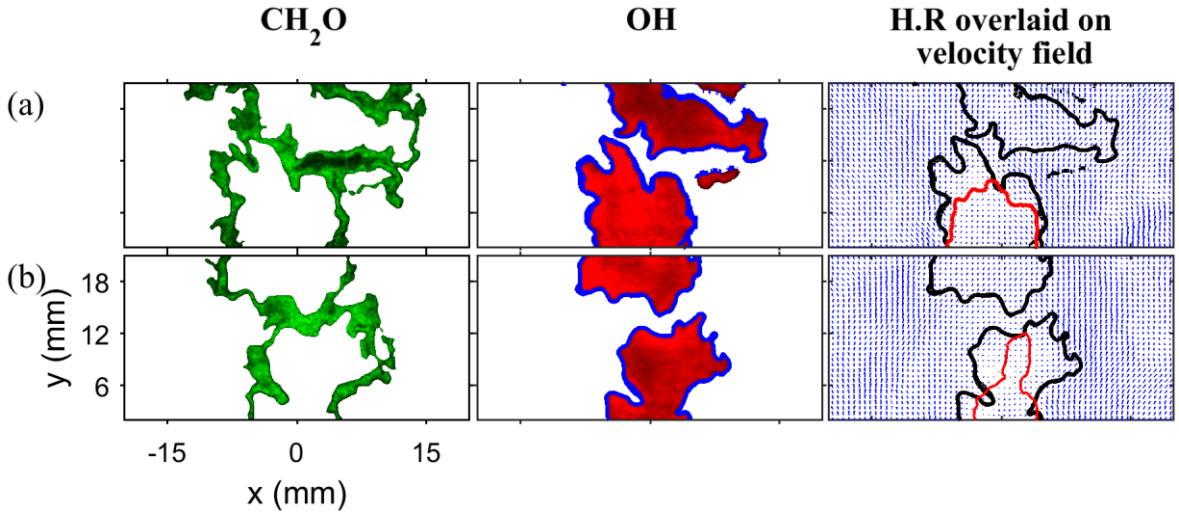

Fig.3.6. Instantaneous images of CH_2O PLIF, OH PLIF and heat release region overlaid on the velocity field for intense turbulence condition (30 %) corresponding to mean velocity of 10 m/s for (a) propane/air flames and (b) ethylene/air flames at ϕ=0.655.

(v) <u>*Asymmetric Flame Structure:*</u> In intense turbulent conditions, the general shape of the flames corresponding to lean propane/- and ethylene/air at ϕ=0.655 was observed to switch from symmetric (varicose) to asymmetric (sinuous) mode, as shown in Fig.3.7. This behavior of bluff body stabilized flames has been linked experimentally, analytically and numerically by various authors in the past (Ref. [30,34,35,61,62]) to the transition between symmetric Kelvin-Helmholtz (KH) shear roll-up and asymmetric Benard-von Karman (BVK) vortex shedding. This behavior has been explained by examining the dilatative and baroclinic vorticity production components in the vorticity transport equation:

$$\frac{D\vec{\omega}}{Dt} = (\vec{\omega}.\vec{\nabla})\vec{V} - \vec{\omega}(\vec{\nabla}.\vec{V}) + \frac{\vec{\nabla}\rho \; X \; \vec{\nabla}p}{\rho^2} + \vec{\nabla} \; X \; \frac{\overrightarrow{\nabla.\Xi}}{\rho} \qquad (1)$$

In reacting flows, vorticity is generated by the baroclinic mechanism, represented by third term on the RHS of the transport equation, due to the misaligned gradients in pressure and density owing to the inclination of the flame with respect to the flow. The vorticity generated by this mechanism is of the opposite direction to that generated by shear near the bluff body. Second term on RHS represents the vorticity damping term due to flow dilatation. The baroclinic mechanism plays an important role in attenuating the Kelvin-Helmholtz instability while vorticity damping has been found to attenuate the Benard-von Karman instability based on computational studies [61]. Thus, the global density ratio across the flame plays an important role in overall flame dynamics.

Entrainment of cold reactants into the flame at high turbulence conditions due to localized extinctions and flamelet merging reduces the global density ratio between the flame region and its surroundings, thus reducing the vorticity damping term discussed above. This results

in stronger influence of the asymmetric vortices which are shed from the flame holder on the flame.

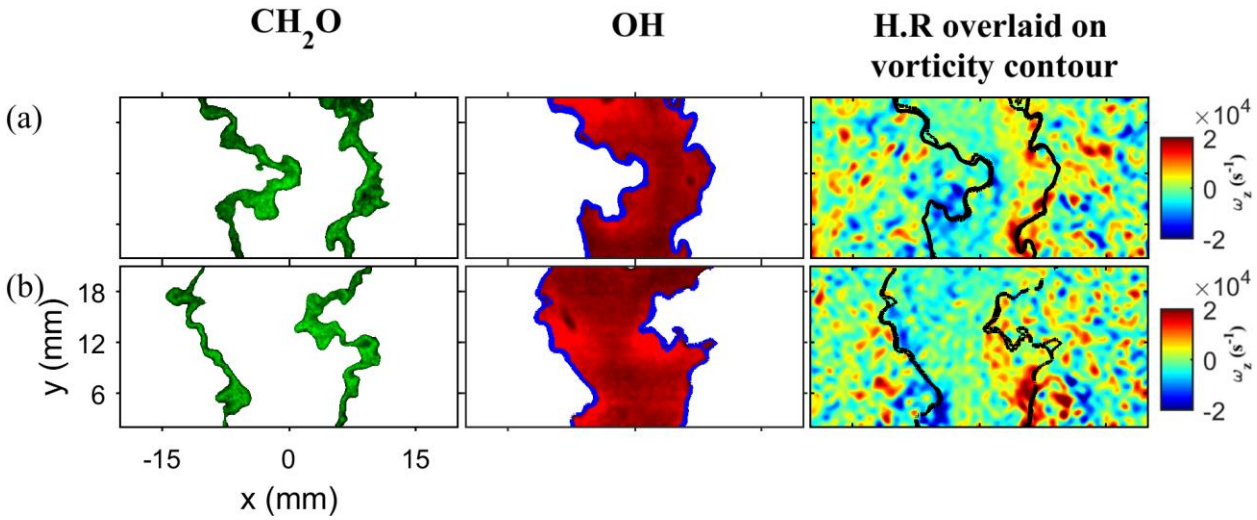

Fig.3.7. Instantaneous PLIF images and heat release region overlaid on the vorticity field showing the asymmetric flame structure for (a) propane/air flames and (b) ethylene/air flames at ϕ=0.655.

While the flames corresponding to the different fuel/air mixtures shows different characteristics when subjected to intense turbulent conditions as discussed above, there is no evidence of broadly distributed heat release zones. The flames under this condition are therefore, characterized by thickened preheat zones and thin reaction zones. Quantification of the flame thickness will be discussed later in the chapter. Similar characteristics were observed for the flames stabilized at a turbulence intensity of 24 %.

Averaged CH_2O PLIF, OH PLIF and heat release images for mean velocity of 10 m/s of different fuel/air mixtures at moderate (~14 %) and intense (~30 %) turbulence intensities are shown in Fig.3.8 and Fig.3.9, respectively. The boundary of the mean recirculation zone for each case is shown by the red line which is defined as the contour of zero mean axial velocity. The mean

PLIF profiles agree with the observations from the instantaneous images. At turbulence intensity of 14%, for all the fuel/air mixture flames, the region behind the bluff body is filled with combustion products marked by the OH signals while CH_2O is observed along the shear layer. The mean flame brush, represented by the average heat release profile, is observed to be relatively thin at the attachment point, where the heat release intensity appears highest, and broadens farther downstream. Owing to higher flame speed, the distribution of the averaged profiles for ethylene/air flames at ϕ=0.85 are observed to be at a much wider flame angle relative to the other fuel/air mixture compositions.

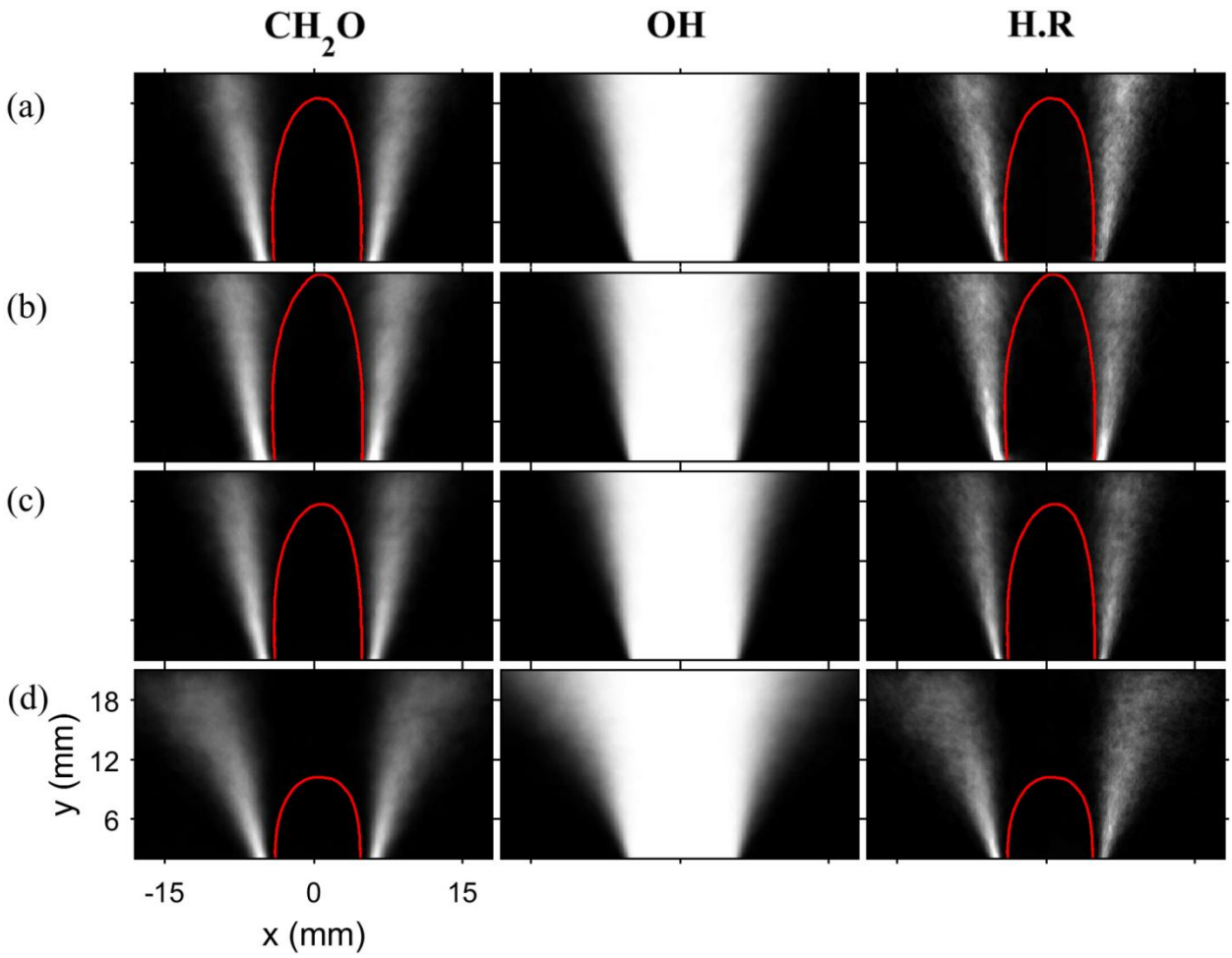

Fig.3.8. Averaged CH_2O PLIF, OH PLIF and heat release images for U_m=10m/s, T.I: 14 % for (a) Methane/air (b) Propane/air (c) Ethylene/air at ϕ=0.655 and (d) Ethylene/air at ϕ=0.85

For the intense turbulence intensity of 30%, wider distributions of the averaged profiles are observed. This can be attributed to the significant wrinkling of the flame front as well as to the different flame front characteristics discussed above. For the methane/- and ethylene/air flames at ϕ=0.85, shown in Fig.3.9 (a) and (d) respectively, the mean CH_2O and heat release signals are observed primarily along the shear layer. However, for propane/air flames at ϕ=0.85 and ethylene/air at ϕ= 0.655 mean CH_2O signals are observed within the mean recirculation zone

especially near the downstream end, as shown in Fig.3.9 (b) and (c), respectively. Also, wider average heat release profile is observed within the recirculation zone at the downstream end indicating that the reaction zone is no longer limited to the shear layer. The difference in behavior of the averaged profiles for these two fuel/air mixture condition at the intense turbulent condition can be attributed to significant localized extinctions, fragmentation and intermittent shift of the flame structure to a sinuous mode as observed in the instantaneous images.

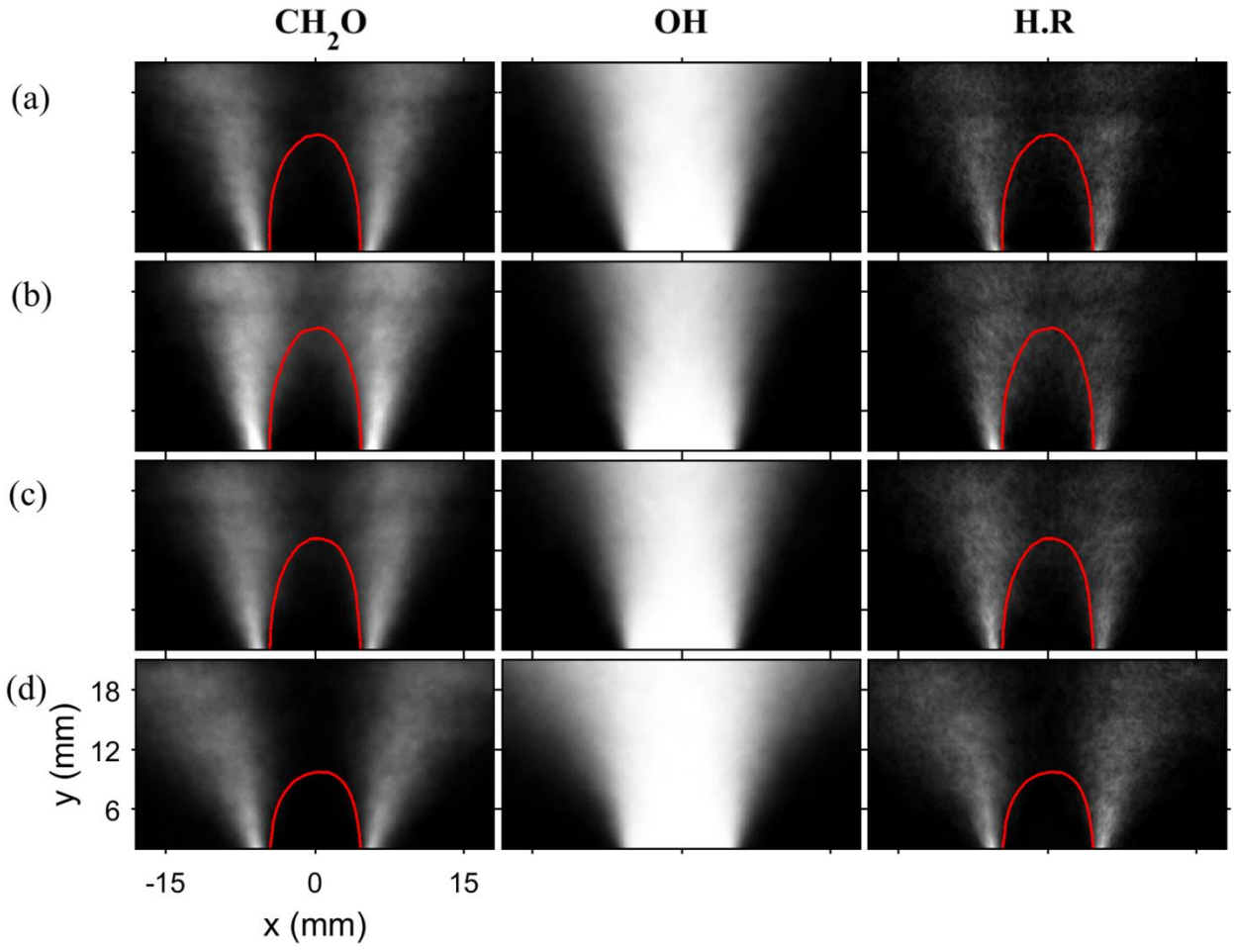

Fig.3.9. Averaged CH_2O PLIF, OH PLIF and heat release images for U_m=10m/s, T.I: 14 % for (a) Methane/air (b) Propane/air (c) Ethylene/air at ϕ=0.655 and (d) Ethylene/air at ϕ=0.85

3.2.2. Average thicknesses of preheat and reaction zones

Average thicknesses of the preheat and reaction zones were estimated for each CH_2O and OH PLIF image pair as detailed in Section 2.3. To examine the effect of turbulence on the thicknesses, an ensemble average of the preheat zone and reaction zone thickness over all the images taken for each case was calculated. The variation of the preheat zone thicknesses normalized by the experimentally obtained laminar preheat zone thickness with respect to turbulence Reynolds number (Re_T) are shown in Fig. 3.10. The normalized quantities for both the fields of view are shown using open and filled symbols for lower and upper fields of view respectively. It clearly shows that for all the preheat zone thickness increases with turbulence Reynolds number. Similar observation has been reported by Skiba *et al.* [10] and Osborne *et al.* [60].

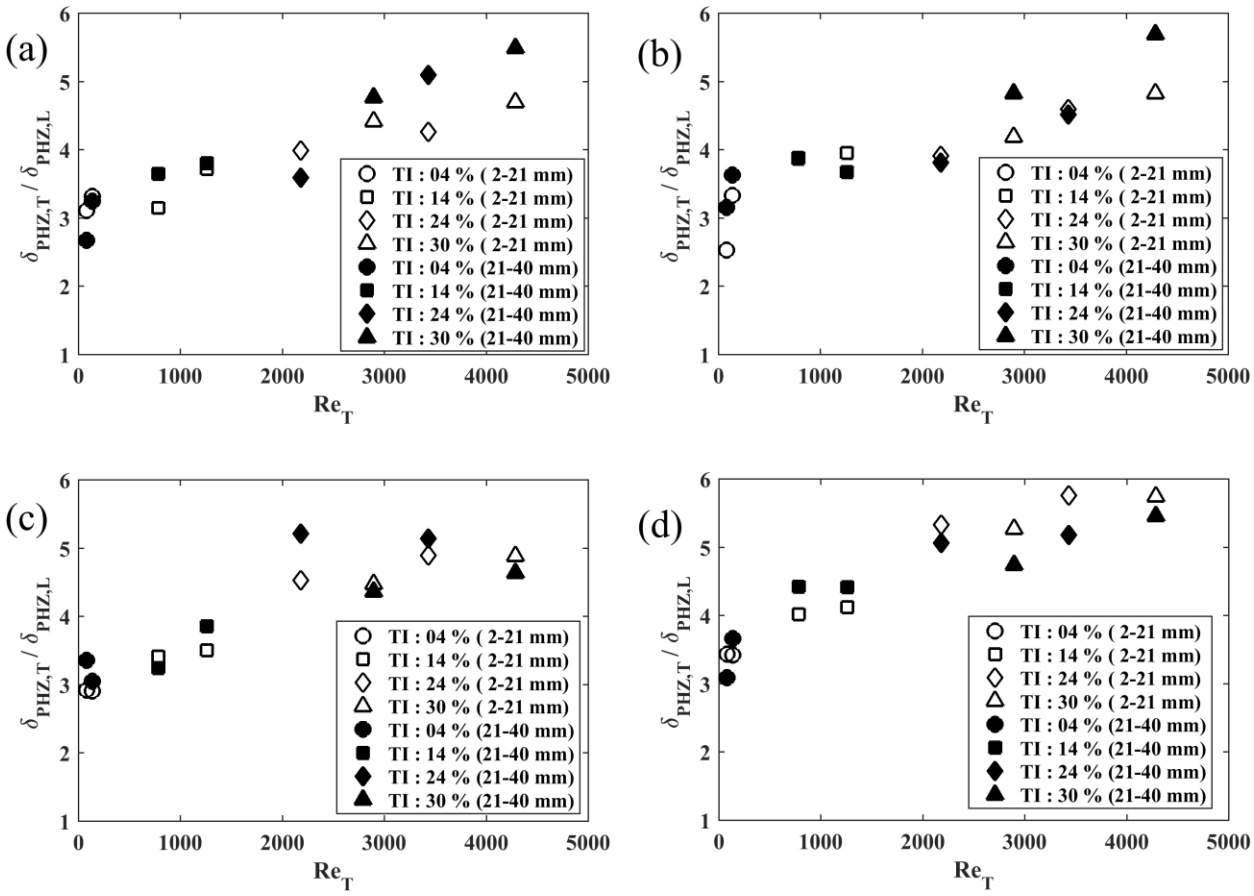

Fig. 3.10. Average turbulent pre-heat zone thickness normalized by experimentally measured values in laminar flame as a function of turbulence Reynolds number (Re_T) for (a) methane/air flames (b) propane/air flames (c) ethylene/air flames (ϕ=0.655) and (d) ethylene/air flames (ϕ=0.85)

In the review paper by Driscoll [2] it has been indicated that a measured flamelet could appear a few (~3-4) times thicker relative to an unstrained laminar flame owing to (1) three dimensional effects on the 2D PLIF measurements (2) limited experimental spatial resolution and (3) applied strain rate. For these reasons, the observation of thickened preheat zone for lower and moderate turbulence intensities might be somewhat attributed to these limitations. However, significant broadening of the preheat zones for turbulent intensities of 24 % (U_m=15 m/s) and 30% cannot

be explained by the limitations of the current diagnostics. Instead the observed thickening might be attributed to penetration of turbulent eddies into the preheat zone.

The variation of normalized reaction zone thickness with turbulence Reynolds number for all the flames is shown in Fig. 3.11. For methane/-, propane/- and ethylene/air (ϕ=0.655), it is observed that reaction zone thickness decreases with turbulence Reynolds number. However, slight increase is observed for the highest turbulence condition which might be due to the occurrence of strong flamelet merging events. Similar trend of the reaction zone thickness has been reported in the experimental work of Buschmann *et al.* [6]. For ethylene/air flames at ϕ=0.85, the reaction zone thickness was observed to increase with increasing level of free stream turbulence. The effect of different levels of turbulence intensities on thickness of the reaction zone has been recently studied in a DNS work by Wang *et al.* [63]. From the flame stretch and flame thickness analysis, the authors had observed that preferential alignment of the flame front with extensive positive strain rate can result in thinning of the reaction zone whereas the presence of high curvature regions along with lower tangential strain can thicken the reaction zone substantially.

The flames subjected to the intense turbulent conditions belong to the category of the thin reaction zone (TRZ) in Borghi's regime diagram, shown in Fig.3.1. Analysis of the PLIF images supports Peters' [64] TRZ regime theory: the preheat zone (marked by the CH_2O layer) is broadened while the inner layer (heat release zone marked by the overlap of OH and CH_2O) remains thin.

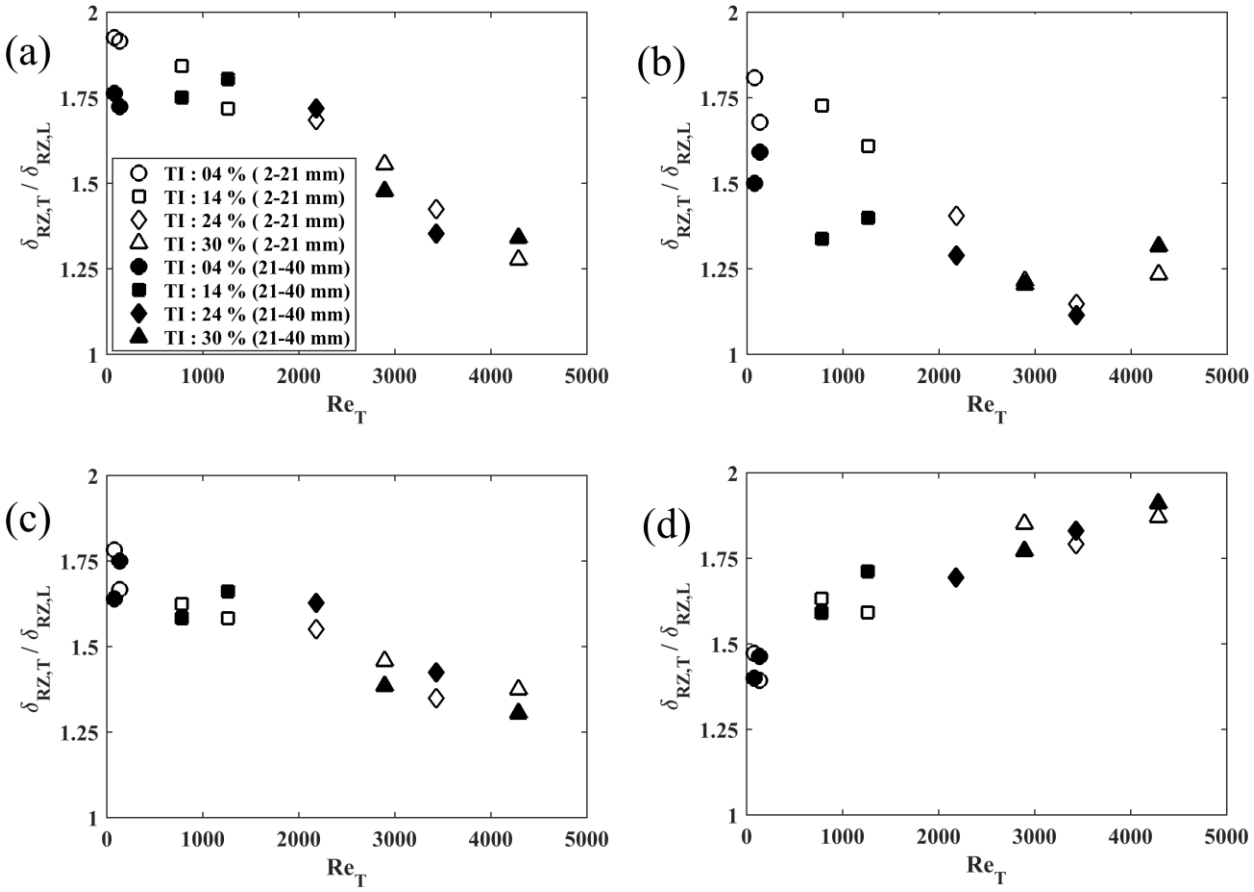

Fig. 3.11. Average turbulent reaction zone thickness normalized by experimentally measured values in laminar flame as a function of turbulence Reynolds number (Re_T) for (a) methane/air flames (b) propane/air flames (c) ethylene/air (ϕ=0.655) flames and (d) ethylene/air (ϕ=0.85) flames

3.2.3. 2-D Estimates of strain rate

The edge of the OH PLIF images represents the leading edge of the flame brush which separates the burned and unburned gas regions. The edge points of the OH PLIF images along which heat release is detected were used in conjunction with the velocity field data to estimate the strain rate information along the flame front. Two-dimensional strain rate was determined using [51]:

$$\kappa_s = -n_x \text{ x } n_y \text{ x } \left(\frac{\partial \text{u}}{\partial \text{y}} + \frac{\partial \text{v}}{\partial \text{x}}\right) + (1 - n_x^2) \text{ x } \frac{\partial \text{u}}{\partial \text{x}} + \left(1 - n_y^2\right) \text{ x } \frac{\partial v}{\partial y} \quad (2)$$

Where u and v velocity components along x and y directions, respectively and n_x and n_y are x and y components of the flame surface normal vector. This is the hydrodynamic strain portion of the overall flame stretch. Additional effects of stretch rate due to flame curvature are not considered in this work and only the two-dimensional hydrodynamic stretch rate accessible by the presently employed diagnostics is computed. Thus, with 600 images collected for each condition, over 5 x 10^5 individual points were used in the calculation of the strain rate statistics.

The pdfs of the hydrodynamic stretch rate for mean velocity of 10 m/s for the stably burning flames of different fuel/air mixtures are shown in Fig.3.12 a-d. The pdfs shown in Fig.3.12 corresponds to the flame segments located near the bluff body (2 to 21 mm from the bluff body). The black lines represent the extinction strain rate computed from OPPDIFF [65] using the mechanism of Wang *et al.* [49]. For estimation of the extinction strain rate in OPPDIF, the configuration included two opposing nozzles, both containing premixed fuel-air mixtures at a temperature of 300 K. As expected, the pdfs are observed to become wider with increasing turbulent intensities. In the experimental work of Filatyev *et al.* [59] and DNS analysis of flame-vortex interaction of Meneveau and Poinsot [66], the stretch efficiency factor was shown to increase as the square of the integral length scale. This indicated that large eddies present in the flow are more efficient in stretching the flame than the small eddies. In the present work, the integral length scale was found to increase with increasing free stream turbulence level of the incoming fuel-air mixture. Also, from the instantaneous images of Fig. 3.2 - Fig.3.7, it was observed that large scale eddies interact more with the flame for the higher turbulence intensity conditions. Therefore, from the observations and discussion in Ref. [59,66], the widening of the strain rate pdfs with turbulence intensity is expected.

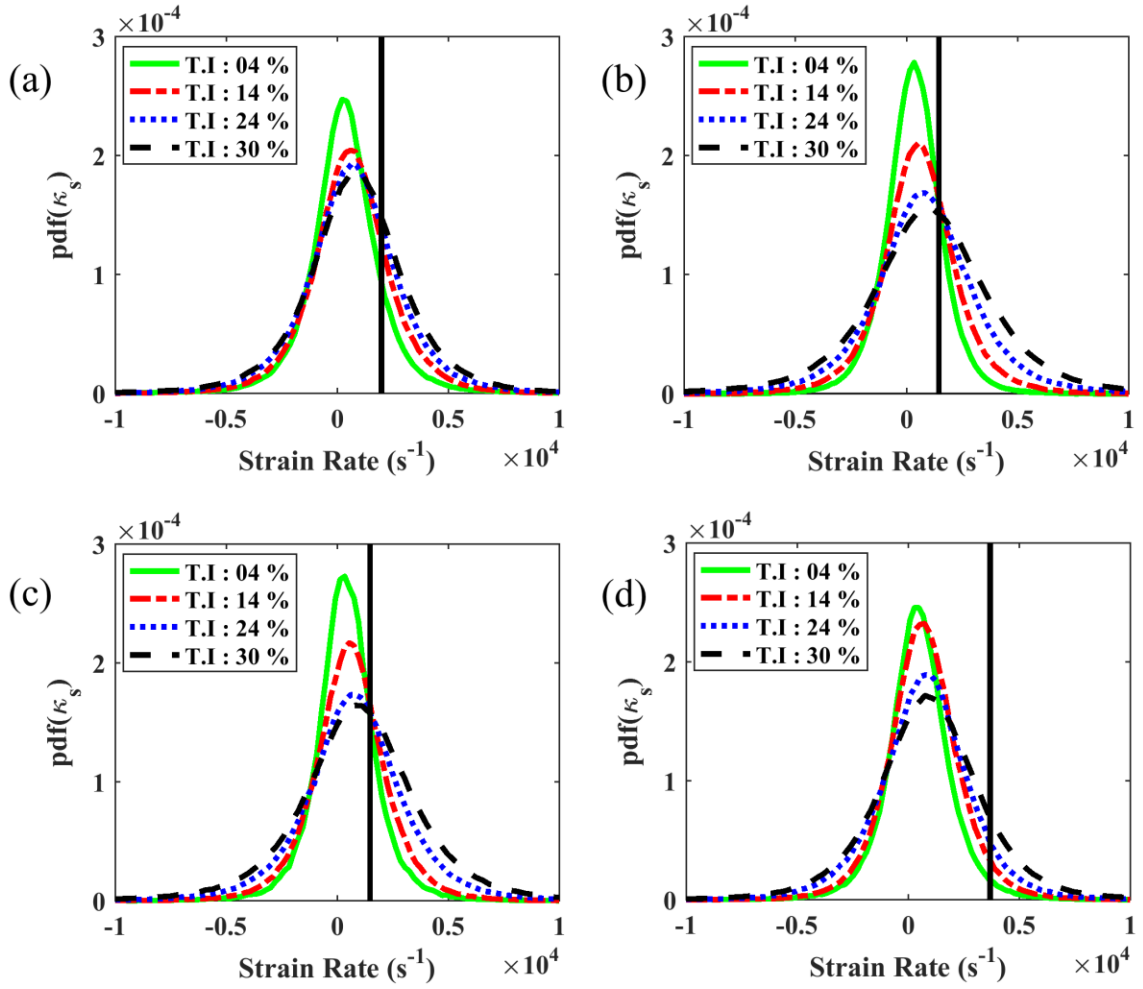

Fig.3.12. Probability distribution functions of the 2-D strain rates for the different turbulent conditions for mean velocity of 10 m/s corresponding to flames of (a) Methane/air (b) Propane/air (c) Ethylene/air at ϕ=0.655 and (d) Ethylene/air at ϕ=0.85.

For flame segments near the flame holder, the strain-rate distribution was skewed towards positive values. Mean strain rate values increased with increasing turbulence levels and were always positive, consistent with the previous studies [67–69]. For example, it increased from $384s^{-1}$ to $1028s^{-1}$ as turbulence intensity was increased from 4 to 30% for the propane/air flame corresponding to 10 m/s mean velocity. For lean methane/air flames which has Lewis number less than unity, the increase of positive stretch rate enhances the burning rate and elevates the

burning temperature [51]. While for the other lean fuel/air mixtures considered in this work which had a Lewis number greater than unity, increase in positive stretch rates will have the opposite effect of reduction in the reaction rate [51].

From the strain rate distributions, it can be clearly seen that for all the conditions there are locations where the instantaneous strain rate exceeds the extinction strain rate computed using OPPDIF. However, the analysis of the instantaneous PLIF images of low and moderate turbulence intensities does not show extinctions. Extinction requires that sufficiently high strain rate be exerted on the flame for a sufficiently long residence time [59] to affect extinction. The larger scale eddies present in the intense turbulent conditions have a longer characteristic roll-over time and therefore, have a higher probability of causing extinction along the flame sheet. This argument supports the observations reported in the discussions on flame topology. However, for the flames of propane/- and ethylene/air at ϕ=0.655, significantly large fraction of the strain rate distribution is observed beyond the corresponding the extinction strain rate relative to that of methane/-and ethylene/air at ϕ=0.85. This indicates that these flames are more susceptible to localized quenching/extinction along the flame sheet at the higher turbulent conditions.

3.2.4. Burning fraction measurements

In order to evaluate the degree of local extinctions for the investigated conditions, the burning fraction of the flames were estimated. The burning fraction has been defined as the length of CH_2O overlapping a reaction zone divided by the total length of CH_2O near the "hot edge" of the reactants[9]:

$$Burning\ Fraction = \frac{Length\ of\ CH_2O\ segment\ burning}{Total\ Length\ of\ CH_2O\ segment} \quad (3)$$

To evaluate the burning fraction, an approach similar to that of Temme *et al.* [9] was followed. The edge of the CH_2O filled regions were divided into multiple segments and then the segments which are not present near a reaction zone were eliminated. From the pool of the selected segments, the length of CH_2O segment was estimated which overlapped with the regions containing OH, and thereby represent the length of the CH_2O segment lying in the reaction zone.

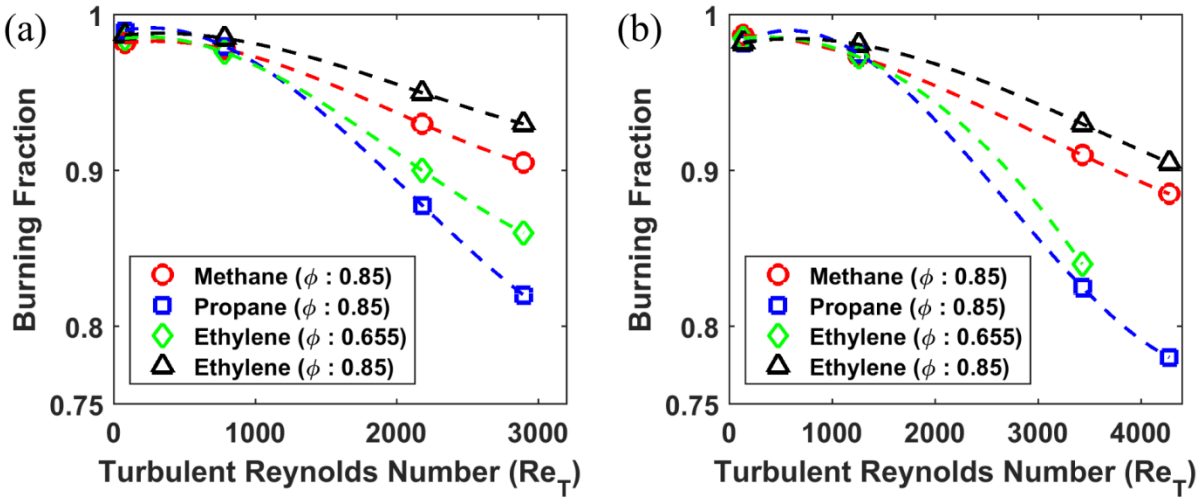

Fig.3.13. Estimate of the burning fraction for the different flames corresponding to mean velocity of (a) 10 m/s and (b) 15 m/s.

The variation of the burning fraction for the different cases corresponding to mean velocity of 10 and 15 m/s is shown in Fig.3.13(a) and (b) respectively. For all the flames, the burning fraction is observed to be close to unity for the low and moderate turbulence intensity conditions. As the turbulence intensity is increased to 24 and 30%, the burning fraction decreases and significant deviation is observed for the different fuel/air mixture flames. For lean ethylene/air flames at ϕ=0.85, the burning fraction is observed to be higher relative to other fuel/air mixtures, indicating the least degree of localized extinctions along the flame sheet. This is expected based on the understanding gained from the strain rate distribution, shown in Fig.3.12, where the area

of the distribution beyond the extinction strain rate was observed to be least. For propane/ and ethylene/air (ϕ=0.655) flames, the strain rate estimates suggest that significant portion of the flame sheet experienced strain rates that exceeded the corresponding extinction strain rate, κ_{ext}. Therefore, the observation of steeper decline of the burning fraction for these flames is reasonable. The presence of significant number of holes along the flame sheet for these fuel/air mixtures provides multiple channels for penetration of the cold reactants and can be a possibility for the observation of the intermittent shift of the flame shape from varicose to sinuous mode. For the lean methane/air flames, the burning fraction was observed to be close to/greater than 0.9 at the intense turbulence conditions. This can be attributed to the observation from strain rate distribution as well as to the opposite behavior of the flames with Lewis number less than 1 when subjected to extensional strain. As the mean velocity is increased to 15 m/s, the strain rate pdfs have been observed to become wider which indicate the imposition of higher strain rate. Consequently, the degree of localized extinctions increases as shown in Fig.3.13 b, in terms of reduction of the burning fraction.

3.2.5. 2-D Curvature

The local flame front curvature illustrates the effect of turbulent flow field on the on wrinkling of the flame sheet and highlights the influence of the flame shape on flamelet burning [70]. The edge of the instantaneous OH-PLIF image conditioned on the occurrence of heat release was considered to mark the flame front. The extracted flame front contour with Cartesian x and y coordinates was parameterized by a path length parameter (s), which denotes the length of the flame front measured from a fixed origin on the contour. For each point along the contour, a 3rd order polynomial, including 9 adjacent contour points, was determined for the x(s) and y(s), parametric contours. Then the local curvature was evaluated using the equation:

$$C = \frac{\dot{x}\ddot{y} - \dot{y}\ddot{x}}{(\dot{x}^2 + \dot{y}^2)^{\frac{3}{2}}} \quad (4)$$

where $\dot{x}$ and $\ddot{x}$ denote the first and second derivatives with respect to *s*, respectively. By convention, the curvature is defined as positive if the flame front is convex towards the reactants. The curvature resolution was limited to ± 5 mm^{-1} based on the thickness of the OH laser sheet.

The pdf of curvature for flames corresponding to the different fuel/air mixtures at mean velocity of 10 m/s and turbulent intensities of 14 and 30% is shown in Fig.3.14 (a) and (b), respectively. The distribution for the near field (2 to 21 mm from the bluff body) and far field (21 to 40 mm from the bluff body) are shown in the first and second column respectively. For moderate turbulence level, the distributions are observed to be approximately Gaussian and symmetrical about zero flame front curvature. The distributions for the higher turbulent conditions are skewed towards positive curvature which shows that at these conditions flames with very high positive curvatures are more likely than those with very high negative curvatures. The occurrence of strong positive wrinkles at intense turbulence conditions indicate higher propensity of generation of flame area as they propagate. For all the fuel/air mixture compositions, the pdfs are observed to become wider for the flame segments in the downstream section relative to the near bluff body region where flame is more constrained and thus, the level of wrinkling increases with distance from the bluff body. At the moderate turbulent condition the distribution is observed to be wider for propane/- and ethylene/air at ϕ=0.655 relative to the methane/air flame in the region near the bluff body. However, at the higher turbulent condition, distributions for these flames become nearly similar with slight variation in their standard deviations. The distribution for ethylene/air flames at ϕ=0.85 for both the turbulent conditions shown in Fig.3.14 is observed to be significantly wider with higher probability of positive curvature wrinkles.

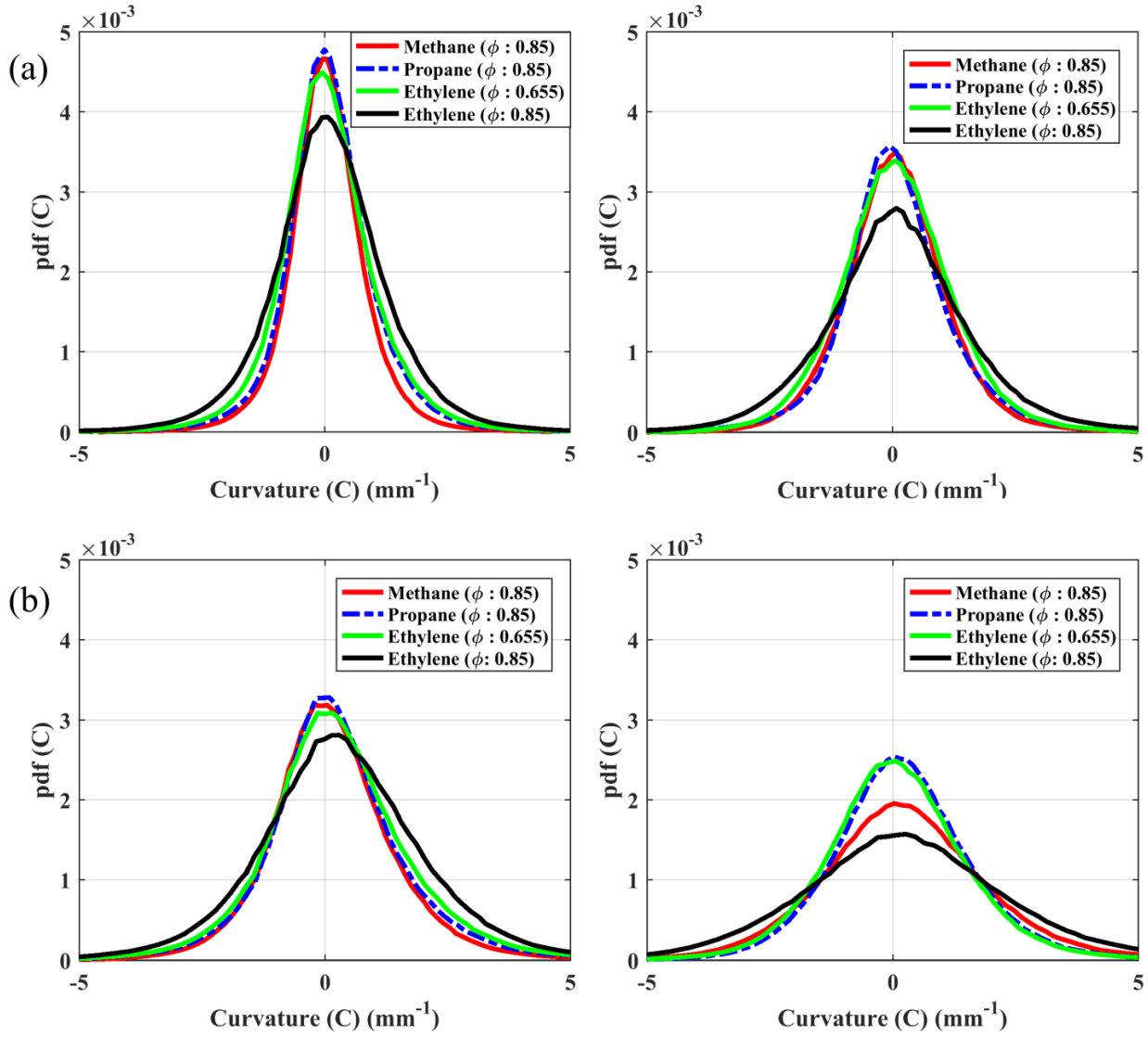

Fig.3.14.Pdfs of 2-D curvature for different fuel/air mixture compositions corresponding to mean velocity of 10 m/s and turbulent intensities of (a) 14 % and (b) 30 %. The first and second column is pdfs of the anchoring and downstream regions respectively.

3.2.6. Flame Brush Thickness

The flame brush thickness is an important parameter describing the average movement of the flame about its mean value and provides an estimate of the region in space where reaction layers are positioned. It is a vital parameter utilized in assesing the accuracy of numerical models [2,4].

For all the tested conditions, brush thickness was evaluated using the mean progress variable ($\bar{c}$) which was determined by averaging the binarized OH-PLIF images. Then the brush thickness was calculated at different axial distances from the bluff body by using the relation [15]:

$$\delta_{t=} \frac{1}{\max(|d\bar{c}/dx|)} \quad (5)$$

The variation of the estimated flame brush thickness for all the experimental conditions is presented in Fig.3.15. For all the fuel/air mixture conditions, it can be clearly seen that free stream turbulence levels significantly influence the flame brush thickness. For low and moderate turbulence conditions, comparison of the flame front structure presented in Fig. 3.2 and Fig.3.3 show that the increase can be attributed to enhanced wrinkling along the flame sheet due to the pronounced formation of unburned mixture fingers. For the intense turbulent conditions, the stronger distortion of the flame front structure which results in the different characteristics can be attributed for the significant increase in the mean flame brush thickness. For the flames corresponding to methane/-, propane/- and ethylene/air at ϕ= 0.655, the flame brush thickness is observed to saturate beyond 24% turbulence intensity with no further increase, as shown in Fig.3.15(c) and (d) and this can be attributed to increased rate of flamelet merging and localized extinctions. This trend agrees with that predicted by the mathematical formulation of Peters [64]. Comparing these results to those in Ref. [15,21] where V-shaped flames were studied using lean premixed mixtures of methane/air, indicates that the trends are similar at low to moderate turbulence intensities (2–17%). The rollover of the brush thickness and departure from the linear increase with downstream distance at higher turbulence intensities have also been observed in these studies. However saturation of the increase of brush thickness with increasing turbulence intensity seen in our data have not been observed, which is most likely due to the lower

turbulence intensities employed in those studies. However, for the ethylene/air flames at ϕ=0.85 higher variation of the flame brush thickness is observed especially at moderate (~14 %) and intense (24 and 30%) turbulent conditions which can be attributed to stronger wrinkling coupled with lower degree of localized extinctions.

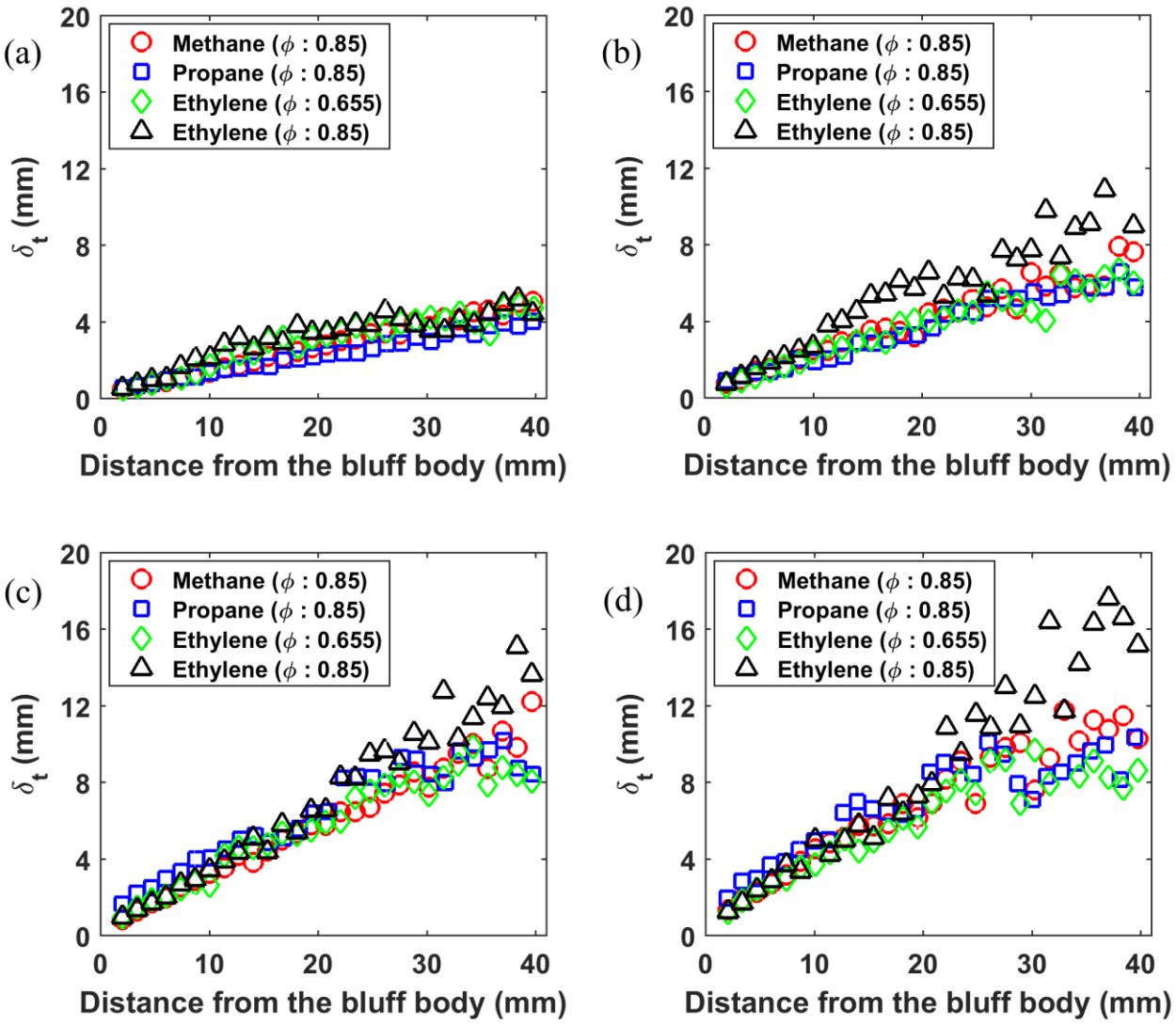

Fig.3.15. Variation of flame brush thickness for U_m=10 m/s and turbulent intensities of (a) 4% (b) 14% (c) 24 % and (d) 30 %.

3.2.7. Flame Surface Density

Flame surface density (FSD) is a measure of the averaged area of the flame surface per unit volume. It describes the effect of wrinkling of the flame front surface and is related to the local consumption speed [2]. In the present work, 2-D FSD was evaluated by the flame length and flame zone area method of Shepherd [5]. In this method, FSD (Σ) is defined in terms of the mean progress variable ($\bar{c}$):

$$\Sigma(\bar{c}) = \frac{L(\bar{c})}{A(\bar{c})} . \frac{1}{n_f} \quad (6)$$

Where $L(\bar{c})$ and $A(\bar{c})$ are the flame length and flame zone area in terms of the mean reaction progress variable and n_f is the number of images used. For estimation of FSD in this work, the mean map of progress variable was divided into 19 sectors with the width of the mean progress variable intervals being 0.05. Following [71], the flame length parameter was estimated by dividing each instantaneous flame front edge obtained from the OH PLIF image into equal segments of 1 pixel length and then superimposed them onto the map of $\bar{c}$. Each segment was then assigned the corresponding $\bar{c}$ value and from the frequency distribution of these values, $L(\bar{c})$ was deduced. The averaged flame length was then calculated by dividing this value with the number of images analyzed for each condition, n_f. Flame zone area, $A(\bar{c})$ was estimated from the frequency distribution of the $\bar{c}$ and the area of each pixel.

The 2-D FSD measurements for all the investigated conditions are shown in Fig.3.16. The first and second columns represent the measurements of FSD for flame segments in the anchoring and downstream regions respectively. For all the flames, the surface density is observed to decrease with increasing turbulence intensity. Similar variation of flame surface density for up to 17 % turbulence intensity has been reported by Kheirkhah and Gülder [16]. Reduction of the FSD

indicates significant increase of flame surface area relative to flame length corresponding to each mean progress variable. Flame surface densities for all cases are observed to decrease in the downstream region compared to the anchoring region.

With increase in the level of free stream turbulence, the flame fronts are observed to have enhanced wrinkling with an increase in the mean volume of the turbulent flame region. The two-dimensional analog to the former parameter refers to an increase in the flame front length as a function of $\bar{c}$, and the two-dimensional analog to the increase in mean volume represents an increase in the flame zone area as a function of $\bar{c}$. It seems that an increase in $A(\bar{c})$ is more pronounced than an increase in $L(\bar{c})$ which results in a decrease of $\Sigma_{,2D}$ with increasing turbulence intensity. For the flames with similar unstrained laminar burning velocity, the FSD measurements are observed to be similar. However, owing to much stronger wrinkling and lower degree of extinction, the ethylene/air (ϕ=0.85) flames have a lower magnitude of two-dimensional FSD.

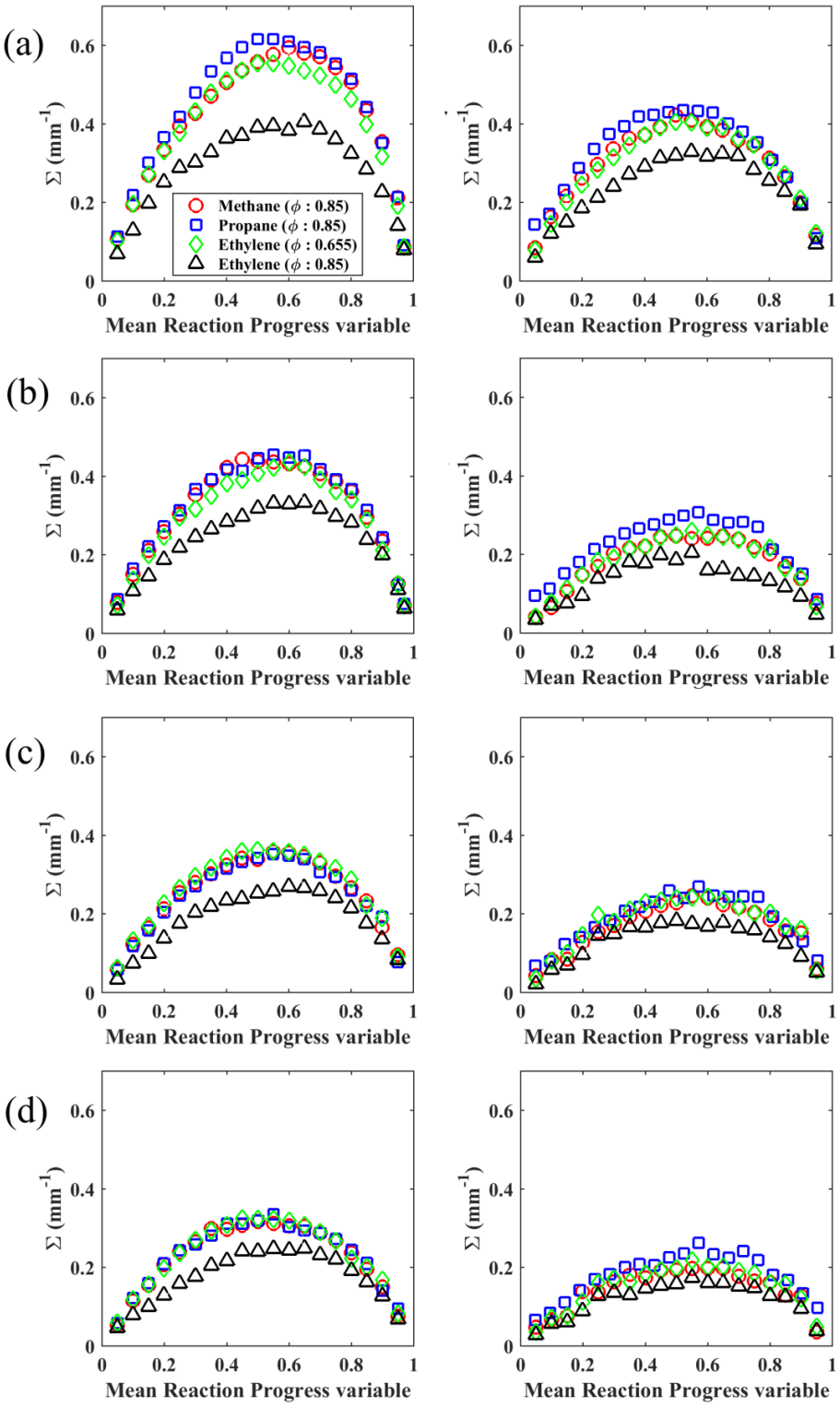

Fig.3.16. Measurements of the flame surface density for U_m=10 m/s and corresponding to turbulent intensities of (a) 4 % (b) 14% (c) 24 % and (d) 30% as a function of mean reaction progress variable ($\bar{c}$)

3.2.8. Ratio of turbulent to laminar flame surface area

Damköhler [72] hypothesized that the main effect of turbulence for flames belonging to the flamelet regime is to wrinkle the thin reaction layers, which retain the local properties of a laminar flame. According to his prediction, the ratio of turbulent to laminar burning velocity (S_T/S_L) is equal to the area ratio (A_T/A_L), where A_T and A_L represent the surface area of wrinkled, turbulent flame and unwrinkled, laminar flame respectively. Following the discussion in Driscoll [2], the local area ratio can be related to flame surface density using the equation:

$$\left(\frac{A_T}{A_L}\right)_L = \int_{-\infty}^{\infty} \Sigma \, d\eta \tag{7}$$

Where η is the axis normal to $\bar{c}$ = 0.5 contour obtained from the averaging the binarized OH PLIF images. To deduce the area ratio by Eq. 7, flame surface density was estimated in spatial coordinates with a procedure similar to the one noted in Ref.[73]. An interrogation box dimension of 0.35 x 0.35 mm was chosen for the FSD computations. The effect of box size on the FSD computation was investigated as discussed in Ref. [59] and it was found that the results were independent of the box size for the chosen values in these computations.

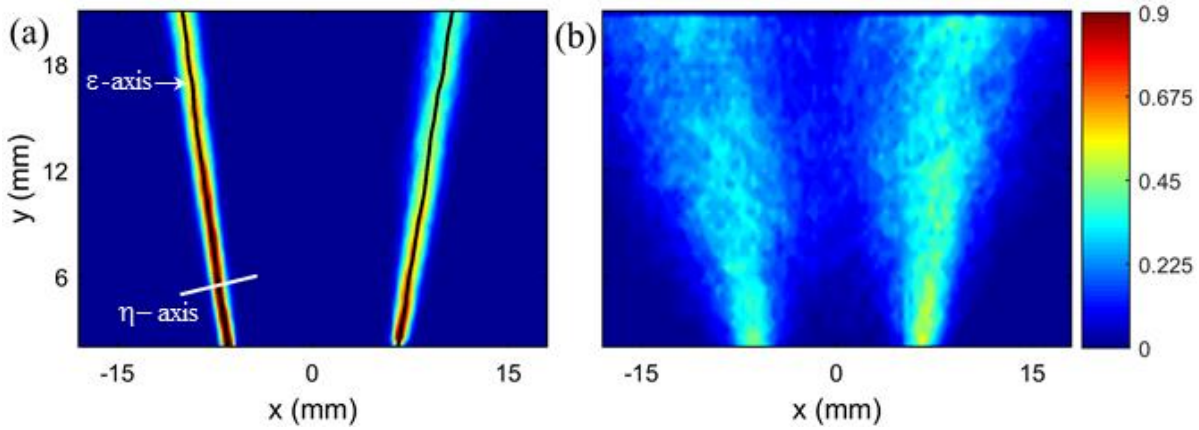

Fig. 3.17. 2D FSD contours for Propane/air flames at U_m = 10 m/s corresponding to (a) T.I : 04 % and (b) T.I : 30%.

In Fig. 3.17, variation of FSD in spatial co-ordinates are shown for propane/air flames corresponding to U_m = 10 m/s and turbulence intensities of 4 and 30%. For the intense turbulent condition, a wider distribution of FSD was observed which broadened further with downstream distance. The broader distribution indicates larger corrugation of the flame due to high level of turbulence as well strong distortion of the flame front. The maximum value of the FSD decreases with downstream distance as the flame brush thickens. Integrating the 2-D FSD along the η−axis as demonstrated by Sattler *et al.* [22], area ratio is obtained for the different cases. The variation of local A_T/A_L for propane/air flames at U_m of 10 m/s and different turbulent intensities are shown in Fig.3.18 at different axial distances from the bluff body. As wrinkling is suppressed by the bluff body; the value of A_T/A_L is close to 1 in its vicinity for all the conditions and then increases with distance from bluff body. At a specific downstream location, flames stabilized in higher turbulent intensity have a higher area ratio. Therefore, based on Damköhler's hypothesis burning velocities of highly turbulent flames are expected to be higher with different burning rates, near and far from the bluff body.

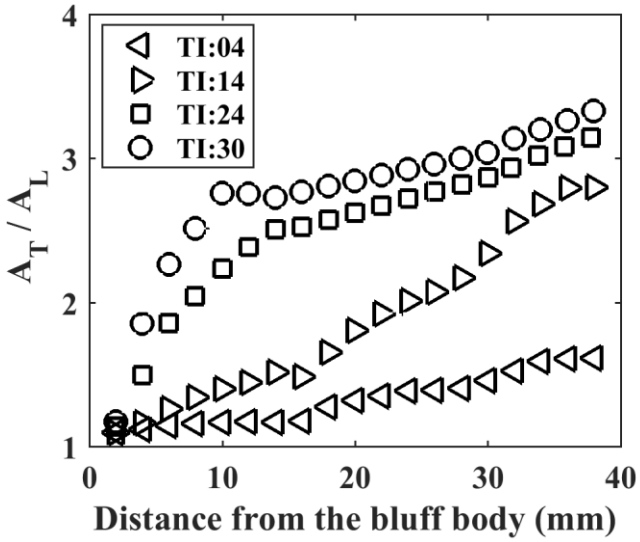

Fig.3.18. Variation of local area ratio for propane/air flames at U_m = 10 m/s subjected to different turbulence levels

To examine the effect of mean velocity and turbulence intensity for the tested conditions, mean area ratio was calculated by using a relation:

$$\frac{\overline{A_T}}{A_L} = \frac{\int_0^l (A_T/A_L)_L \, d\xi}{\int_0^l d\xi} \tag{8}$$

The plot of mean area ratio for all the tested conditions is shown in Fig.3.19. The area ratio is observed to be strongly influenced by the mean velocity of the flow as well as the free stream turbulence level. With increase in turbulence levels, the variation of the mean area ratio exhibits a non-linear behavior. For U_m=10 m/s, growth rate of mean area ratio is observed to decrease for the propane/- and ethylene/air (ϕ= 0.655) flames. However, a steeper increase is observed for the methane/- and ethylene/air (ϕ= 0.85) flames. For U_m=15 m/s, the area ratio for propane/air flames display a non-linear bending behavior owing to the decrease at the highest turbulent condition. The flames corresponding to methane/- and ethylene/air (ϕ= 0.85) exhibit a behavior

similar to that for U_m=10 m/s. The mean area ratio of a turbulent flame is governed by the increase due to enhancement of wrinkling along the flame front while an opposite effect is played by flamelet merging and localized extinctions which reduce the burning area. For, the ethylene/air flames at ϕ=0.85, significant increase in flame front wrinkling was observed from the pdf of curvature, shown in Fig.3.14, while the burning fraction measurements showed that its degree of localized extinctions was the lowest. Hence, the increase of the mean area for this flame is expected. For the propane/- and ethylene/air (ϕ=0.655), the degree of extinctions was observed to increase at the higher turbulent conditions. Therefore, the non-linear bending behavior can be attributed to the occurrence of localized extinctions and fragmentation events which offset the gain in flame area due to wrinkling. Methane/air flames showed a similar variation of the curvature distribution as of propane and ethylene/air (ϕ=0.655) but its burning fraction estimates was higher. Thus, the variation of the mean area ratio for the different fuel/air mixtures agrees with the observations of the instantaneous images shown in Fig. 3.2 - Fig.3.7 as well as the variation of the different statistical parameters.

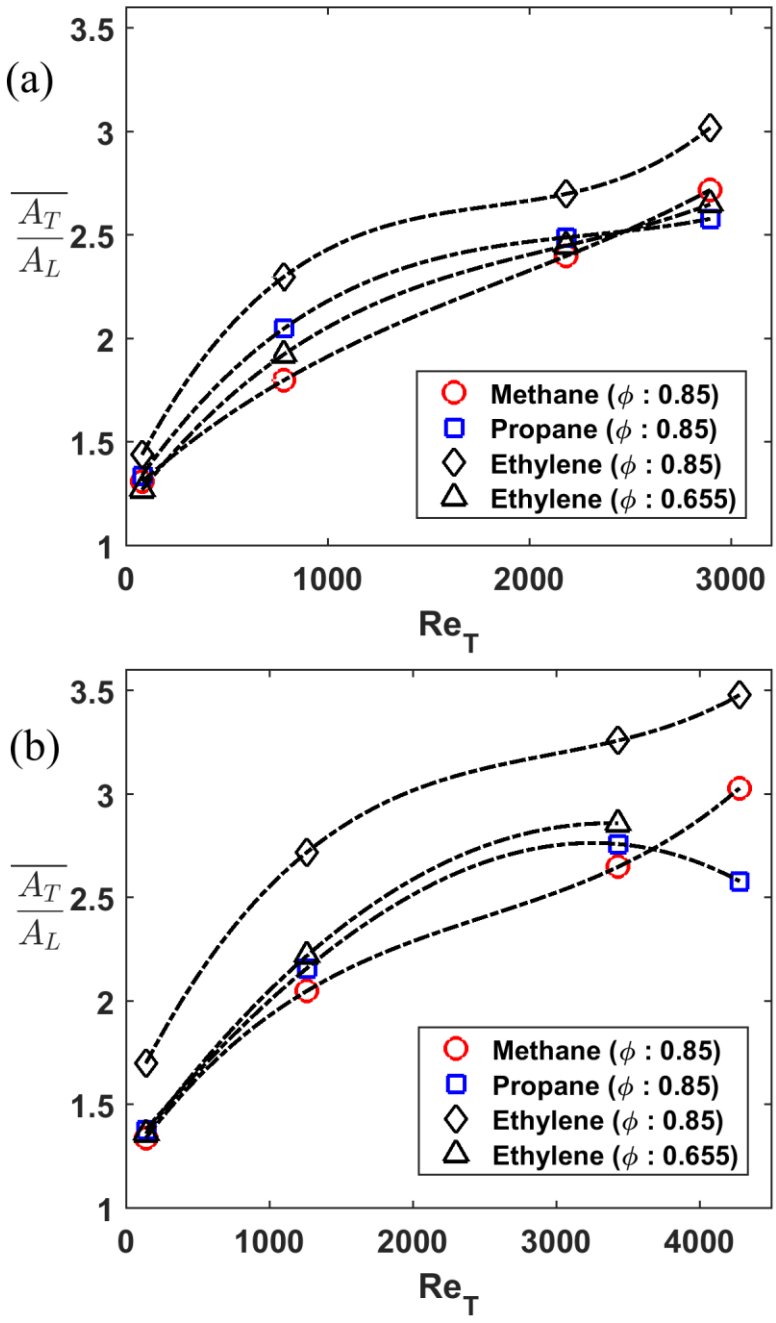

Fig.3.19. Variation of the measured area ratio for the all tested conditions for mean velocity of (a) 10 m/s and (b) 15 m/s

3.2.9. Flame Speed

Flame speed is an important parameter used to characterize turbulent flames. It is one of the parameters used by modelers to validate against experimental data. In this work, turbulent flame speed is presented in terms of displacement speed, which is often used for V-shaped flames [2]. As the V-flame is stationary in the laboratory coordinates, the mean displacement speed has been computed by using the relation:

$$S_{T,D} = U_m \sin \alpha \quad (9)$$

Where U_m is the mean velocity of the reactants and α is the mean half angle of the V-flame. The half angle was determined using a similar method as described in [21]. First, a line was fitted through the isocontour of $\bar{c} = 0.5$ obtained from the averaged binarized OH PLIF images. Subsequently, α was determined as the angle between the line and vertical axis. The mean velocity U_m was determined by spatially averaging the exit velocities along the plane of the bluff body. From the theoretical and experimental results of the past studies, a semi-empirical correlation has been developed for turbulent flame speed and is given by [64]:

$$\frac{S_T}{S_{L,O}} = 1 + C \left(\frac{u'}{S_{L,O}}\right)^n \quad (10)$$

The exponent n is determined by finding the best fit of Eqn. 10 to the experimental data. In the previous studies, different variations of this correlation have been developed to fit the experimental data based on the value of parameter *C*. The parameter C is expected to be a function of turbulent Reynolds number (Re_T) [2,3] or be proportional to integral length scale normalized by the flame thickness [64]. However, as discussed in Driscoll [2], Lipatnikov and Chomiak [4] and Peters [64], the dependency of C on the length scale or Re_t is still not clear

owing to large scatter in the experimental results of the past and no single correlation has been found to collapse all available data.

Displacement speed measured for all the tested conditions is shown in Fig. 3.20 as a function of the normalized velocity fluctuation of the flow, $u'/S_{L,O}$. The turbulent flame speed $S_{T,D}$ increases with increase in normalized velocity fluctuations, $u'/S_{L,O}$. At a fixed normalized turbulence level, flames corresponding to methane/-, propane/- at ϕ=0.85 and ethylene/air at ϕ=0.655, which have close unstrained, laminar burning velocities, their turbulent displacement speeds are found to vary inversely with their respective Lewis numbers. Similar observation has been reported in several experiments in different configurations, as summarized in [2,4]. For each fuel/air mixture, a least-square fit of Eqn.10 to the experimental data gives a best fit correlation where C is a function of turbulence Reynolds number (Re_T) as shown in Fig. 3. **21**. The best fit correlations indicate that both the turbulence levels ($u'/S_{L,O}$) as well as length scales influence the turbulent displacement speed of the bluff body stabilized flames studied in this work.

Utilizing the measured displacement speed data for all the 31 investigated flames; a best fit correlation was deduced of the form:

$$\frac{S_{T,D}}{S_{L,O}} = 1 + 9.8\,Re_T^{-0.11}\,Le^{-0.57}\left(\frac{u'}{S_{L,O}}\right)^{0.53} \qquad (11)$$

The plot of experimental flame speed against the values obtained from Eqn (11) is shown in Fig. 3. 22. The data along the diagonal line indicate perfect match of the correlation to the experimental values. The experimental data could be collapsed using this correlation which represents the best fit. It captures the observation for the effect of integral length scale of the flow field and molecular diffusivity on the displacement speed by the presence of turbulent Reynolds Number and Lewis number, respectively.

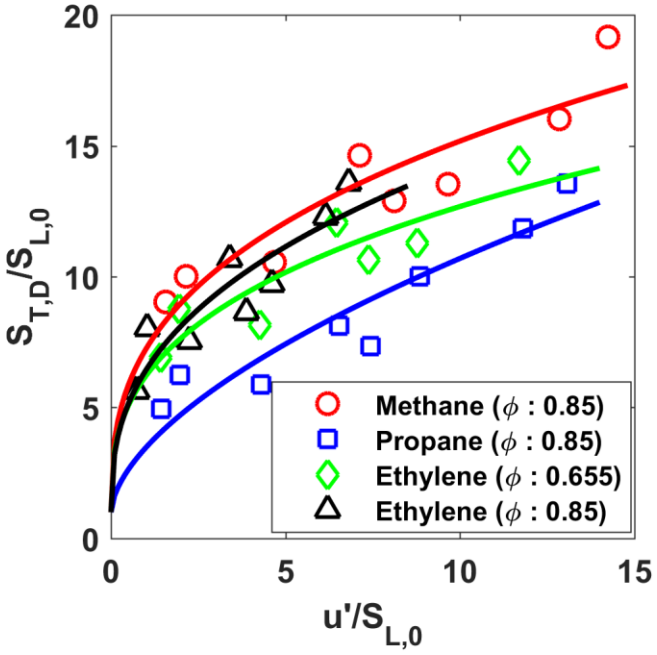

Fig. 3.20. Variation of normalized turbulent displacement speed as a function of the normalized velocity fluctuation of the flow for the tested conditions

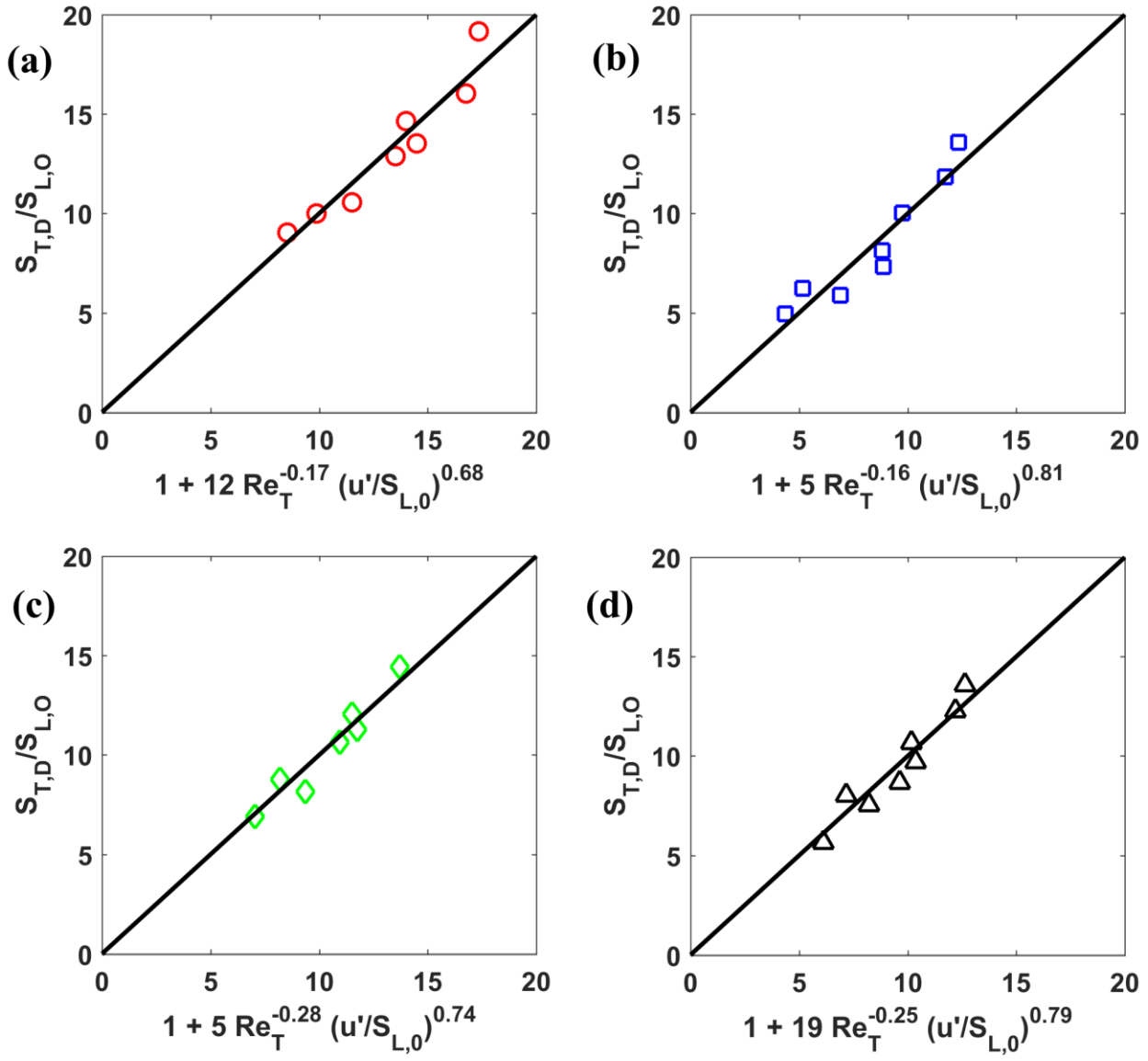

Fig. 3. 21. Best fit correlation of the normalized turbulent flame speed for (a) Methane/air (R^2 = 0.91) (b) Propane/air (R^2 = 0.9) (c) Ethylene/air (ϕ=0.655) (R^2 = 0.92) and (d) Ethylene/air (ϕ=0.85) (R^2 = 0.92).

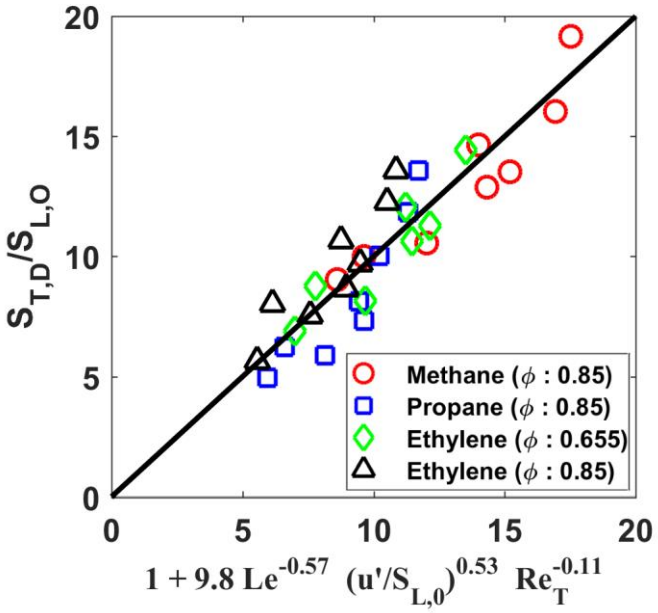

Fig. 3. 22. Normalized turbulent displacement speed as a function of the best fit (R^2 = 0.89)

3.3 Summary

In this chapter, the effect of fuel properties and different levels of turbulence intensities on the flame structure was investigated by simultaneous OH PLIF, CH_2O PLIF and PIV. The flame front structure was observed to be strongly dependent on the free stream turbulence level of the incoming fuel/air mixture as well on the properties of the fuel/air mixture. Formation of cusps and unburnt mixture fingers were observed as the turbulence intensity was increased from 4 to 14 % but, the heat release region remained continuous. For the intense turbulence conditions, different characteristics of the flame front were observed which strongly depended on the properties of fuel/air mixture. For methane/- and ethylene/air (ϕ=0.85), localized extinctions along the flame sheet and flamelet merging were observed which created isolated pockets of reactants in the flame envelope with heat release regions along their boundary. In addition to these features, propane/- and ethylene/air (ϕ=0.655) flames exhibited the occurrence of flame fragmentation events which created multiple islands of OH filled regions separated by thick

layers of CH_2O. The overall flame shape for these conditions was observed to change intermittently from symmetric to asymmetric mode with increasing turbulence intensity. The strain rate pdfs showed that flames under highly turbulent conditions experienced larger strain rates which lead to localized extinction zones along the flame surface. The degree of localized extinctions has been quantified by burning fraction measurements which were found to be highest for lean propane/air flames and least for ethylene/air flames at ϕ=0.85. Enhanced wrinkling along with modification of the flame fronts resulted in broadening of the curvature pdfs. The brush thickness increased with increasing turbulence intensity but for methane/-, propane/- and ethylene/air (ϕ=0.655) saturated beyond 24 % while the two-dimensional flame surface density decreased for all the investigated conditions. As turbulence intensity was increased, the mean flame surface area ratio was observed to grow and eventually result in a non-linear behavior owing to merging, extinction and fragmentation events. Turbulent flame speed was computed based on the mean flame structure and their correlation revealed the dependency of molecular diffusivity and flow straining.

CHAPTER FOUR

4. Effects of free stream flow turbulence on blowoff characteristics

Introduction

The lean blowoff limits are strongly governed by the characteristics of the inlet flow as well by the properties of the fuel/air mixture. In this chapter, the effect of different levels of free stream turbulence (turbulence intensity varying from ~ 4 to 30%) on flame blowoff phenomenon of lean, turbulent and nominally axisymmetric propane-air flames will be discussed. In chapter 3, it was shown that the presence of different levels of turbulence in the flow can strongly modify the flame front structure. It will be shown in this chapter that the free stream turbulence can also affect the lean blowoff limits. Therefore, a systematic study of bluff-body stabilized flame near blowoff conditions under different free stream turbulence levels has been performed. Detailed study of the flame/flow interaction at conditions close to blowoff has been performed by simultaneous OH PLIF, CH_2O PLIF and particle image velocimetry (PIV) to examine the underlying physics. Measurements of strain rate and curvature statistics, burning fraction, asymmetric index and the average duration of the extinction event have been obtained for a range of experimental test conditions. The experimental conditions are discussed in the next section, followed by a discussion of the results and a summary of the important conclusions.

4.1 Experimental conditions

Lean premixed mixture of propane and air at room temperature has been used. The flame blowoff equivalence ratios were determined for three mean velocities of 5, 10 and 15 m/s. For each mean streamwise exit velocity, turbulence intensities of 4, 14, 24 and 30% have been studied. The simultaneous OH PLIF, CH_2O PLIF and PIV has been applied primarily to the

flames corresponding to the mean velocities of 5 and 10 m/s subjected to the different free stream turbulent conditions. To study the dynamics of the flames near blowoff for each inlet condition, the measurements were first performed at two equivalence ratios representing near blowoff conditions – equivalence ratios 0.05 and 0.02 above the blowoff equivalence ratio for the given condition. These flames spanned the regimes of wrinkled flames, corrugated flames and thin reaction zones in Borghi's regime diagram [12], as shown in Fig. 4.1. For normalization in the Borghi diagram, unstrained laminar flame speed and thickness values were computed using the PREMIX code [48] and the propane-air mechanism of Wang *et al.* [49]. The unstretched laminar flame thickness (δ_f) was defined as the temperature difference across a laminar flame divided by the maximum temperature gradient.

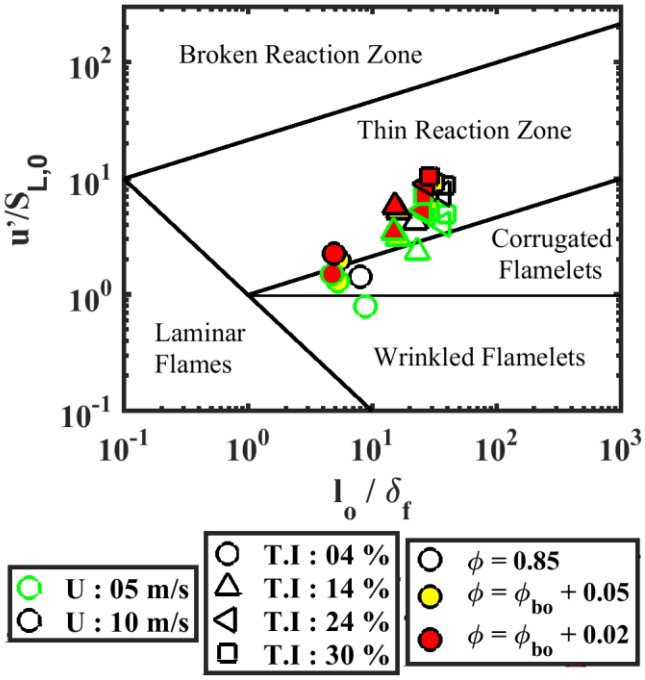

Fig. 4.1. Experimental conditions studied by laser diagnostics overlaid on the premixed combustion regime diagram

4.2 Results and Discussion

In this section, results of the experiments are presented and discussed. The variation of the blowoff equivalence ratio for the different turbulent conditions is presented in Section 4.2.1 followed by the results of simultaneous OH, CH_2O PLIF and PIV for the flames at conditions near blowoff.

4.2.1. Flame blowoff characteristics

Blowoff equivalence ratios of the lean, conical flames at different mean velocities and free stream turbulence levels were measured by determining the equivalence ratio at the point of rapid reduction of the PMT signal from the flame base. Determination of the blowoff point is unambiguous owing to the fully automated approach in which the mixture equivalence is reduced gradually from the stably burning condition (ϕ=0.85) to the point of flame blowoff with simultaneous monitoring of the CH* emission using the PMT detector. The change in the mass-flow rate and mean velocity due to reduction of the fuel flow rate as the blowoff is approached was estimated to be less than 2% for all the investigated conditions.

The variation of the blowoff equivalence ratios for the different experimental conditions is shown in Fig. 4.2. The flame blowoff equivalence ratios were determined at least thrice for each experimental condition to ensure their repeatability. For the approach velocity of 5 m/s, the blowoff equivalence ratio was observed to increase with increasing levels of free stream turbulence, with a maximum increase of about 15% at 24% turbulence intensity. However, with further increase in turbulence intensity to 30%, the flame regained some stability and blowoff equivalence ratio underwent a reduction by about 7% relative to the 24% turbulence intensity condition. This result aside from being interesting, is an example of how free stream turbulence

can influence the flame blowoff in an an unexpected manner at this particular condition. This flow condition will be futher interrogated later in the chapter in the context of the PLIF/PIV images. For the approach velocities of 10 and 15 m/s, the blowoff equivalence ratio was found to increase with increasing free stream turbulence intensity. Typical increase in the blowoff equivalence ratio from low (4%) to highest (30%) turbulence condition is 17% and 20 % for the 10 and 15 m/s cases respectively. Apart from the condition of 5 m/s approach velocity at a turbulence intensity of 30 %, increasing turbulence intensity was found to reduce the flame stability (i.e. increase flame blowoff equivalence ratio).

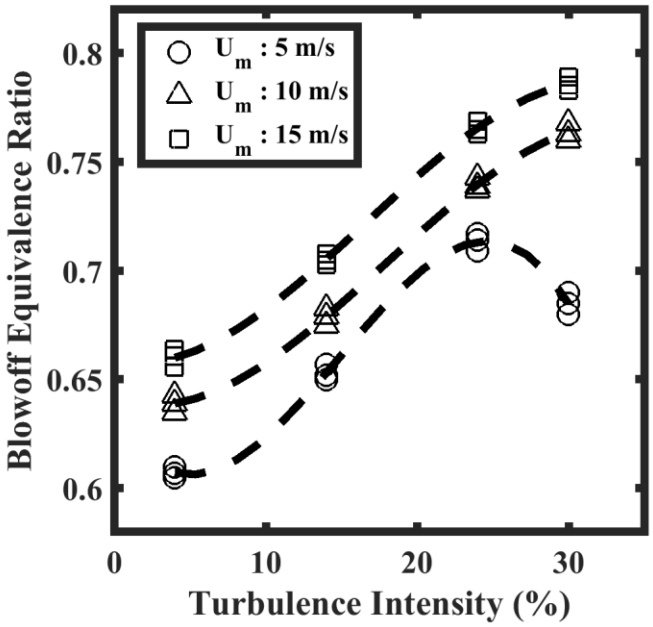

Fig. 4.2. Variation of the blowoff equivalence ratio for mean approach velocities of 5, 10 and 15 m/s. Three repeated experimental results are shown in each case.

4.2.2. Variation of the recirculation zone length

Before proceeding with the discussion on the flame front topology, it is worth examining the effect of different levels of free stream turbulence on the recirculation zone structure as it plays a

pivotal role in stabilizing the flame. The effect of different levels of free stream turbulence on the mean streamwise length of the recirculation zone normalized by the bluff-body diameter is shown in Fig. 4.3. The recirculation zone length was determined as the axial location along the center of the bluff-body flame holder where the mean streamwise velocity changes from negative to positive. With increase in turbulent intensity, the length of the recirculation zone is observed to decrease significantly. Similar observation has been reported by Pan *et al.* [74] and the variation has been attributed to increase in turbulent burning velocity. As blowoff is approached, shortening of the recirculation zone is observed due to lower dilatation.

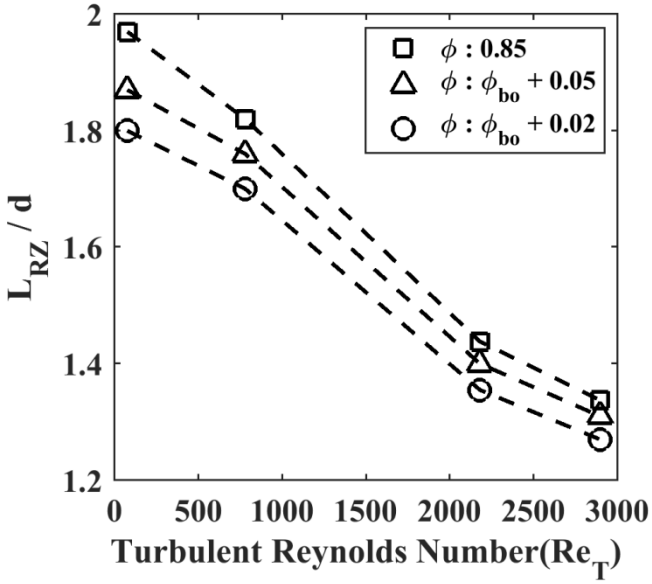

Fig. 4.3. Variation of the mean recirculation zone for the different flames investigated corresponding to mean velocity of 10 m/s.

4.2.3. Flame front topology

The flame front topology is strongly dependent on the free stream turbulence intensity of the incoming mixture as had been discussed in the previous chapter. Instantaneous PLIF images for

stably burning lean propane/air flames at different turbulence intensities are shown in Fig. 4.4 to elucidate the difference in the flame structure as blowoff is approached. For all the conditions studied at $\phi = 0.85$, overlaying the heat release regions on the vorticity field showed that the flame sheet predominantly lies outside the high vorticity regions of the shear layer, except in the cases where the flame shape changes from varicose to sinuous mode at high turbulence levels.

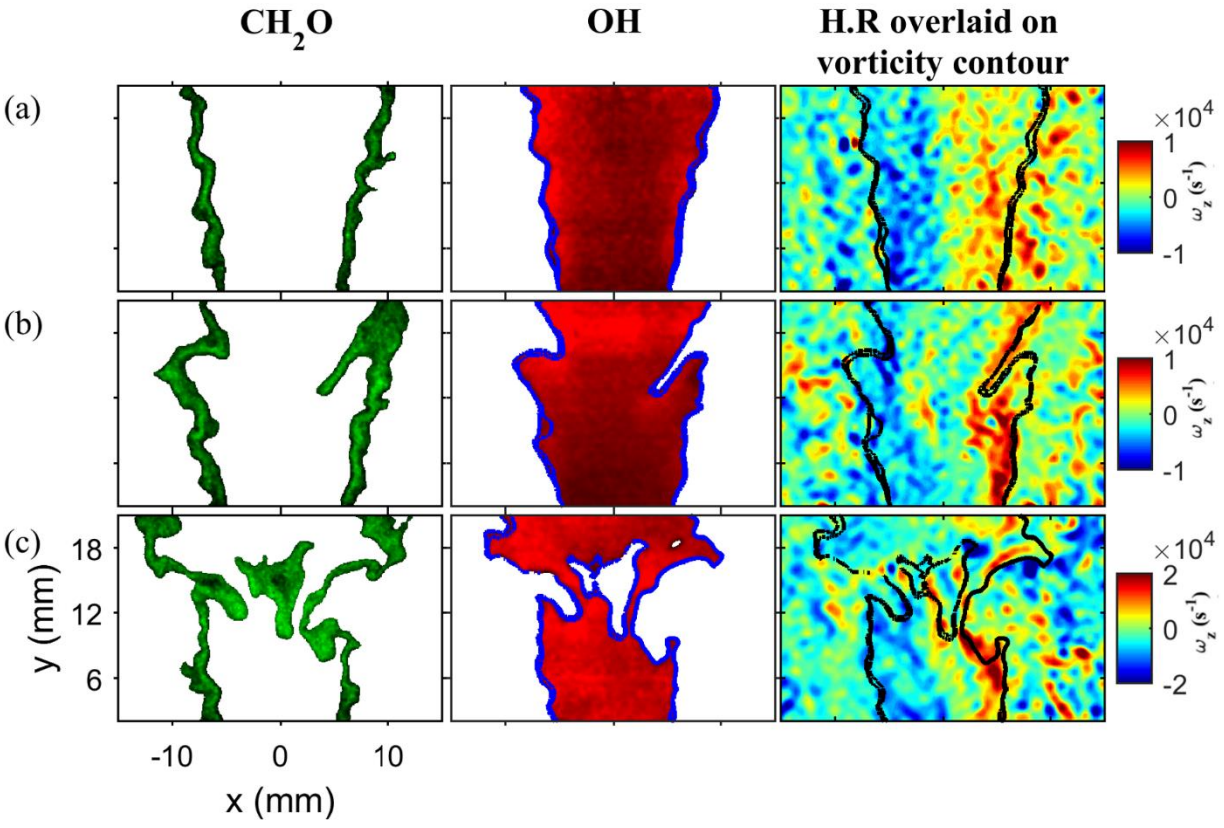

Fig. 4.4. Instantaneous images of CH_2O PLIF, OH PLIF and heat release region overlaid on the vorticity contours for mean velocity of 10 m/s and corresponding to (a) low turbulence (4%) (b) moderate turbulence (14%) and (c) intense turbulence (30%).

To investigate the flame structure close to blowoff, simultaneous PLIF imaging and PIV has been performed at two equivalence ratios – 0.05 and 0.02 above the corresponding blowoff

equivalence ratio for each case. Instantaneous images for mean velocity of 10 m/s and low (4%), moderate (14%) and intense (30%) turbulent conditions at equivalence ratios 0.05 above the corresponding blowoff equivalence ratios are shown in Fig. 4.5. As blowoff is approached, the flame speed decreases due to reduction of the equivalence ratio. Therefore, the flame front moves inward to maintain kinematic balance with the incoming fuel-air mixture. It is observed that the flame becomes narrower in shape with more corrugated edges and the flame front moves into the high vorticity regions of the shear layer. In these regions, flame fronts are subjected to higher aerodynamic strain rates as will be further discussed later in the chapter. For the low and moderate turbulent intensity conditions, localized extinctions are observed along the shear layer as can be seen by the breaks along the overlapping regions of OH and CH_2O in Fig. 4.5(a) and (b), respectively. For the intense turbulent condition, the breaks along the heat release region are observed to increase in frequency and size as shown in Fig. 4.5(c). This provides multiple channels for penetration of reactants into the recirculation zone and mix with the hot combustion products residing in the recirculation zone. In most cases, regions void of OH within the recirculation zone are filled with CH_2O. Heat release is observed to occur along the boundary of the isolated pockets of CH_2O where the preheated and partially reacted gases come in contact with hot combustion products. Also, at the intensely turbulent conditions, pronounced formation of cusps are observed particularly near the bluff-body as shown in Fig. 4.5 (c) for the right wing of the flame where the flame front is observed to be wrapped around a vortical structure. As the equivalence ratio is reduced, the magnitude of the flame generated baroclinic vorticity also decreases owing to the decreasing density jump across the flame. Also, the vorticity damping term due to flow dilatation decreases. Both of these effects result in a higher magnitude of bluff-body generated vorticity as compared to the low turbulence, robustly burning flames [34]. This

higher magnitude of shear generated vorticity leads to stronger interaction with the flame sheet leading to (i) asymmetric global flame structure (sinuous flame shape as compared to more varicose shape at lower turbulence, higher equivalence ratio conditions); (ii) formation of flame front structures with negative and large values of curvature near the attachment point.

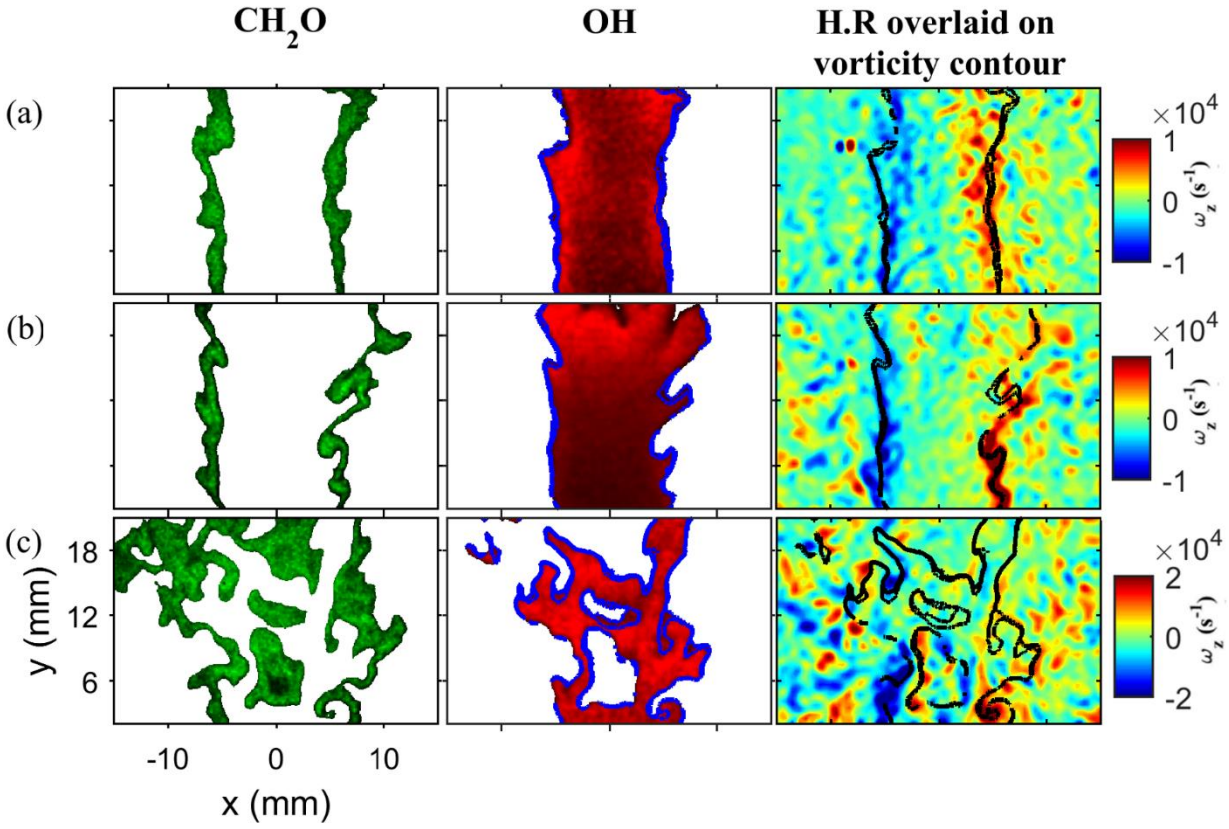

Fig. 4.5. Instantaneous images of CH_2O PLIF, OH PLIF and heat release region overlaid on the vorticity contours for mean velocity of 10 m/s and corresponding to (a) low turbulence (4%) at ϕ=0.69 (b) moderate turbulence (14%) at ϕ=0.73 and (c) intense turbulence (30%) at ϕ=0.81.

For flames closest to blowoff, at an equivalence ratio 0.02 above the corresponding blowoff equivalence ratio, as shown in Fig. 4.6, greater changes are observed in both the OH and CH_2O PLIF signals. Significant localized extinctions are observed along the shear layer for all the

flames investigated at this condition. For the lower turbulent intensity condition (4%), breaks along the heat release regions are observed to increase in frequency and size, particularly at the downstream parts of the recirculation zone which are in the vicinity of the recirculation zone closure point as shown in Fig. 4.6(a). For moderate turbulent intensity (14%), it is observed that local extinction and disintegration of the flame has intensified. At this condition, the flame is occasionally observed to recede to the tip of the recirculation zone. Thicker regions of CH_2O are observed near the closure point of the recirculation zone. To illustrate this, the instantaneous recirculation zone represented by the contour of $U_y = 0$ is shown by the dashed red lines on the velocity field data in Fig. 4.6(b) and the heat release regions are overlaid on the velocity field. Thin reaction zones are observed along its boundary, importantly along the reattachment point. Similar observation of retreatment of the flame front at conditions close to blowoff had been reported by Chaudhuri *et al.* [35]. Under favorable flow residence times, the shear layer is able to re-ignite and the flame is observed to survive at this condition. The laminar flame simulations show only a minor increase in the width of the CH_2O profile as ϕ was reduced from 0.85 to 0.70. The wide regions of CH_2O observed near the end of the recirculation zone in this case are therefore not likely to result from widening of the CH_2O profile across the flame front, but indicate the presence of preheated reactants or partially burned gases.

For the intense turbulence condition, significant fragmentation of the flame and localized extinctions are observed which provides channels for penetration of reactants into the recirculation zone as shown in Fig. 4.6(c). The instantaneous recirculation zone is marked by the red dashed lines on the velocity field. The region marked by the box shows an instance of break in the flame front along shear layer. The velocity vectors in the vicinity of the flame hole indicate the movement of preheated reactants / partially burned gases into the recirculation zone which

lowers the temperature of the hot product gases that reside there and play an important role in flame stabilization. Also, the occurrence of flame fragmentation further weakens the stabilization process. Fig. 4.6(c) shows that the flame has disintegrated into fragments - bottom flame segment which is anchored on the flame holder while the other flame segment represented by the island of OH filled region is observed downstream. There may be two likely scenarios leading to this type of flame structure. (1) significant localized extinction along the flame sheets through which the reactants enter all the way to the central part of the flame and heat-up there (formaldehyde signal region) and/or (2) flame pinching events resulting in fragmentation of the flame. The exact mechanism for the occurrence of this phenomenon is still speculative and is a subject of active research. Of interest is the bottom flame fragment, where breaks along the heat release region are observed in the segment within the recirculation zone and velocity vectors indicate the movement of reactants from the top of the recirculation zone. To enable a better visualization of these events, velocity vectors have been overlaid on the CH_2O PLIF image as shown in Fig. 4.7, with the boundaries of the reaction zone and instantaneous recirculation zone marked by thick blue and red (dashed) line respectively. However, the flame can re-ignite in the shear layers which enable it to survive at this condition through a series of extinction/re-ignition events.

For the approach velocity of 5 m/s, similar behavior is observed for the low and moderate turbulent intensity conditions. For the 24% turbulence intensity condition, at conditions close to blowoff the flame front is observed to predominantly lie on the high vorticity regions of the shear layer as shown in Fig. 4.8(a). As the turbulence intensity is increased to 30%, the flame front shows a strongly intermittent behavior with respect to its location in relation to the shear layer at conditions close to blowoff as shown in Fig. 4.8(b) and Fig. 4.8(c). Under certain conditions the

flame becomes columnar in shape with the reaction zone overlapping with the high vorticity regions of the shear layer as shown in Fig. 4.8(b) while occasionally the flame shape becomes wider with the reaction zone positioning itself outside the highly strained region as shown in Fig. 4.8(c). Such strongly intermittent behavior has not been observed for the approach velocity of 10 m/s at 24 and 30% turbulent intensity conditions. This behavior can be attributed to higher mixing rate and favorable flow residence time scale relative to the mean velocity of 10 m/s, which enables in re-igniting the locally extinguished regions along the flame sheet and propagation of the flame front. This peculiar behavior observed at 5 m/s, 30% turbulence intensity condition is also supported by the burning fraction measurements discussed later. However, explanation of this behavior is somewhat speculative based on the analysis of the PLIF/PIV data. Application of detailed time resolved diagnostics will enable better understanding of this behavior.

These instantaneous images of the flame structure at conditions close to blowoff clearly illustrate the advantage of simultaneous PLIF imaging of OH and CH_2O along with PIV as it provides a much more comprehensive visualization of the localized extinctions along the flame sheet and the pathways for entrainment of the reactants into the recirculation zone.

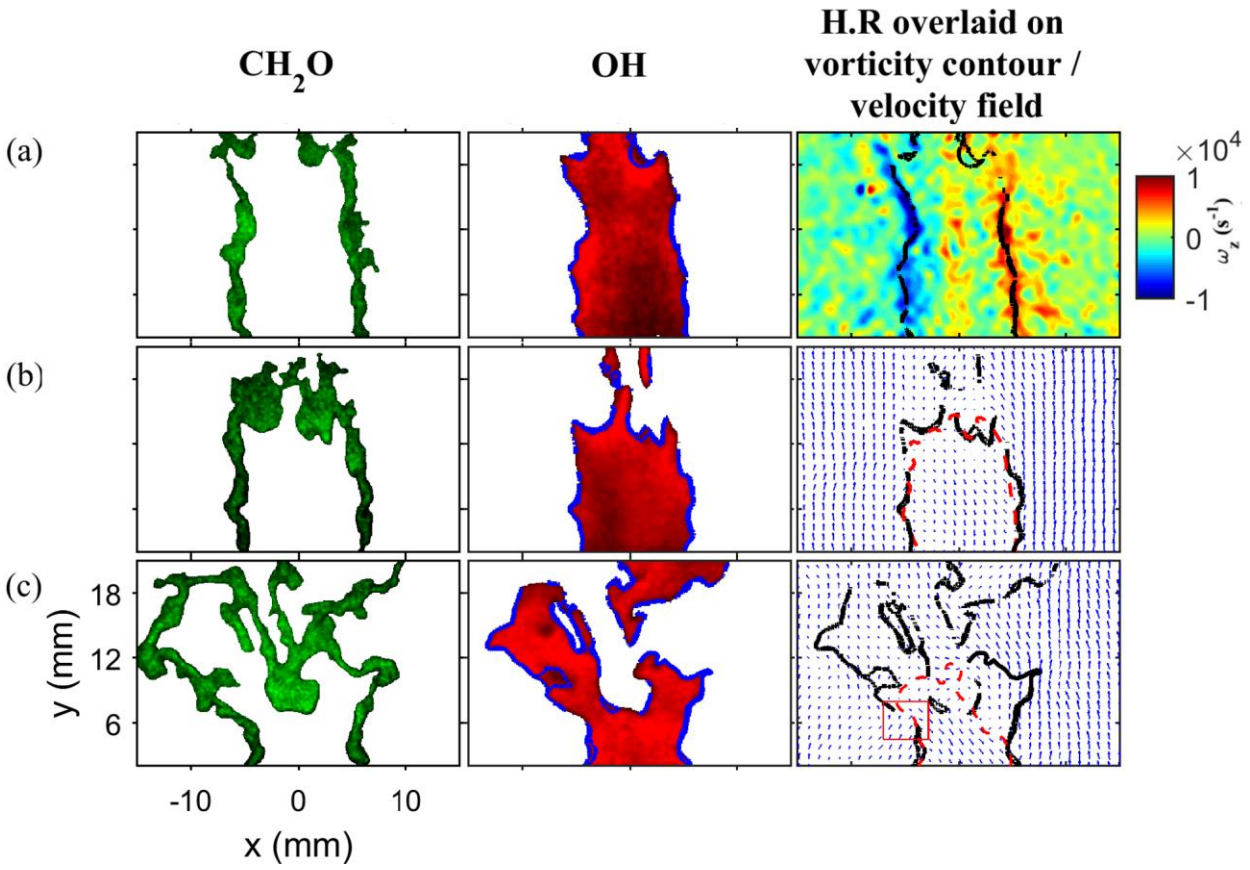

Fig. 4.6. Instantaneous images of CH_2O PLIF, OH PLIF and heat release region overlaid on the vorticity contours / velocity field for mean velocity of 10 m/s and corresponding to (a) low turbulence (4%) at ϕ=0.66 (b) moderate turbulence (14%) at ϕ=0.70 and (c) intense turbulence (30%) at ϕ=0.78

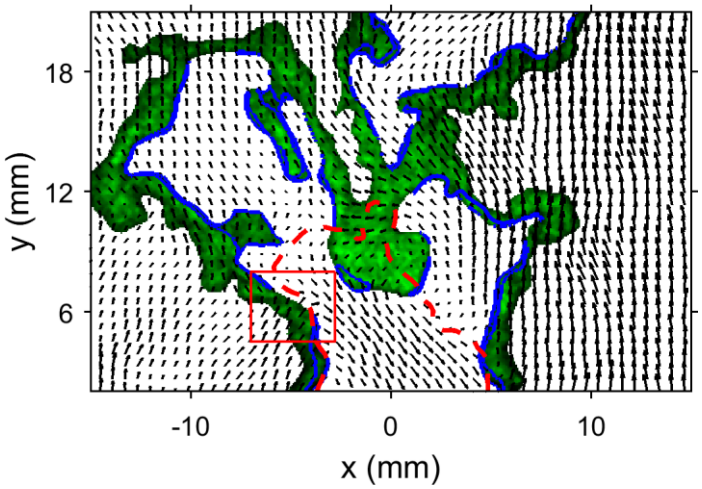

Fig. 4.7. Velocity vectors overlaid on the CH_2O PLIF image

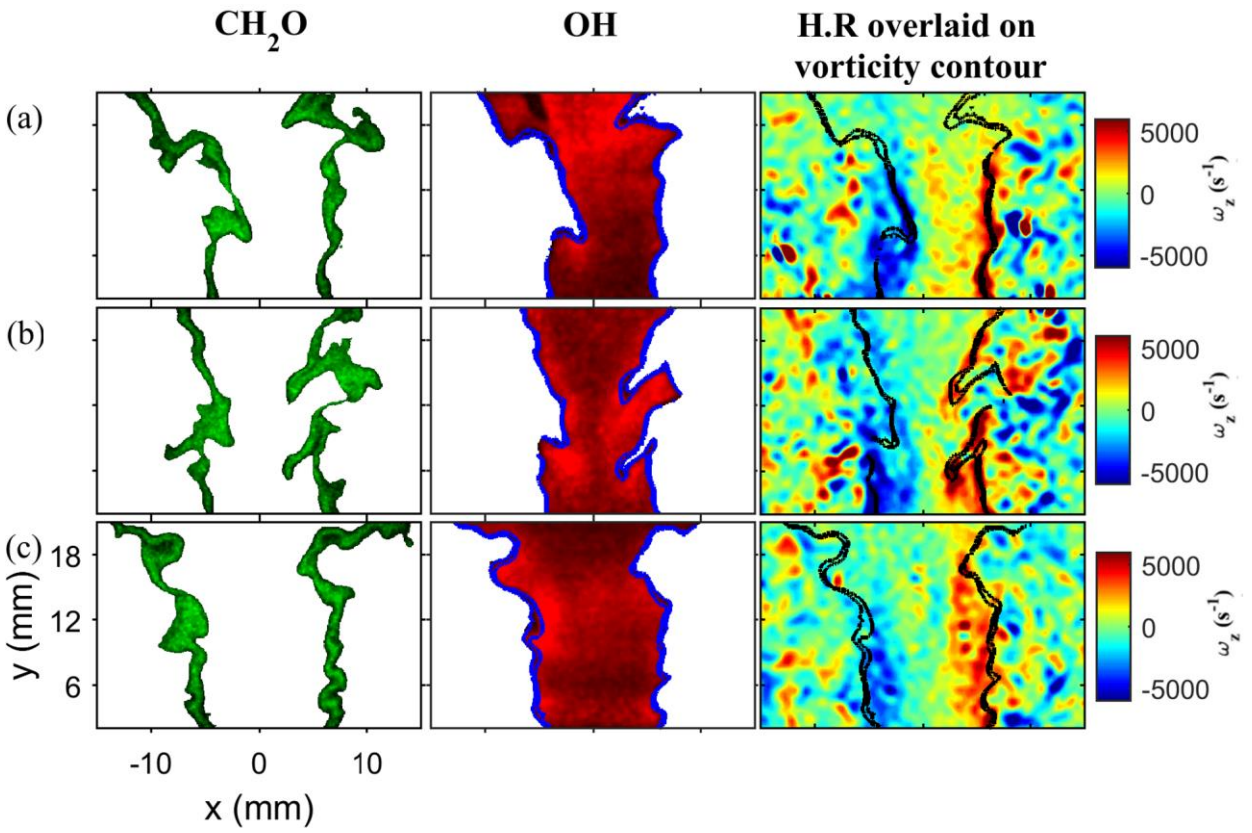

Fig. 4.8. Instantaneous images of CH_2O PLIF, OH PLIF and heat release region overlaid on the vorticity contours / velocity field for mean velocity of 5 m/s and corresponding to (a) T.I: 24% at ϕ=0.76, (b) T.I: 30% at ϕ=0.73 showing the overlapping of the reaction zones with the shear layer vortices and (c) T.I: 30% at ϕ=0.73 showing the movement of the flame front away from the high vorticity regions.

4.2.4. 2-D Estimates of strain rate

From the instantaneous PLIF images discussed in the previous section, it is clear that the frequency of localized extinction along the shear layers intensifies as flame blowoff is approached. The cause for this can be examined using the strain rate measurements. The two - dimensional hydrodynamic strain rate has been computed in a similar manner as outlined in Section 3.2.3.

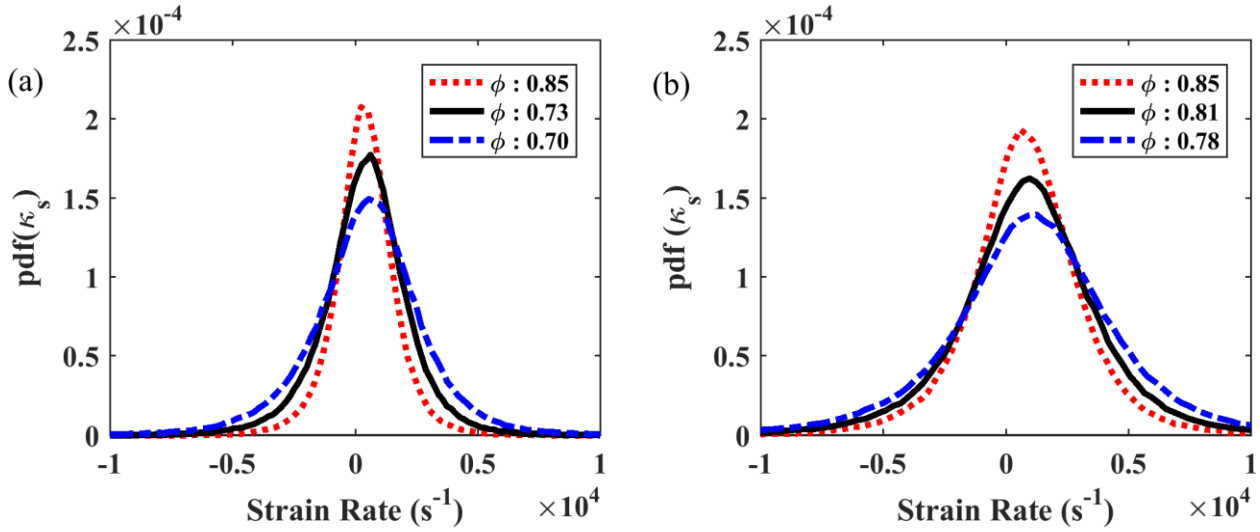

Fig. 4.9. Probability distribution functions of the 2D strain rates for mean velocity of 10 m/s corresponding to turbulent intensities of (a) 14% and (b) 30%.

The pdfs of the hydrodynamic stretch rate for the mean velocity of 10 m/s for moderate and high turbulence intensities at conditions of robustly burning as well as near blowoff conditions are shown in Fig. 4.9. For both of the cases, it is clearly observed that as blowoff is approached the strain rate pdfs become wider. This can be attributed to two possible reasons: (i) Under the robustly burning condition, the flame fronts represented by the thin heat release regions were observed to envelope the higher vorticity regions of the shear layer. As blowoff is approached, the flame front migrates into the higher vorticity regions and experiences higher strains; (ii) As the equivalence ratio decreases, the flame segment in the near field of the bluff-body experiences higher vorticity magnitudes due to reduction of the flame generated baroclinic vorticity and the vorticity damping term which play an important role in reducing the shear generated vorticity in the near field. This has been demonstrated in the work of Nair and Lieuwen [34] by estimating the average vorticity along a flame segment by sequentially reducing the equivalence ratio to approach blowoff. Therefore, the flame segments in the vicinity of the anchoring point

experience higher hydrodynamic strain as blowoff is approached. Also, as blowoff is approached the strain rate distributions are observed to be skewed towards positive values with increasing mean strain rate values. The increase in extensional strain rate results in creating holes along the flame sheet.

As expected, the pdfs are observed to become wider with increasing turbulence intensities. Past experimental work of Filatyev *et al.* [59] and DNS analysis of flame-vortex interaction of Meneveau and Poinsot [66], have demonstrated the stretch efficiency factor to increase as the square of the integral length scale. This indicated that large eddies present in the flow are more efficient at stretching the flame than small eddies. In the present work, the integral length scale was found to increase with increasing free stream turbulence level of the incoming fuel-air mixture and therefore, the widening of the strain rates pdfs with increasing turbulence intensity is reasonable and consistent with previous studies.

4.2.5. Burning fraction measurements

In order to evaluate the degree of local extinctions at the investigated conditions, the burning fraction of the flames were estimated by the algorithm outlined in Section 3.2.4. The variation of the burning fraction for the different cases corresponding to mean velocity of 10 m/s is shown in Fig. 4.10(a). For the robustly burning flames stabilized at an equivalence ratio of 0.85, a clear decrease in the burning fraction is observed with increase in the free stream turbulence levels. The variation of the pdfs of the strain rate shown in Fig. 4.9 illustrate that the flames stabilized in intensely turbulent conditions (24 and 30%) are subjected to higher magnitudes of strain rates. As blowoff is approached, the burning fraction is observed to decrease for all the cases. The flames near blowoff are subjected to higher strain rates relative to the stably burning flames at the corresponding flow conditions. Furthermore, the near blowoff flame is also more vulnerable

to strain, as extinction strain rate decreases with reduction of the equivalence ratio [75,76]. This is apparently the reason for the appearance of local points of extinctions along the flame sheet for the near blowoff flames at low and moderate turbulent intensity conditions and increase in frequency and size of breaks along the reaction zone for the intensely turbulent conditions as discussed in Section 4.2.3 and quantitatively, shown by the variation of the burning fraction.

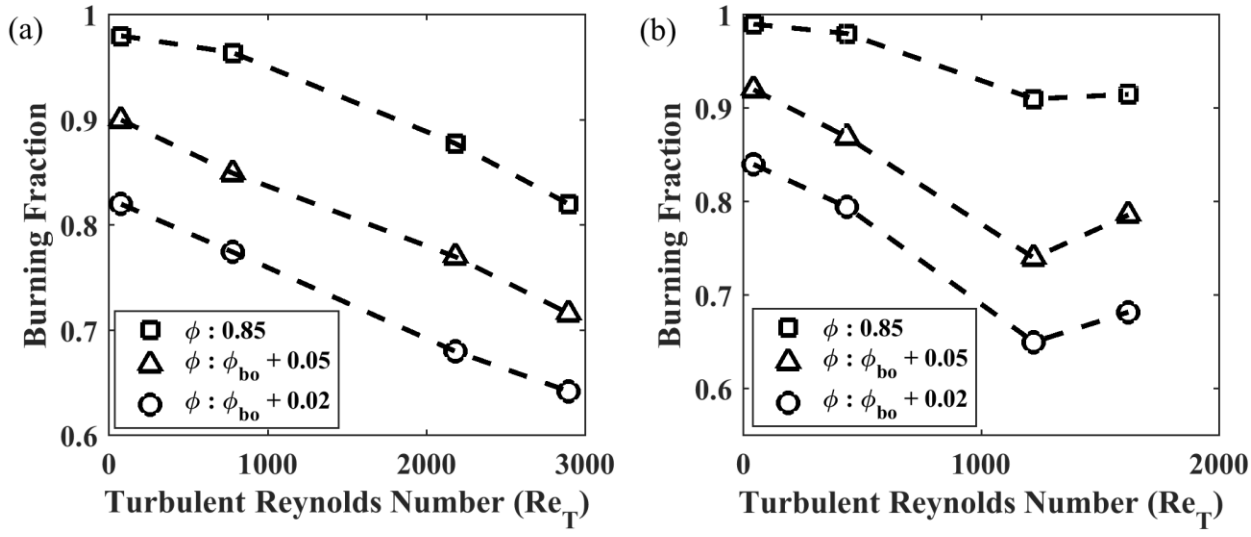

Fig. 4.10. Estimates of the burning fraction for mean velocity of (a) 10 m/s and (b) 5 m/s corresponding to different turbulent conditions for flames away and near blowoff.

The variation of burning fraction for the different cases corresponding to approach velocity of 5 m/s is shown in Fig. 4.10b. For the robustly burning flame, the burning fraction decreases as turbulence intensity is increased from 4 to 24%. No significant difference is observed as the turbulence intensity of the approach flow is increased to 30%. As expected, the burning fraction is observed to decrease for all the cases as blowoff is approached. However, at conditions near blowoff the burning fraction for the turbulent intensity of 24% is observed to be lower than that of the 30% condition. This behavior can be attributed to the observation that for the turbulent

intensity of 24%, the flame front predominantly overlapped with the high vorticity region of the shear layer. Therefore, the flame is subjected to higher strain rate for a significant duration which makes it more susceptible to localized extinction along the flame sheet. However, for turbulence intensity of 30%, as the flame front has an intermittent behavior with respect to the highly strained region of the shear layer, it is less susceptible to localized extinctions as illustrated by the relatively higher burning fraction. The variation of the flame front position and measurements of burning fraction explain the observation of the decrease of the blowoff equivalence ratio for the mean velocity of 5 m/s at turbulent intensity of 30%.

With the reduction of burning fraction as blowoff is approached, there is significant entrainment of pre-heated/partially reacted gases into the recirculation zone which can affect the stabilization dynamics. To illustrate this behavior, averaged CH_2O and heat release images for the turbulence intensities of 14 and 30% are shown in Fig. 4.11 and Fig. 4.12, respectively. The boundary of the mean recirculation zone for each case is shown by the red line which is defined as the contour of zero mean axial velocity.

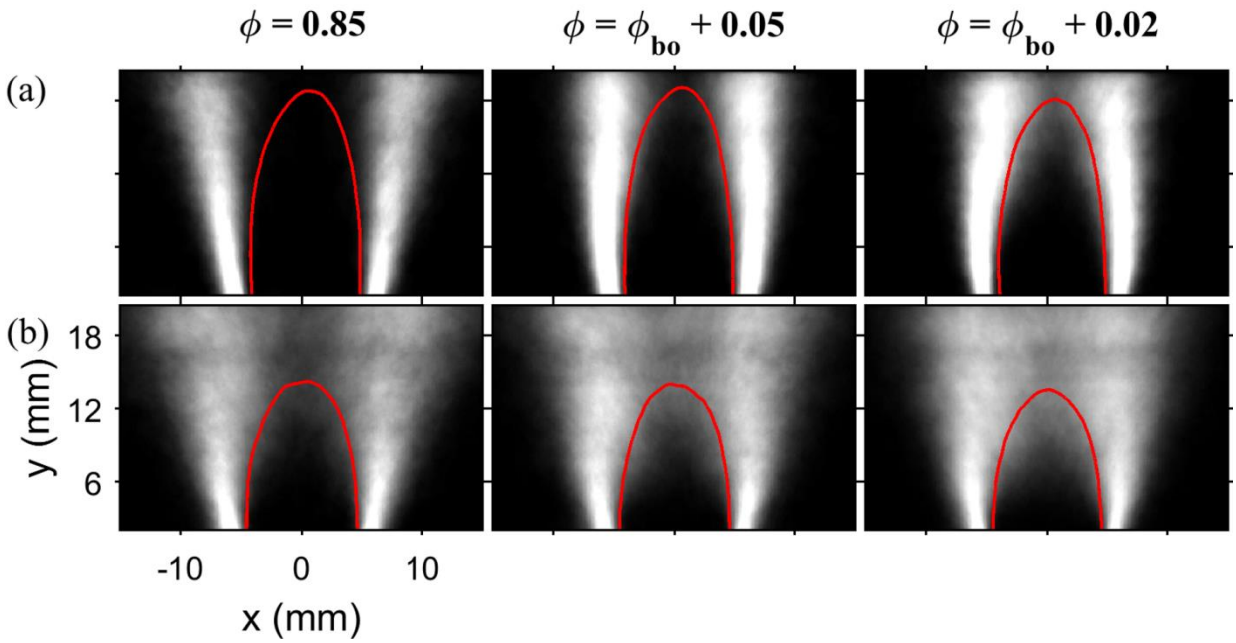

Fig. 4.11. Averaged formaldehyde images for U_m=10 m/s at (a) T.I: 14% and (b) T.I: 30%

At the moderate turbulence intensity condition, the robustly burning flame at ϕ=0.85 has the mean CH_2O signal along the shear layer. The mean flame brush, marked by the profile of average heat release is observed to be thin, with relatively high intensity near the attachment point and widening downstream. As the equivalence ratio is reduced to the condition closest to blowoff, mean CH_2O signal within the recirculation zone increases, especially within the tip of the recirculation zone as shown in Fig. 4.11(a). Similarly, a wider average heat release profile is observed within the recirculation zone at the downstream end (shown in Fig. 4.12(a)), indicating that the reaction zone is no longer located along the shear layer but envelopes the recirculation zone boundary including its tip. However, the heat release profile near the attachment point is still thin and has a relatively higher intensity.

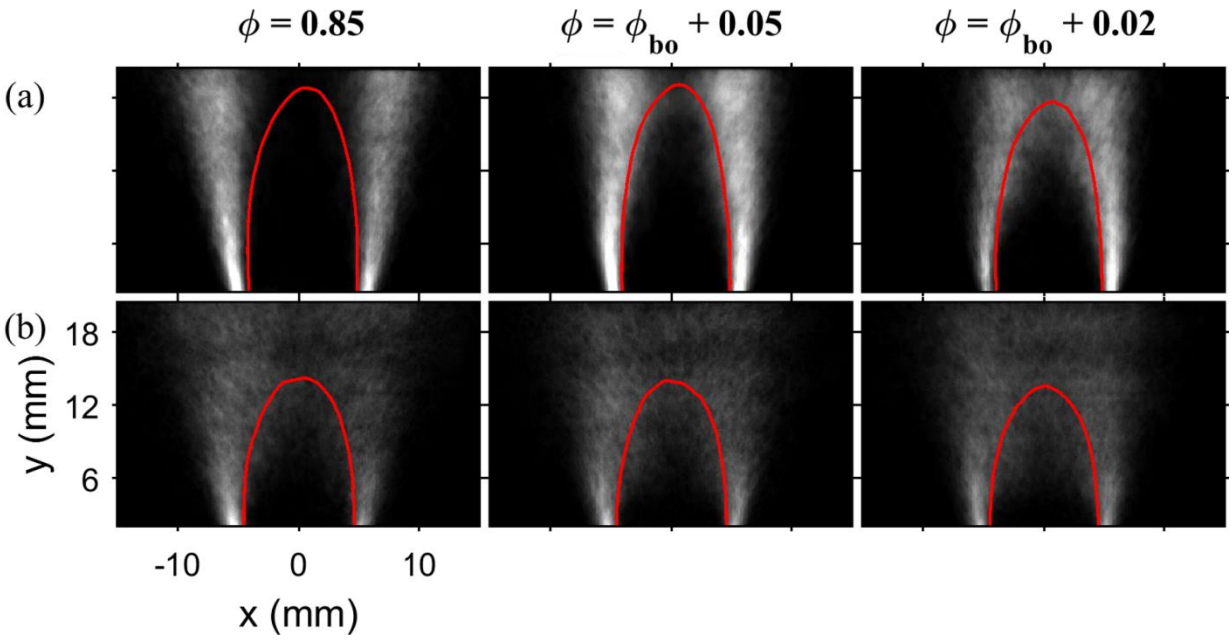

Fig. 4.12. Averaged heat release images for U_m=10 m/s at (a) T.I: 14% and (b) T.I: 30%

At the turbulence intensity of 30%, the robustly burning flame has a lower burning fraction relatively to the other turbulence conditions. Thus, it is expected to observe more CH_2O signal inside the recirculation zone as shown in Fig. 4.11(b). Similar to the moderate turbulent intensity condition, as blowoff is approached the concentration of preheated/partially burned gases as well as heat release profiles increase significantly within the recirculation zone as observed by the rising mean signal strength.

From the instantaneous as well as averaged PLIF images, it is clear that the probability of localized extinctions varies within the length of the recirculation zone and it would be useful to determine the most probable location of flame extinctions. For this assessment, the flame sheet was divided into five sections: the recirculation zone was divided into four sections of equal length and the wake region downstream of the recirculation zone. The variation of the burning fraction along the flame sheet for the turbulent intensity of 30% is shown in Fig. 4.13 as a function of the normalized distance from the bluff-body. It clearly shows that the percentage of

extinctions is more in the shear layer relative to the downstream wake region. Within the recirculation zone, burning fraction decreases with increasing distance from the flame holder with lowest being in the section nearest to the tip of the recirculation zone. Similar observation has been reported in the recent numerical work of Geikie and Ahmed [77]. Of interest is that as the blowoff condition is approached, there is a stronger reduction of the burning fraction at locations close to the bluff-body as exhibited by the decreasing slope of the variation especially in the sections - 2 (within 0.25-0.5 L_{RZ}) and 3 (within 0.5 – 0.75 L_{RZ}). However, the region closest to the attachment point maintains a relatively high burning fraction all throughout which agrees with the observation of high intensity in the averaged heat release images.

In an experimental work using the opposed flow configuration, Mastorakos *et al.* [78] had investigated the effect of strain on a lean, premixed flame stabilized by opposed jet of hot, combustion products of varying temperature. It was demonstrated that increasing the temperature of the opposed jet of combustion products aided in flame stability. Though the experiments were carried out using natural gas/air mixture, similar behavior is observed from the OPPDIF simulations for propane/air mixtures and can be attributed to the increasing value of extinction strain rate. The configuration simulated in OPPDIF included two opposing nozzles where one of the nozzle contained premixed propane-air mixtures at a temperature of 300 K while the other nozzle contained hot, combustion products of varying temperature. Based on this observation, it is possible that as the cooling of the recirculation zone occurs due to dilution with the entrained reactant gases through the flame holes, the corresponding extinction strain rate κ_{ext} decreases. Therefore, the extinction strain rate at the downstream portion of the recirculation zone is low and this results in the lowest burning fraction.

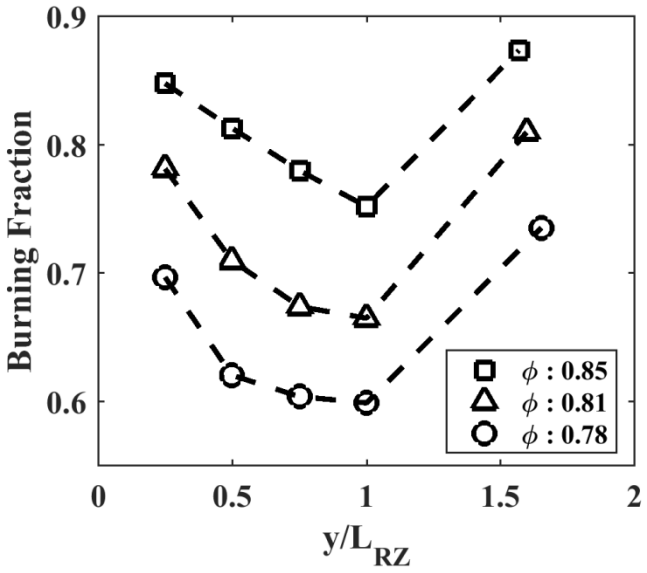

Fig. 4.13. Variation of burning fraction across the flame segments for mean velocity of 10 m/s and turbulent intensity of 30%

4.2.6. Asymmetric Index

As blowoff is approached, the general shape of the flame was observed to intermittently shift from symmetric (varicose) to asymmetric (sinuous) mode as shown in Fig. 4.14. Similar observations have been reported for near blowoff flames by Nair and Lieuwen [34], Kiel *et* al [32] and Chaudhuri *et al.* [35] and it has been termed as the "second stage" which leads to flame blowoff [30]. The physics behind the reversal of the flame to a global asymmetric structure has been studied in detail by Emerson *et al.* [62] and Mehta and Soteriou [61] and has been primarily attributed to the decrease in density ratio across the flame sheet and its effect on global stability. The reduction of density ratio results in lessening of the dilatation effect on vorticity and the baroclinic vorticity generation, both of which amplify the importance of shear generated vorticity and the von Karman instability.

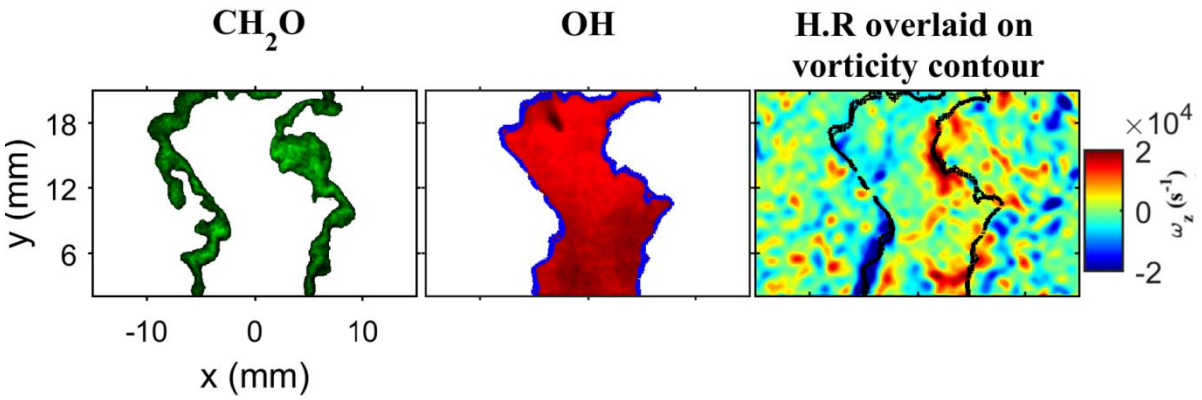

Fig. 4.14. Instantaneous PLIF image for U_m=10 m/s, T.I: 14% at ϕ=0.73 ($\phi_{b.o}$: $\phi_{b.o}$ + 0.05).

To investigate the flame dynamics near blowoff, an asymmetric index was estimated for all the cases following an approach similar to Emerson *et al.* [62]. Flame dynamics were quantified using the transverse position of the left and right flame edges, $\zeta_L(y,t)$ and $\zeta_R(y,t)$, as a function of axial position and time as shown in Fig. 4.15. To characterize the degree of sinuous oscillation, a correlation has been estimated between the wrinkling of the left and right flame edges with the condition of detected heat release and is given by:

$$r_{L,R}(y) = \frac{\langle \zeta_L(y,t)\zeta_R(y,t)\rangle}{\sqrt{\langle(\zeta_L(y,t))^2\rangle\langle(\zeta_R(y,t))^2\rangle}} \quad (1)$$

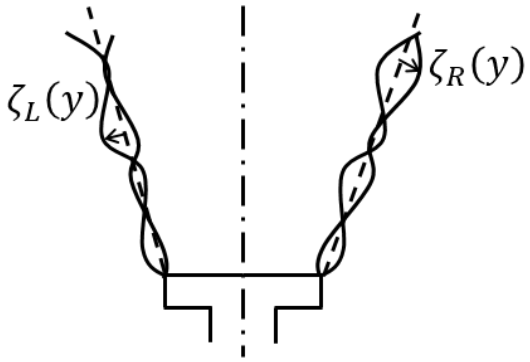

Fig. 4.15. Typical OH PLIF flame edge showing the function

The negative and positive correlation coefficients imply asymmetric and symmetric flame wrinkling, respectively. Furthermore, a nearly zero correlation coefficient implies that the flame branches are disturbed by uncorrelated structures with a scale much smaller than their transverse separation distance. The variation of the correlation coefficient for the different turbulent conditions is shown in Fig. 4.16

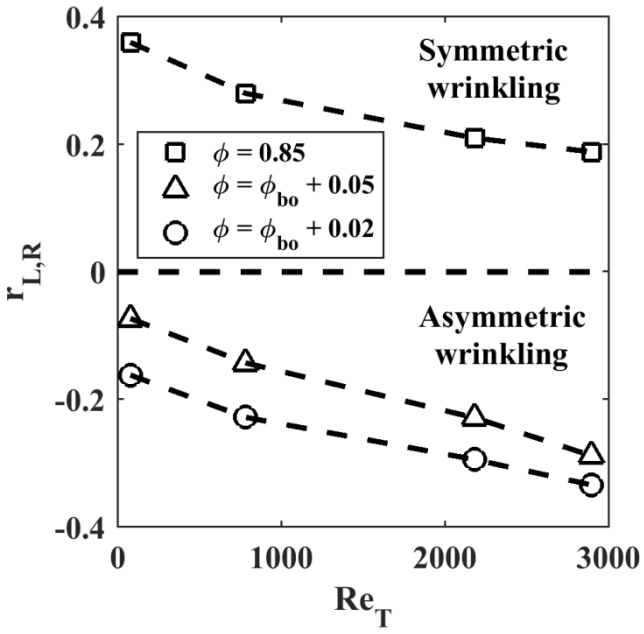

Fig. 4.16. Variation of the correlation coefficient for flames near and far from blowoff at U_m=10 m/s. Measurements are shown for the axial position of peak flame response

For each turbulence condition, as the equivalence ratio is lowered from 0.85 to 0.05 above the blowoff equivalence ratio, the correlation coefficient is observed to switch sign from positive to negative and it further decreases for the condition closest to blowoff. This is indicative of growing asymmetric motion across the flame edges as blowoff is approached. As the turbulence intensity is increased, significant reduction of the coefficient is also observed. Based on the understanding from the previous research [61,62], this variation can be attributed to decreasing

temperature ratio across the flame sheet. This validates the hypothesis that as the frequency of local extinctions increase, significant penetration of preheated gases occurs diluting the hot combustion products present in the recirculation zone and thereby, lowering its temperature. However, a direct measurement of the temperature would be more conclusive.

4.2.7. 2-D Curvature

The local response of the flame front surface was assessed by evaluating the local 2-D flame front curvature statistics using the process mentioned in Section 3.2.5. Fig. 4.17 shows the probability distribution function of the curvature for the turbulent intensities of 14 and 30%. For moderate turbulence intensity, the distributions are observed to be approximately Gaussian, and symmetrical about C = 0. At conditions approaching blowoff, the pdfs are seen to widen which agree with discussions of the instantaneous PLIF images in Section 4.2.3. For the intensely turbulent condition, the distributions are not symmetric. The stably burning flame has a mean positive curvature with longer tails towards the positive curvature side. Near blowoff the distribution widens but there is a higher probability of the formation of negative curvature surfaces. This agrees with the observation of increased frequency of cusps in the flame segment near the bluff-body.

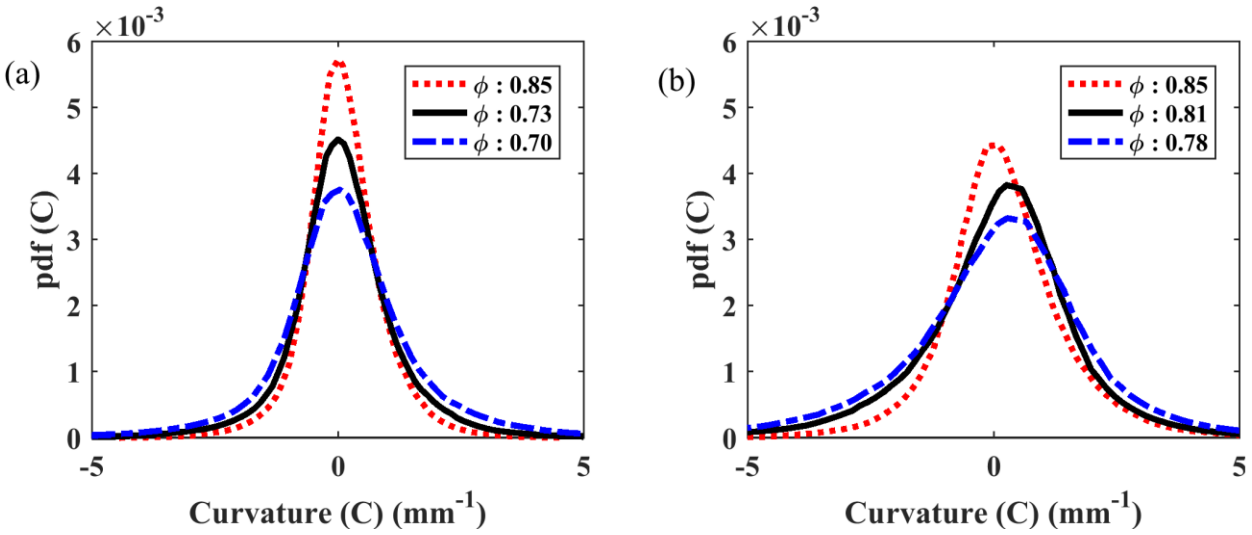

Fig. 4.17. Pdfs of 2-D curvature for the different flame conditions corresponding to mean velocity of 10 m/s at (a) T.I: 14 % and (b) T.I: 30%.

4.2.8. Duration of the blowoff transient

The motivation to quantify the duration of the blowoff event is based on the observation of Chaudhuri *et al.* [35] and Dawson *et al.* [39] who used time- resolved chemiluminescence imaging to show that the blowoff event occurs over a period of few milliseconds. Kariuki *et al.* [40] quantified the duration of the blowoff events by processing the OH* emission time series obtained using a photomultiplier tube and validated the observation of Dawson *et al.* [39]. The PLIF images illustrated the differences in the flame structure near blowoff as the free stream turbulence levels were varied. Therefore, it is worth examining the effect of this modification on the duration of the blowoff events. For this assessment, the CH* emission signal collected by the PMT detector was analyzed using the approach demonstrated by Kariuki *et al.* [40].

For each condition, five independent time series were recorded by operating the PMT at 50 kHz and ramping down the equivalence ratio from 0.85. The last one second of the data was used for this analysis. Each time series was time shifted such that the blowoff occurred at an arbitrary

chosen time. Each time series was normalized by the mean value of CH* which was estimated from the beginning of this subset to start of the decay process. These were then averaged to obtain the average behavior of the blowoff event. The average duration of the blowoff event was defined as the time needed for the emission to decrease from 90 to 10% of the $\langle CH^* \rangle$ before the start of the decay. In an additional experiment, the trends of the estimated durations were verified by high speed chemiluminescence imaging at 1 kHz. The results for mean velocity of 10 m/s are presented in Table 4.1. Values of τ_{ext} are observed to decrease with increasing turbulence levels. Significant reduction is observed for the intensely turbulent conditions of 24 and 30% relative to the other two cases. This indicates that the significant cooling of the recirculation zone due to penetration of reactants strongly weakens the flame stabilization. However, a direct measurement of temperature of the recirculation zone region can provide some more insight into the effects of heat transfer on the blowoff mechanism. The values of τ_{ext} are observed to be at least an order of magnitude greater than the characteristic residence time, L_{RZ}/U_m for all the conditions indicating that the events during the final stages of the blowoff process influence the flame structure over larger time scales than those of chemistry and flow field turbulence.

Table 4.1. Values of τ_{ext} evaluated for U_m=10 m/s

Turbulence Intensity (%)	Re_T	τ_{ext} (ms)	$\tau_{ext}/(L_{RZ}/U_m)$
4	79	37.3	20.7
14	783	30.7	18.1
24	2182	18.9	13.9
30	2898	15.3	12.0

4.3 Concluding remarks

In this chapter, the effect of different levels of free stream turbulence on the blowoff dynamics of a bluff-body stabilized flame is presented. Detailed flame structure was investigated by simultaneous OH PLIF, CH_2O PLIF and PIV to determine the sequence of events leading to blowoff. Apart from the condition of 5 m/s approach velocity at a turbulence intensity of 30 %, increasing turbulence intensity was found to reduce the flame stability. It was found that with reduction of equivalence ratio as blowoff was approached, the flame shape changed from a conical to a more columnar shape and the degree of interaction of the flame front with the shear layer consequently increased. Near blowoff, the flame front and the high vorticity region along the shear layer overlap to induce high local strain that exceed the corresponding extinction stretch rates, resulting in local flame holes. As blowoff was approached, significant increase in the frequency of breaks along the reaction zone was observed for low and moderate turbulence conditions. For the higher turbulence conditions, fragmentation of the flame was observed which provided additional pathways for penetration of reactants into the recirculation zone, leading to the presence of low temperature combustion processes inside the recirculation zone at conditions very close to lean extinction. The length of the recirculation zone was observed to decrease significantly with increasing turbulence levels while only a slight decrease was observed as blowoff was approached. Measurements of the burning fraction quantified the degree of local extinctions for varying turbulence levels and at conditions away from and near blowoff. Enhanced corrugations along with modification of the flame fronts resulted in broadening of the curvature pdfs. At conditions near blowoff, increasing the turbulence levels showed a greater response of the flames to absolute instability.

CHAPTER FIVE

5. Effect of fuel properties on the blowoff dynamics

Introduction

In Chapter 3, it was shown that under identical characteristics of the inlet flow, the properties of the fuel/air mixture play an important role in governing the flame front topology. Therefore, the motivation of the work presented in this chapter is to examine the corresponding effect of the fuel properties on the blowoff dynamics of lean premixed flames. Lean premixed flames of methane/- and ethylene/air have been studied at conditions close to blowoff by simultaneous PLIF imaging of OH and CH_2O and PIV. Measurements of blowoff equivalence ratio, burning fraction, asymmetric index, curvature statistics and mean strain rates have been obtained for a range of experimental test conditions. In the next section,experimental conditions are summarized followed by a discussion of the results and a summary of the important conclusions.

5.1 Experimental conditions

Lean premixed mixture of methane/- and ethylene/air at room temperature has been used. The flame blowoff equivalence ratios were determined for three mean velocities of 5, 10 and 15 m/s. For each mean axial velocity, turbulence intensities of 4, 14, 24 and 30% have been studied. The simultaneous OH PLIF, CH_2O PLIF and PIV have been applied primarily to the flames corresponding to mean velocity of 10 m/s subjected to the different free stream turbulence conditions. To study the dynamics of the flames near blowoff for each inlet condition, the measurements were performed at two equivalence ratios representing near blowoff conditions – equivalence ratios 0.05 and 0.02 above the blowoff equivalence ratio for the given condition and compared with results of the stably burning flames discussed in Chapter 3. The flames

investigated by this diagnostic technique spanned the regimes of wrinkled flames, corrugated flames and thin reaction zones in Borghi's regime diagram[12], as shown in Fig. 5.1. For normalization in the Borghi diagram, unstrained laminar flame speed and thickness values were computed using the PREMIX code [48] and USC Mech Version II of Wang *et al.* [49]. The unstretched laminar flame thickness (δ_f) was defined as the temperature difference across a laminar flame divided by the maximum temperature gradient.

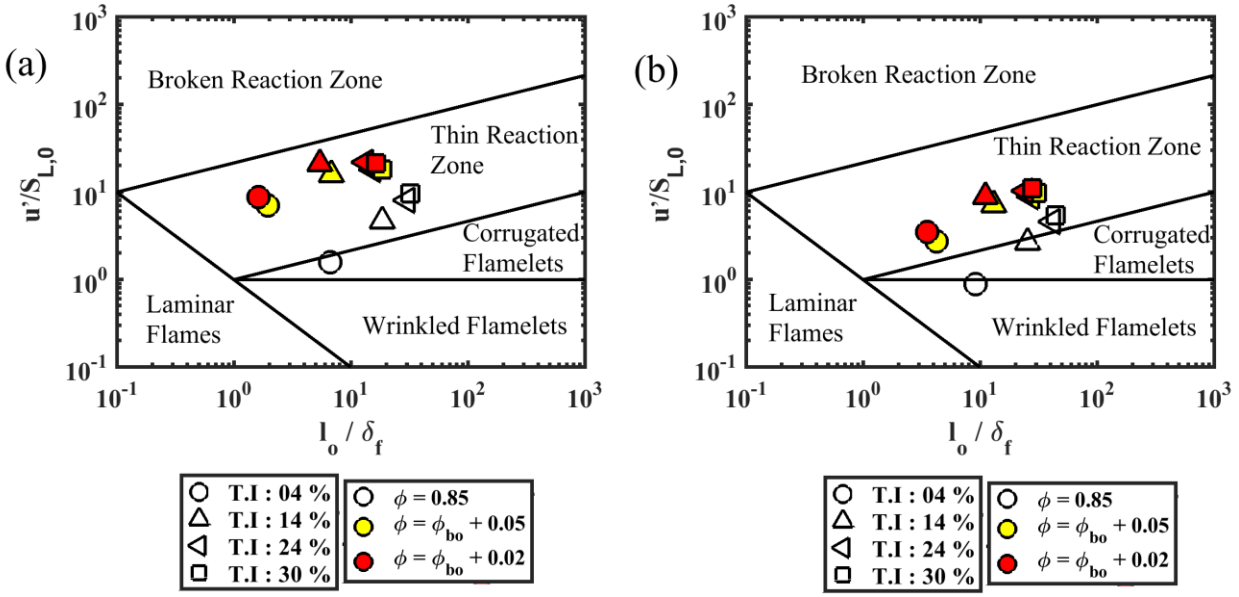

Fig. 5.1. Experimental conditions studied by laser diagnostics overlaid on the premixed combustion regime diagram for (a) methane/air flames and (b) ethylene/air flames

5.2 Results and Discussions

In this section, the variation of the blowoff equivalence ratio for the different turbulent conditions is presented in Section 5.2.1 followed by the results of simultaneous OH, CH_2O PLIF and PIV for the flames at conditions near blowoff.

5.2.1. Variation of blowoff equivalence ratio

The variation of the blowoff equivalence ratios for lean methane/-, propane/- and ethylene/air flames for the different experimental conditions is shown in Fig. 5.2. To ensure repeatability, the flame blowoff equivalence ratios were determined at least thrice for each inlet condition. For lean methane/air flames, as turbulence intensity was increased from 4 to 30 %, a monotonic increase of the blowoff equivalence ratio was observed for all the mean velocities, as shown in Fig. 5.2a. Typical increase in the blowoff equivalence ratio from low (4%) to highest (30%) turbulence condition is about 25 % for mean velocities of 5 and 10 m/s and 32% for mean velocity of 15 m/s. For ethylene/air flames, a similar trend of increase in blowoff equivalence ratio with increasing levels of turbulence intensity is observed for the three mean velocities studied in this work, as shown in Fig. 5.2b. For mean velocities of 5 and 10 m/s, the blowoff equivalence ratios increased by about 22% as the turbulence intensity was increased from 4 to 30%, while for the mean velocity of 15 m/s, the blowoff equivalence ratio increased by about 31%. The variation of blowoff equivalence ratio for lean propane/air flames at identical flow conditions is shown in Fig. 5.2c. From the plots shown in Fig. 5.2, it is interesting to note for the identical flow conditions, the blowoff equivalence ratios for lean methane/- and ethylene/air flames are significantly lower than those of propane/air flames. Also, the peculiar behavior of propane/air flames for mean velocity of 5 m/s and intense turbulence condition of 30% is not observed for methane/- and ethylene/air flames. This clearly indicates the important role played by the properties of the fuel/air mixtures in governing the extinction limits for lean, premixed bluff body stabilized flames.

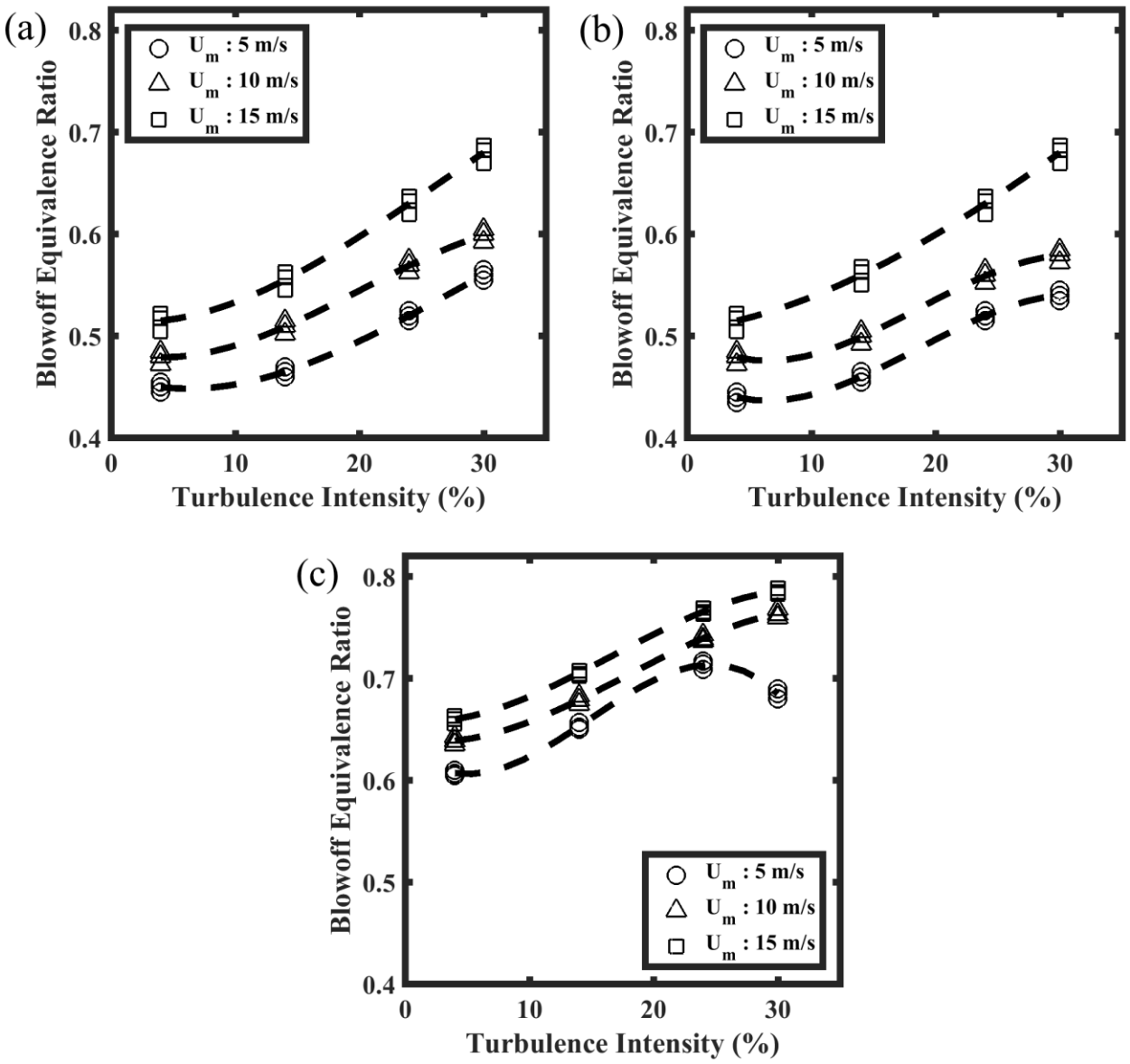

Fig. 5.2. Variation of blowoff equivalence ratio for the different inlet conditions corresponding to lean flames of (a) Methane (b) Ethylene and (c) Propane. Three repeated experimental results are shown in each case.

5.2.2. Flame front topology

To elucidate the difference in the flame structure at conditions close to blowoff and provide a direct comparison with the stably burning flames, instantaneous PLIF images for robustly burning methane/- and ethylene/air flames at $\phi = 0.85$ are shown in Fig. 5.3 and Fig. 5.4, respectively. Because of the higher flame speed of ethylene flame envelope is situated at significantly wider cone angle than those of methane and propane fuels. At low turbulence intensity (4 %), methane/- and ethylene/air flames exhibit weak corrugations along the flame sheet. As the turbulence intensity was increased to 14%, pronounced formation of cusps were observed due to formation of the unburned mixture fingers. For both the low and moderate turbulence levels, mostly continuous reaction zones were observed. At the intense turbulent condition (30 %), significant modification of the flame front was observed owing to the occurrence of flamelet merging, localized extinctions and pocket formation. It is important to note that for all the conditions studied at $\phi = 0.85$, overlaying the heat release regions on the vorticity field show that the flame sheet predominantly lies outside the high vorticity regions of the shear layer, as shown in Fig. 5.3 and Fig. 5.4, and the variation of the flame structure can be attributed primarily to the different levels of turbulence intensity in the approach flow.

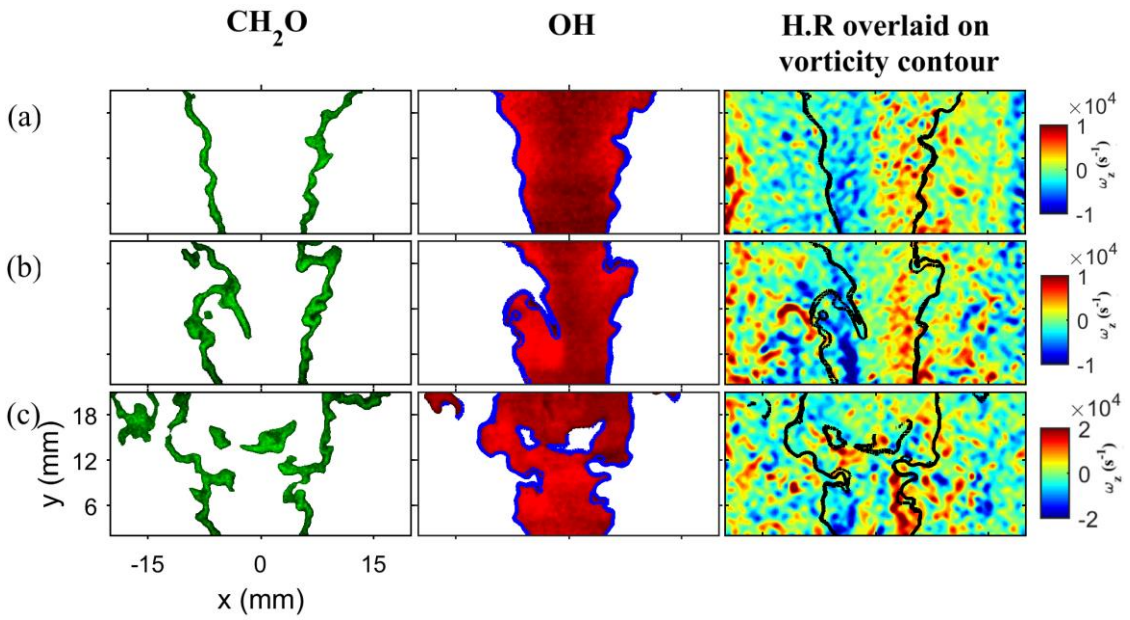

Fig. 5.3. Instantaneous images of stably burning methane/air flames (ϕ=0.85) for mean velocity of 10 m/s and corresponding to (a) low turbulence (4%) (b) moderate turbulence (14%) and (c) intense turbulence (30%)

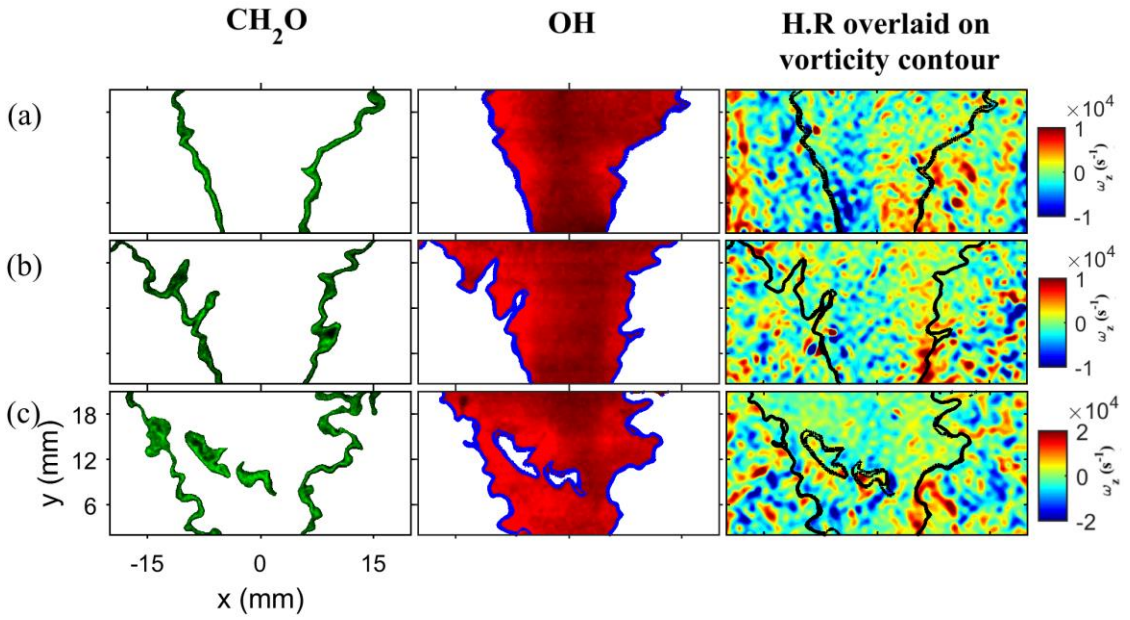

Fig. 5.4. Instantaneous images of stably burning ethylene/air flames (ϕ=0.85) for mean velocity of 10 m/s and corresponding to (a) low turbulence (4%) (b) moderate turbulence (14%) and (c) intense turbulence (30%)

To investigate the flame structure close to blowoff, simultaneous PLIF imaging and PIV has been performed at two equivalence ratios – 0.05 and 0.02 above the corresponding blowoff equivalence ratio for each case. Instantaneous images for mean velocity of 10 m/s and low (4%), moderate (14%) and intense (30%) turbulent conditions at equivalence ratios 0.05 above the corresponding blowoff equivalence ratios for methane/- and ethylene/air flames are shown in Fig. 5.5 and Fig. 5.6, respectively. For low and moderate turbulence conditions, comparison of these instantaneous images with those of the stably burning flames show that the flame shape becomes columnar as blowoff is approached owing to reduction of the flame speed. At these conditions flame front overlaps with the high vorticity regions of the shear layer and they are consequently subjected to higher aerodynamic strain rates which result in localized extinctions along the shear layer as can be seen by the breaks along the overlapping regions of OH and CH_2O in Fig. 5.5a-b and Fig. 5.6a-b. . For both methane/- and ethylene/air flames at the intense turbulence condition, breaks along the reaction zones are observed to increase in frequency and size as shown in Fig. 5.5c and Fig. 5.6c, respectively. This provides multiple channels for penetration of reactants into the burnt region that is normally filled with hot combustion products. Comparing the PLIF images of methane/- and ethylene/air flames obtained at this near blowoff condition with those of the stably burning flames at the intense turbulent conditions, indicate a higher propensity of formation of these islands of CH_2O within the OH filled regions. Overlap of the OH and CH_2O layers indicate the occurrence of heat release along the boundaries of the isolated pockets of CH_2O where the preheated and partially reacted gases come in contact with hot combustion products. Also, at the intensely turbulent conditions, pronounced formation of cusps are observed particularly near the bluff-body as shown in Fig. 5.5c for the left wing of the flame where the flame front is observed to be wrapped around a vortical structure.

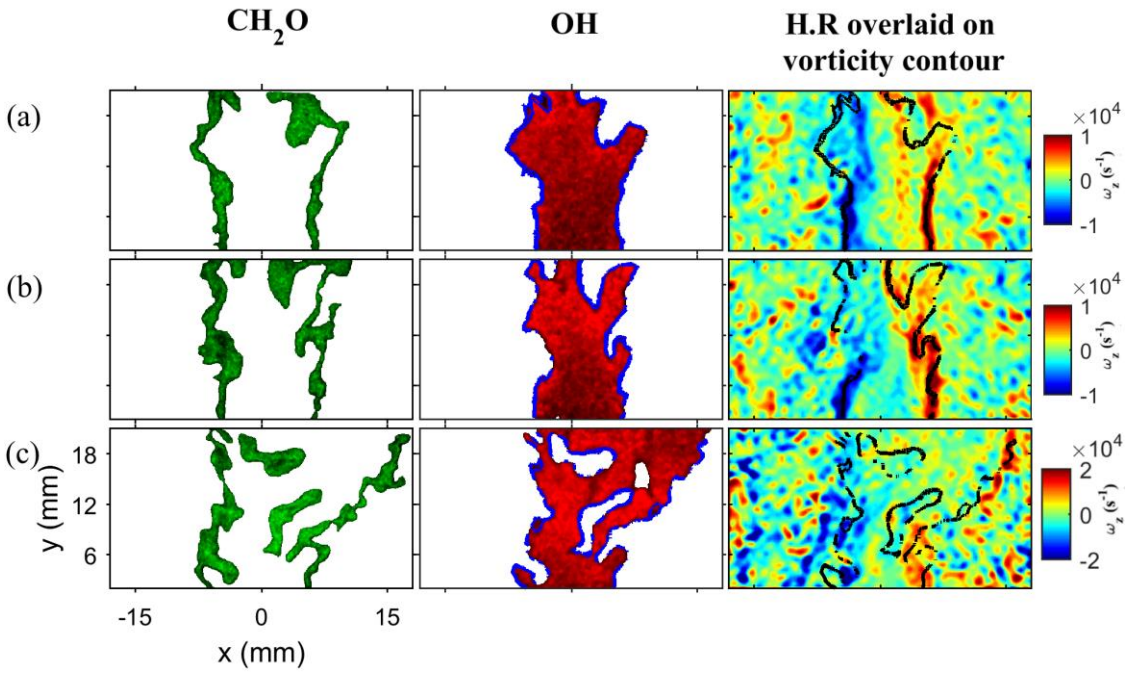

Fig. 5.5. Instantaneous images of methane/air flames at mean velocity of 10 m/s corresponding to (a) low turbulence (4%) at ϕ=0.53 (b) moderate turbulence (14%) at ϕ=0.56 and (c) intense turbulence (30%) at ϕ=0.65.

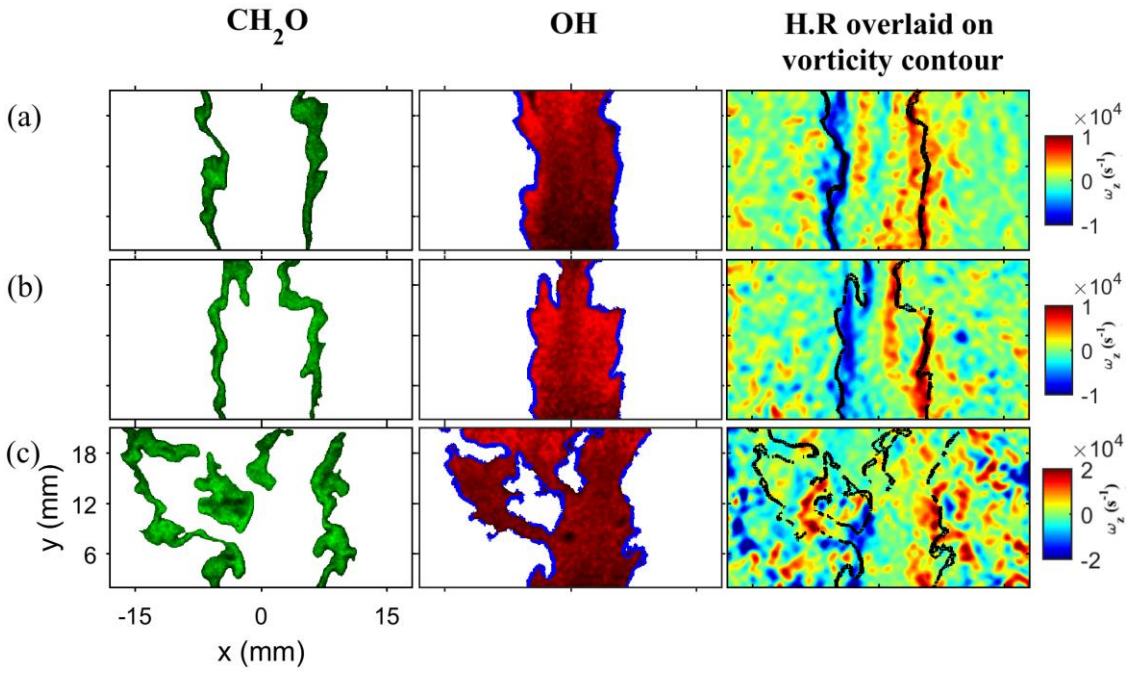

Fig. 5.6. Instantaneous images of ethylene/air flames at mean velocity of 10 m/s corresponding to (a) low turbulence (4%) at ϕ=0.53 (b) moderate turbulence (14%) at ϕ=0.55 and (c) intense turbulence (30%) at ϕ=0.63.

As the equivalence ratio is reduced towards blowoff, significant modification of the flame front structure is observed. Instantaneous PLIF images for methane/- and ethylene/air flames at an equivalence ratio of 0.02 above their corresponding blowoff equivalence ratios are shown in Fig. 5.7 and Fig. 5.8, respectively. For the lower turbulence intensity condition (4%), breaks along the reaction zones are observed to increase in frequency and size, particularly near the downstream end of the recirculation zone , as shown in Fig. 5.7a and Fig. 5.8a. At the moderate turbulence condition (14 %), significant localized extinctions and fragmentation of the flame is observed. At certain occasions, the flame is observed to recede into the recirculation zone. Such an event is shown for methane/- and ethylene/air flame in Fig. 5.7b and Fig. 5.8b, respectively. The instantaneous recirculation zone has been represented by the contour of $U_y = 0$ and is shown by the solid red line. The occurrence of this reduction in the instantaneous flame height can lead to two possibilities: (1) in the top part of the flame segment, regions void of overlap of OH and CH_2O are observed. The presence of these local holes provides pathways for entrainment of reactants into the recirculation zone. Higher rate of entrainment can reduce the temperature of the hot combustion products residing in the recirculation zone due to dilution and can drive the flame towards blowoff. Similar observation of reduction of flame height prior to blowoff has been reported by Kariuki *et al.* [41,42] for methane/- and ethylene/air flames and the occurrence of this possibility has been hypothesized as the route to blowoff for shorter premixed flame stabilized using a large axisymmetric bluff body. (2) The other possibility is that owing to favorable residence time in the recirculation zone, re-ignition of the flame along the shear layer can occur. In the present study, the second possibility is observed to occur and the flame is able to survive at this condition. The occurrence of the extinction/re-ignition events has been also been observed by high speed chemiluminescence imaging.

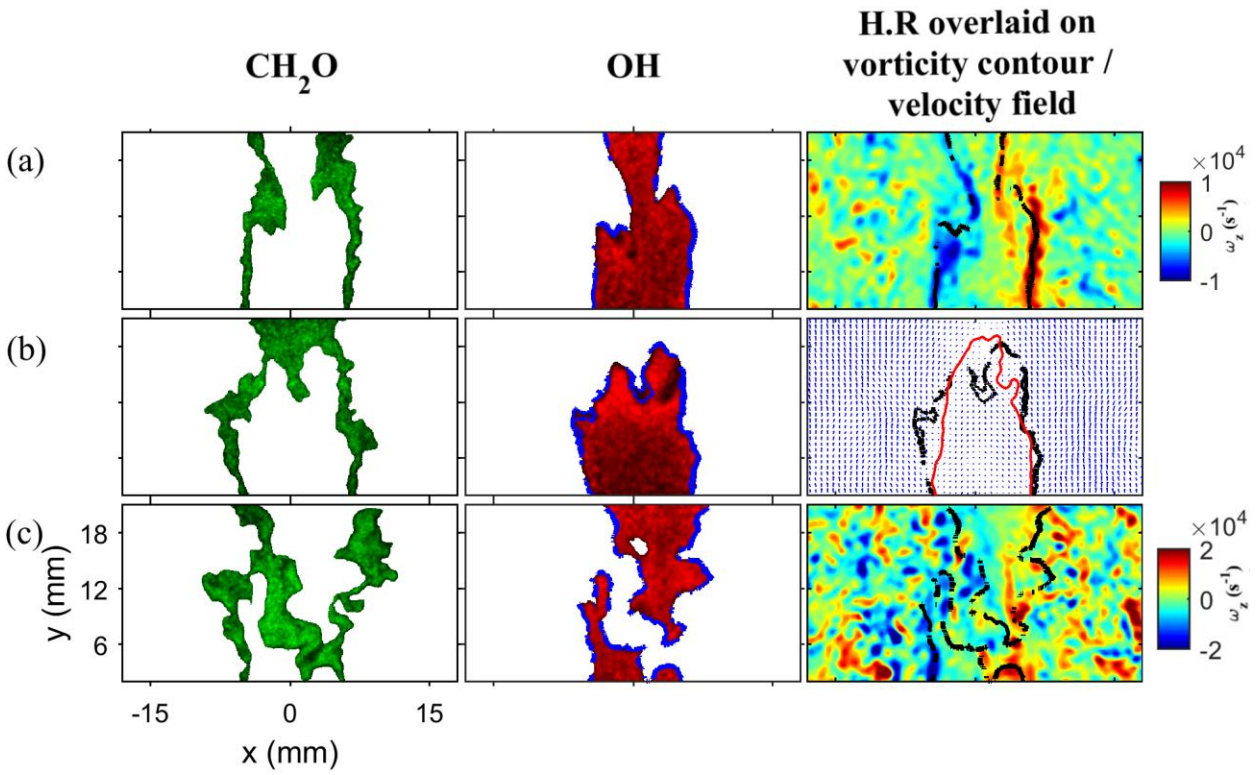

Fig. 5.7. Instantaneous images of methane/air flames for mean velocity of 10 m/s corresponding to (a) low turbulence (4%) at ϕ=0.5 (b) moderate turbulence (14%) at ϕ=0.53 and (c) intense turbulence (30%) at ϕ=0.62.

At the intense turbulence condition, significant localized quenching and disintegration of the flame sheet is observed to occur which provide areas for penetration of reactants into the recirculation zone. The reduction of the density ratio between the flame and its surrounding can strengthen the Benard-von Karman (BVK) instability. This can result in the formation of a sinuous wake which can aid in the penetration of unburned reactants into the recirculation zone through the locally quenched regions of the flame sheet. Such an event is shown for methane/- and ethylene/air flames in Fig. 5.7c and Fig. 5.8c, respectively. To enable a better visualization of this event, an enlarged image of Fig. 5.8c is shown in Fig. 5.9. The instantaneous recirculation zone is shown by the solid red line. In Fig. 5.9a, it can be seen that the lower left wing of the

flame is subjected to a strong negative vorticity field which has been possibly generated by the bluff body. This tends to pull unburned reactants into the recirculation zone. To illustrate the latter point, velocity vectors have been overlaid on the CH_2O PLIF image as shown in Fig. 5.9b. The direction of the velocity vectors and presence of formaldehyde in the recirculation zone illustrates the role played by the bluff body generated vorticity at conditions close to blowoff in entrainment of reactants in the recirculation zone. By LES analysis of the blowout process, Smith *et al.* [79] illustrated the effect of the simultaneous presence of BVK instability and localized extinctions along the flame sheet that result in entrainment of cold reactants which subsequently, reduced the temperature of the gases present in the recirculation zone and ultimately led to flame blowout.

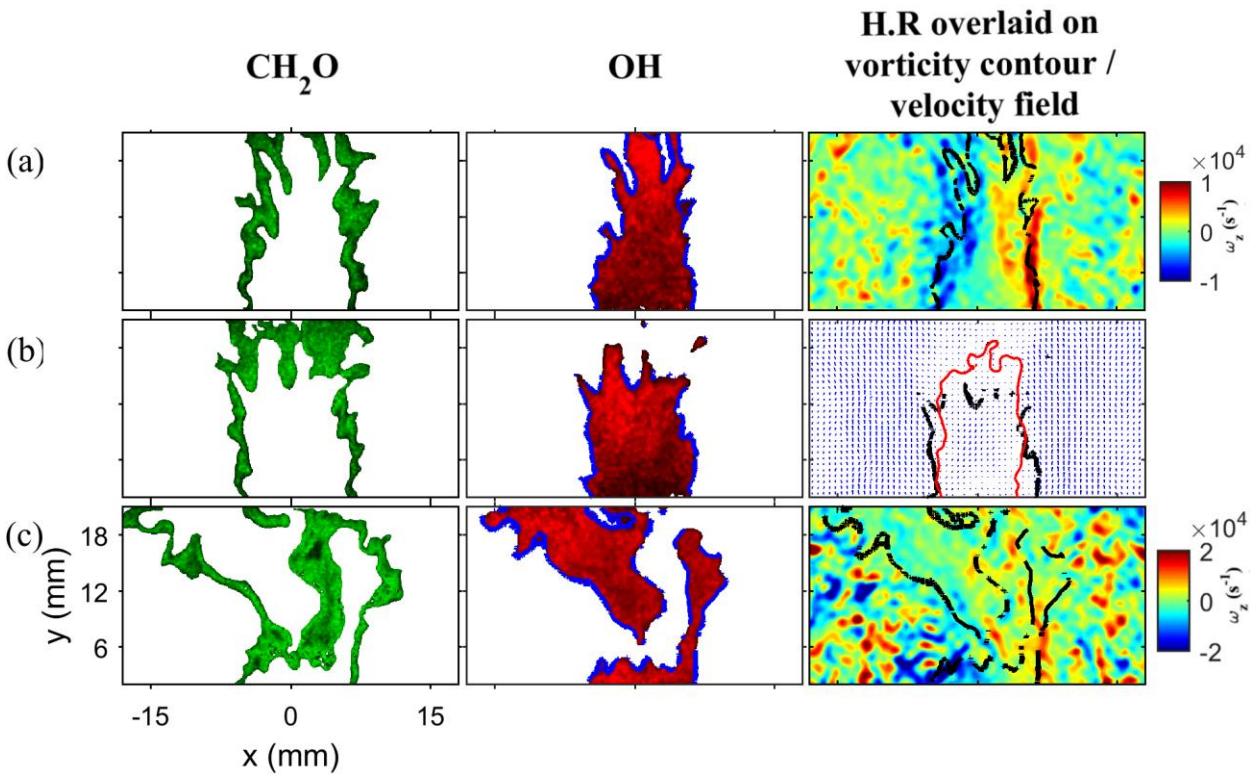

Fig. 5.8. Instantaneous images of ethylene/air flames for mean velocity of 10 m/s corresponding to (a) low turbulence (4%) at ϕ=0.5 (b) moderate turbulence (14%) at ϕ=0.52 and (c) intense turbulence (30%) at ϕ=0.6

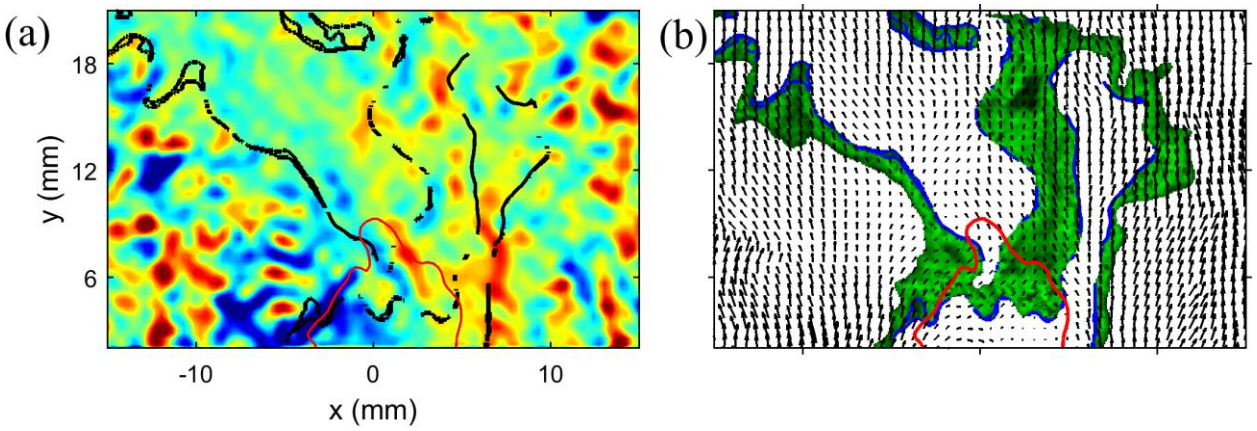

Fig. 5.9. (a) Heat release regions of the ethylene/air flame is overlaid on the vorticity contour (b) Velocity vectors overlaid on the CH_2O PLIF image

The averaged profiles for CH_2O PLIF and heat release signals for methane/air flames at moderate and intense turbulence levels are shown in Fig. 5.10 and Fig. 5.11. The boundary of the mean recirculation zone for each case is shown by the red line which is defined as the contour of zero mean axial velocity. At the moderate turbulence intensity condition (14%), the robustly burning flame at $\phi = 0.85$ has the mean CH_2O signal along the shear layer. The mean flame brush, marked by the profile of average heat release is observed to have relatively high intensity near the attachment point and widens downstream. As the equivalence ratio is decreased to the condition closest to blowoff, mean CH_2O signal is observed within the recirculation zone, as shown in Fig. 5.10a. Similarly, a wider average heat release profile is observed with strong signals near the downstream end of the recirculation zone (shown in Fig. 5.11a), indicating that the reaction zone is no longer located along the shear layer but envelopes the recirculation zone boundary including its tip. At the intense turbulence condition (30%), the robustly burning flame has a wider profile of CH_2O and heat release that is primarily located along the shear layer. At conditions near blowoff, the concentration of preheated/partially burned gases as well as heat release profiles increase significantly within the recirculation zone as observed by the rising mean signal strength relative to the moderate turbulence condition, as shown in Fig. 5.10b and Fig. 5.11b. The averaged images validate the observation reported for the instantaneous images at conditions near blowoff. For ethylene/air flames, similar variation is observed for the mean CH_2O and heat release profiles at conditions approaching blowoff.

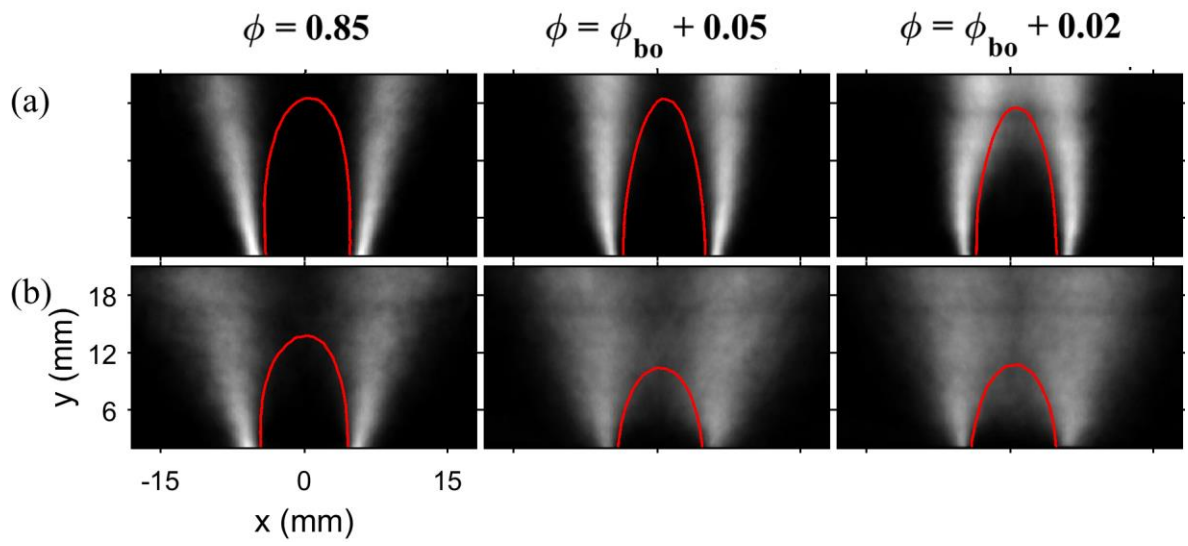

Fig. 5.10. Averaged formaldehyde images of methane/air flames for U_m=10 m/s at (a) T.I: 14% and (b) T.I: 30%

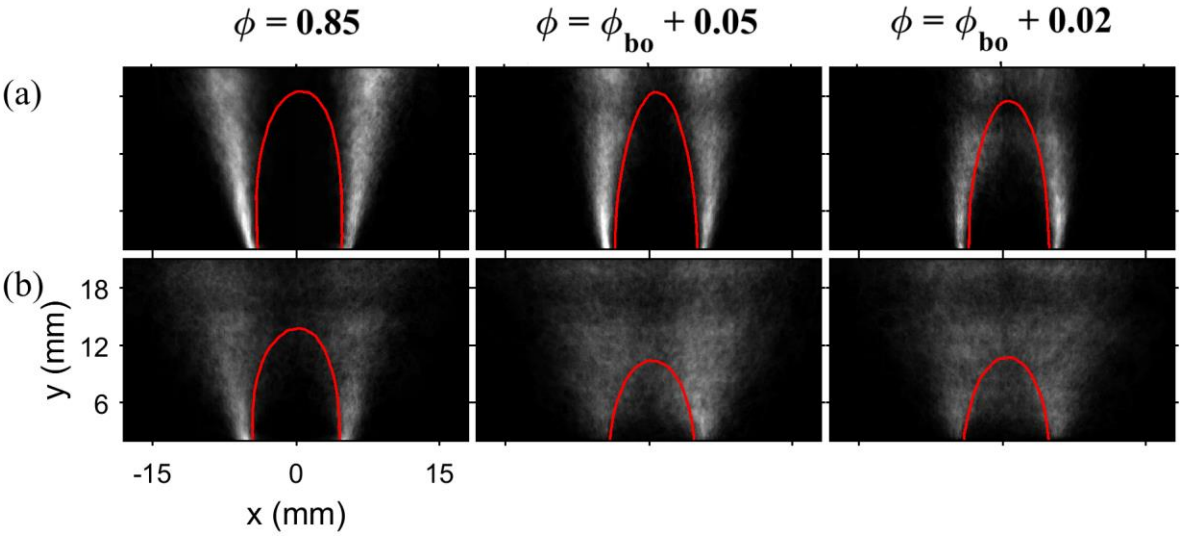

Fig. 5.11.Averaged heat release images for U_m=10 m/s at (a) T.I: 14% and (b) T.I: 30%

5.2.3. 2-D Estimates of strain rate

Two dimensional estimates of aerodynamic strain rates were evaluated for methane/- and ethylene/air flames at conditions close to blowoff in an identical manner as described in Section 3.2.3. The variation of the strain rate for methane/- and ethylene/air flames is shown in Fig. 5.12. The first and second column represents the variation at moderate (14 %) and intense (30 %) turbulence levels. Extinction strain rates were evaluated for each flame condition using OPPDIF[65]. For estimation of the extinction strain rate in OPPDIF, the configuration included two opposing nozzles, both containing premixed fuel-air mixtures at a temperature of 300 K. The solid green and blue lines represent the extinction strain rates for robustly burning flame (ϕ=0.85) and at the condition closest to blowoff ($\phi=\phi_{b.o}$ + 0.02). Fig. 5.12 clearly shows that as blowoff is approached the strain rate pdfs become wider for all the cases. This is expected based on the observation that at conditions near blowoff, the flame front overlaps with the higher vorticity regions of the shear layer which induces higher strain rate on the flame relative to the robustly burning condition. It can also be clearly observed that the strain rate which the flame can withstand significantly reduces as the equivalence ratio is lowered to approach blowoff. For conditions close to blowoff the area of the pdf curve that lies beyond the extinction strain rate is significantly higher relative to the stably burning flames. Thus, the opposing trend of the extinction strain rate and the hydrodynamic strain rate experienced by the flame at conditions close to blowoff increases the possibility of occurrence of localized quenching/extinction along the flame sheet. For both methane/- and ethylene/air flames, the strain rates pdfs at the intense turbulence condition are much wider relative to that of the moderate turbulence levels which explains the observation of significantly higher degree of extinctions for these cases.

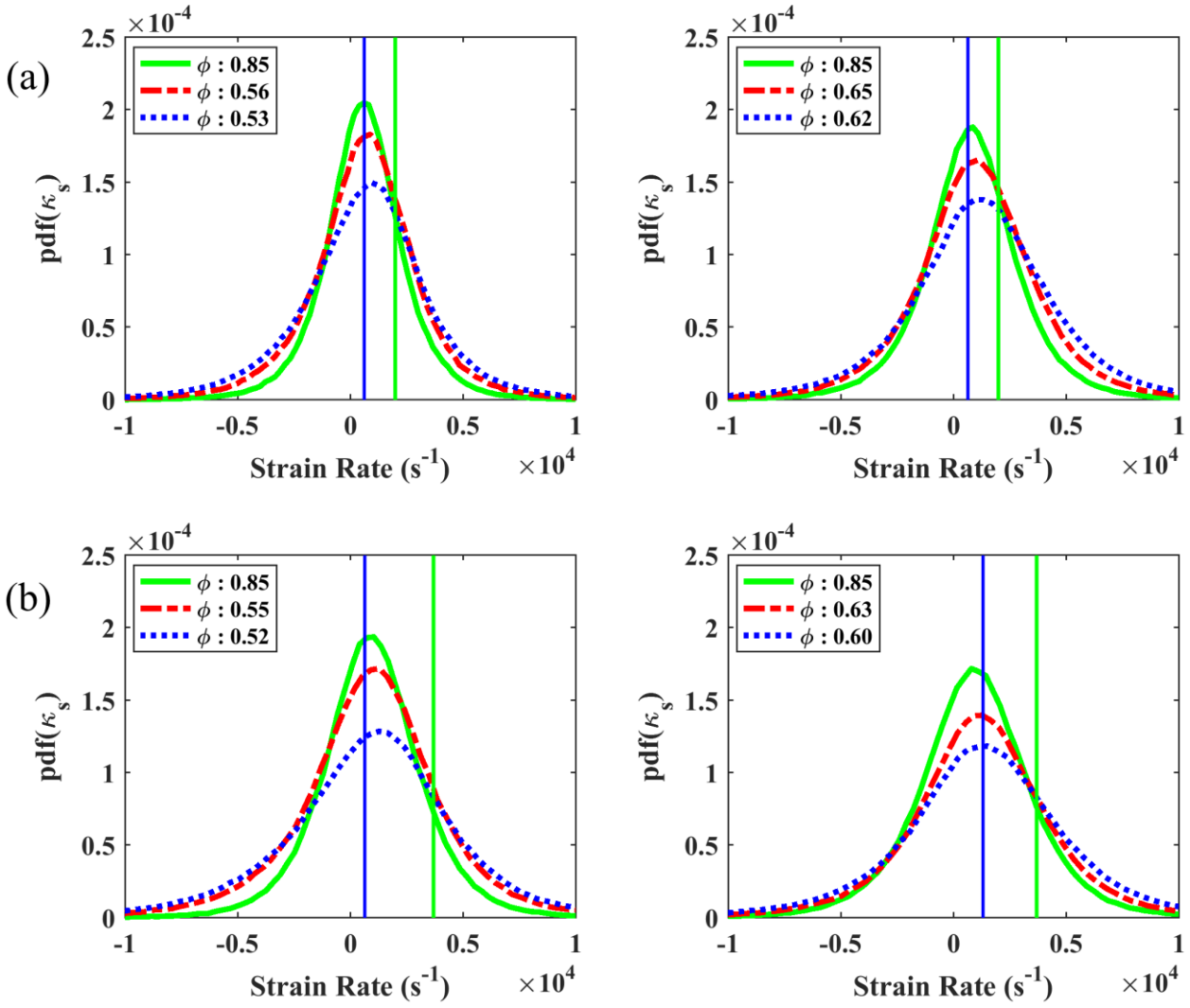

Fig. 5.12. Probability distribution functions of the 2-D strain rates for flames corresponding to (a) methane/air and (b) ethylene/air. The first and second column represents the variation for turbulence intensities of 14 and 30%, respectively.

5.2.4. Burning fraction measurements

To estimate the degree of localized extinctions for the investigated flames, burning fraction was evaluated for each condition. The variation of burning fraction for flames at conditions far and near to blowoff is shown in Fig. 5.13 for methane/- and ethylene/air flames. For both the flames

stabilized at an equivalence ratio of 0.85, a clear decrease in the burning fraction is observed with increase in the free stream turbulence levels which has been discussed in Chapter 3. As blowoff is approached, the burning fraction is observed to decrease for all the cases owing to the imposition of higher strain rates relative to the stably burning flames at the identical flow conditions. Furthermore, the near blowoff flame is also more prone to localized extinction owing to significant reduction of the extinction strain rate as shown in Fig. 5.12. Thus, the observation of significant increase in frequency and size of breaks along the reaction zone with increasing turbulence intensity shown quantitatively by the variation of the burning fraction is consistent with strain induced extinctions leading to flame blowoff.

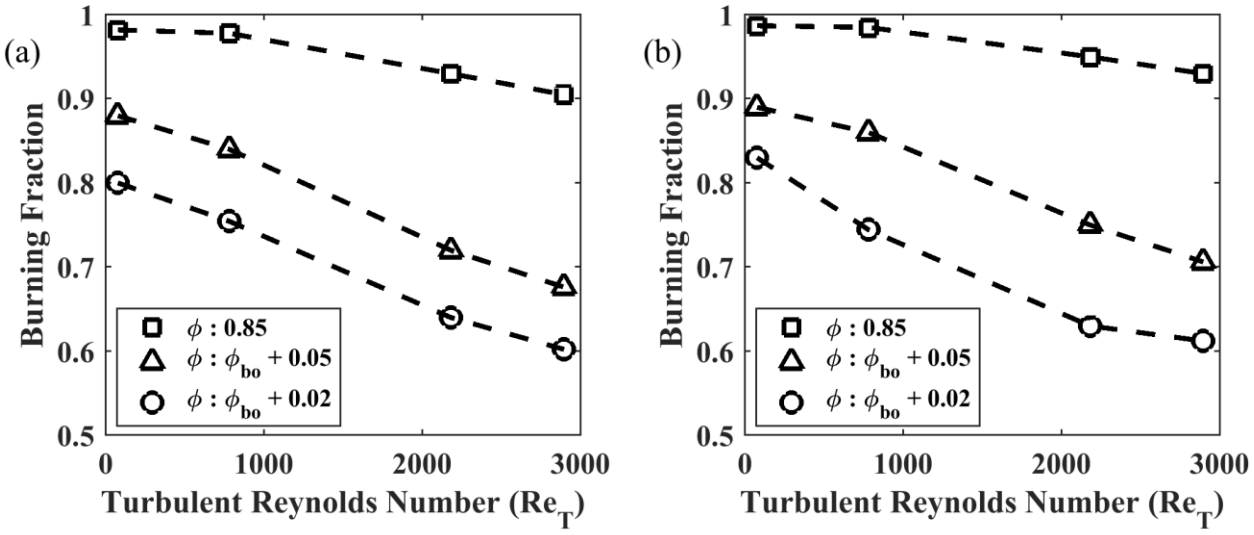

Fig. 5.13. Estimates of burning fraction for flames away and near to blowoff corresponding to (a) methane/air and (b) ethylene/air

5.2.5. Asymmetric Index

As blowoff is approached, the general shape of methane/- and ethylene/air flames were observed to intermittently shift from varicose to sinuous mode, as had been observed for propane/air flames. Lieuwen *et al.* [80] has proposed that the simultaneous presence of the sinuous wake and flame extinction events are required for flame blowoff. The effect of the sinuous wake in pulling the unburned reactants into the recirculation zone has been shown for ethylene/air flames in Fig. 5.9. From the past works of Mehta *et al.* [61] and Emerson *et al.* [62], it is known that this shift in the flame shape primarily occurs due to reduction of the density ratio between the flame and its surrounding. Analysis of the PLIF images show that relative to propane/air flame, more number of images are observed for methane/- and ethylene/air flames which have flame structures and vorticity field similar to those shown in Fig. 5.7c and Fig. 5.8c. Therefore, to quantify this observation asymmetric index has been evaluated by estimating the correlation coefficient between the left and right wings of the flame segment as outlined in Section 4.2.6. The variation of the correlation coefficient for methane/- and ethylene/air flames is shown in Fig. 5.14 a and b, respectively. For comparison with propane/air flames, its correlation coefficient is also shown in Fig. 5.14c. For all the near blowoff flames, the correlation coefficient is observed to switch sign from positive to negative which is indicative of growing asymmetric motion across the flame edges. As the turbulence intensity is increased, significant reduction of the coefficient is also observed. However, it is interesting to note that for methane/- and ethylene/air flames, the magnitude of the negative correlations are higher relative to that of propane/air flames as the turbulence Reynolds number increases. This indicates stronger interaction of the sinuous wake with the near blowoff flames of methane/- and ethylene/air. Based on the understanding from the previous research [61,62], this variation can be attributed to lower

temperature ratio across the flame sheet. This can be partially attributed to the fact that near blowoff methane/- and ethylene/air flames have lower adiabatic flame temperature relative to that of propane/air flames as their blowoff equivalence ratios were significantly lower. However, this argument is speculative at the moment and a direct measurement of the entrainment rate and temperature would be more conclusive.

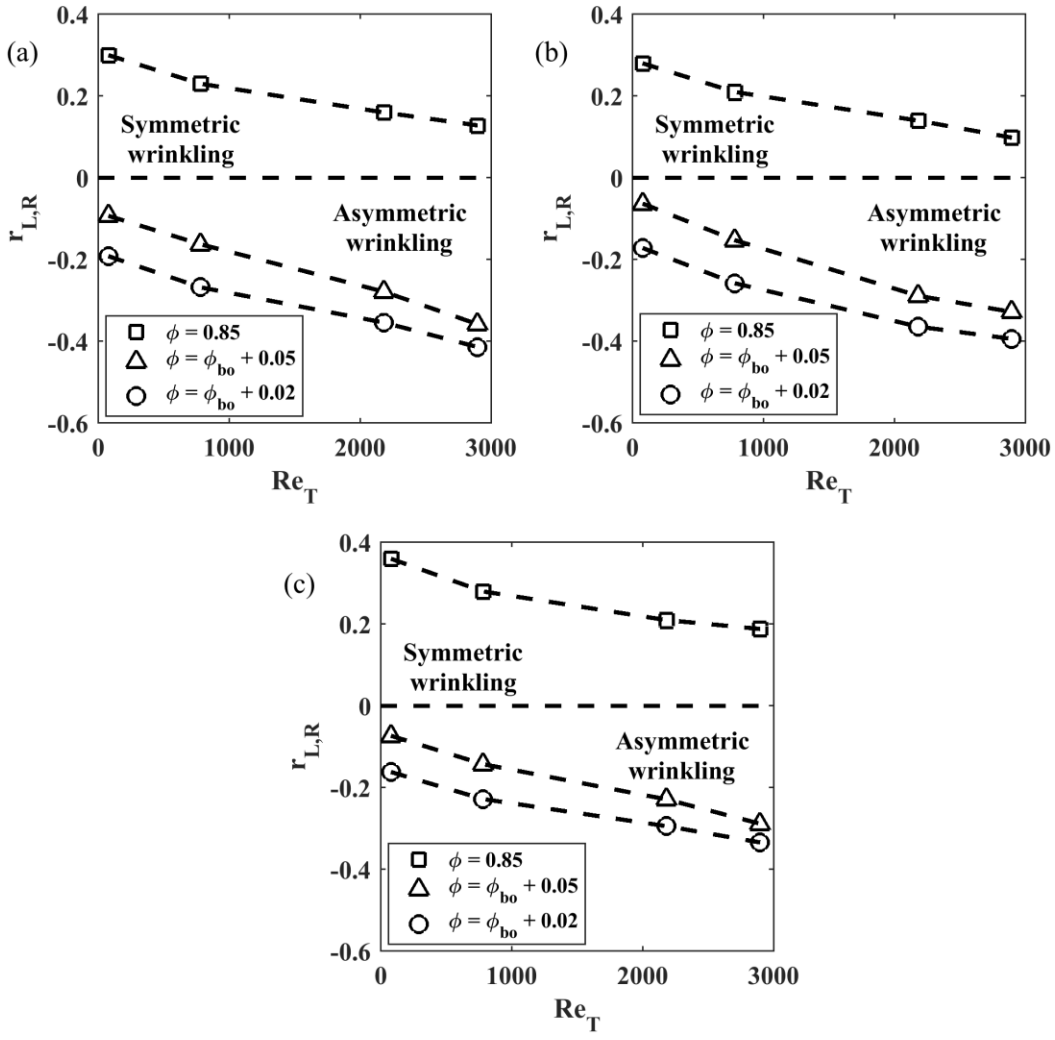

Fig. 5.14. Variation of correlation coefficient for (a) methane/air flames (b) ethylene/air flames and (c) propane/air flames. Measurements are shown for the axial position of peak flame response.

5.2.6. 2-D Curvature

From the instantaneous PLIF images shown in Fig. 5.3 –Fig. 5.8, it was observed that flame front edge had significant distortion as blowoff was approached. This local response of the flame front surface was assessed by evaluating the 2-D flame front curvature statistics. The variation of the pdfs of curvature for methane/- and ethylene/air flames are shown in Fig. 5.15 at turbulence intensities of 14 and 30%. For all the flames, at conditions approaching blowoff the pdfs are seen to widen owing to stronger corrugations of the flame front due to interaction with the shear layer vortices as well as due to the presence of strong sinuous wake in the flow. For near blowoff flames, the distributions are slightly skewed towards positive curvature. The distribution is seen to be wider at the intense turbulence condition for both methane/- and ethylene/air flames.

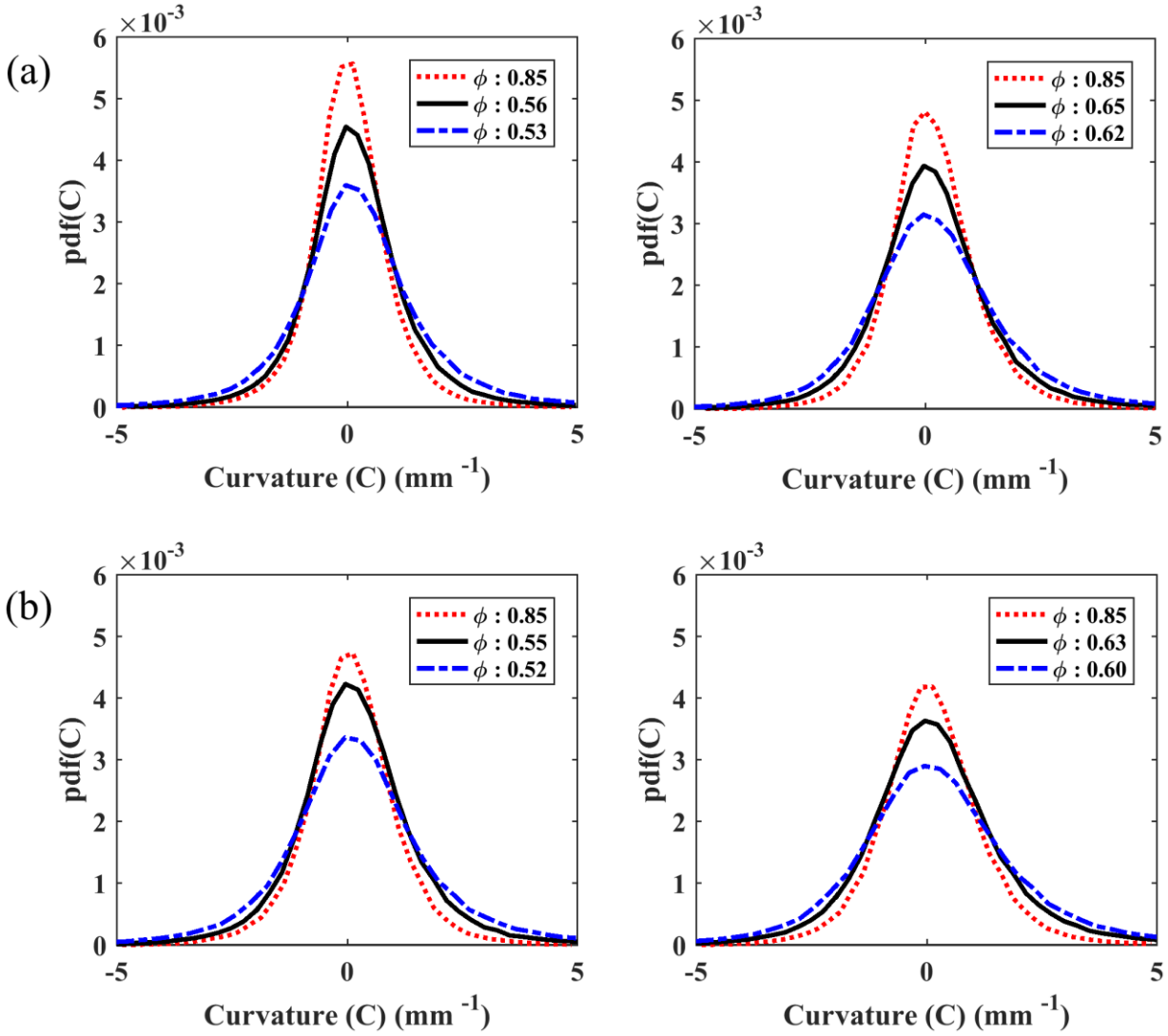

Fig. 5.15. Pdfs of 2-D curvature for (a) methane/air flames (b) ethylene/air flames. First and second column represent the variation for turbulence intensities of 14 and 30%.

5.3 Discussion

Based on the PLIF images and velocity field information acquired for near blowoff flames of methane/-, propane/- and ethylene/air, it is observed that the sequence of events through which the bluff body stabilized flame transitions to blowoff is similar which can be summarized as follows: As the equivalence ratio is lowered, the flame becomes narrower in shape owing to

reduction of flame speed and the flame fronts overlaps with the higher vorticity regions of the shear layer. This induces high strain rates on the flame which results in localized extinctions along the flame sheet where local strain rate exceeds the extinction strain rate which provides multiple regions for penetration of unburned reactants into the recirculation zone. The resulting reduction of the density between flame and its surrounding strengthens the BVK instability and thus, sinuous wakes are observed at conditions close to blowoff. The presence of sinuous wake and localized extinctions aid in the penetration of the cold reactants into the recirculation zone and thus, lowering the temperature of the recirculation zone. This ultimately leads to blowoff when the shear layer fails to re-ignite.

From this understanding of the sequence of events, it is realized that the most important factor governing the inception of the blowoff process is the turbulent flame speed. From the results discussed in Chapter 3, it is known that at for robustly burning flames at ϕ= 0.85 and identical turbulence intensity, the flame speed for propane/air was lowest followed by methane/- and ethylene/air. Thus, at robustly burning condition propane/air flames reside in closest proximity to the shear layer relative to methane/- and ethylene/air flames and for a lower reduction in equivalence ratio, the flame speed decreases such that the flame fronts shift onto the higher vorticity regions of the shear layer whereas significant reduction in equivalence ratio is required for the methane/- and ethylene/air flames.

To examine the effect of strain rate exerted on the flame based on its position, mean strain rate was estimated for each flame at different axial distances from the bluff body by using the relation:

$$\kappa_s = -n_x \text{ x } n_y \text{ x } \left(\frac{\partial \text{u}}{\partial \text{y}} + \frac{\partial \text{v}}{\partial \text{x}}\right) + (1 - n_x^2) \text{ x } \frac{\partial \text{u}}{\partial \text{x}} + \left(1 - n_y^2\right) \text{ x } \frac{\partial v}{\partial y} \quad (1)$$

The individual terms in Equation (1) can be decomposed into the contribution of shear ($\kappa_{s,shear}$) and normal strain ($\kappa_{s,normal}$) with respect to the flame sheet [81,82], where

$$\kappa_{s,shear} = -n_x \text{ x } n_y \text{ x } \left(\frac{\partial \text{u}}{\partial \text{y}} + \frac{\partial \text{v}}{\partial \text{x}}\right) \quad (2)$$

$$\kappa_{s,normal} = (1 - n_x^2) \text{ x } \frac{\partial \text{u}}{\partial \text{x}} + \left(1 - n_y^2\right) x \frac{\partial v}{\partial y} \quad (3)$$

The $\kappa_{s,normal}$ term describes the impact of flow acceleration and deceleration, while $\kappa_{s,shear}$ quantifies the manner in which shearing flow strain translates into flame stretch. Both terms are clearly non-zero in regions of high shear in flame stabilization regions. The contribution of the shear and normal flow components are highly sensitive to the relative inclination of the flame to the flow, through the n_x and n_y terms in Eqs. (2-3). The data presented in this section is for the intense turbulence condition. Similar variation has been observed at other turbulence intensities.

The variation of mean strain rate and its components for methane/-, propane/- and ethylene/air flames at conditions away and near to blowoff are shown in Fig. 5.16 - Fig. 5.18. For each case, the normal, shear and total strain has been normalized by the corresponding extinction strain rate evaluated using OPPDIF [65]. From Fig. 5.16 - Fig. 5.18, it is clearly seen that as blowoff is approached, the strain rates exerted on the flame increases significantly. At conditions closest to blowoff, it is observed that significant portion of the flame sheet experiences mean strain rates that exceed their corresponding extinction strain rate. For methane/air flames, the normal strain component is observed to play a dominating role at conditions near blowoff whereas for propane/air flames, the shear strain component contributes significantly to the total strain. However, for ethylene/air flames the two components are observed to be of comparable

magnitude. This variation of mean strain rate clearly explains the observation that frequency of localized extinction increases significantly as blowoff is approached.

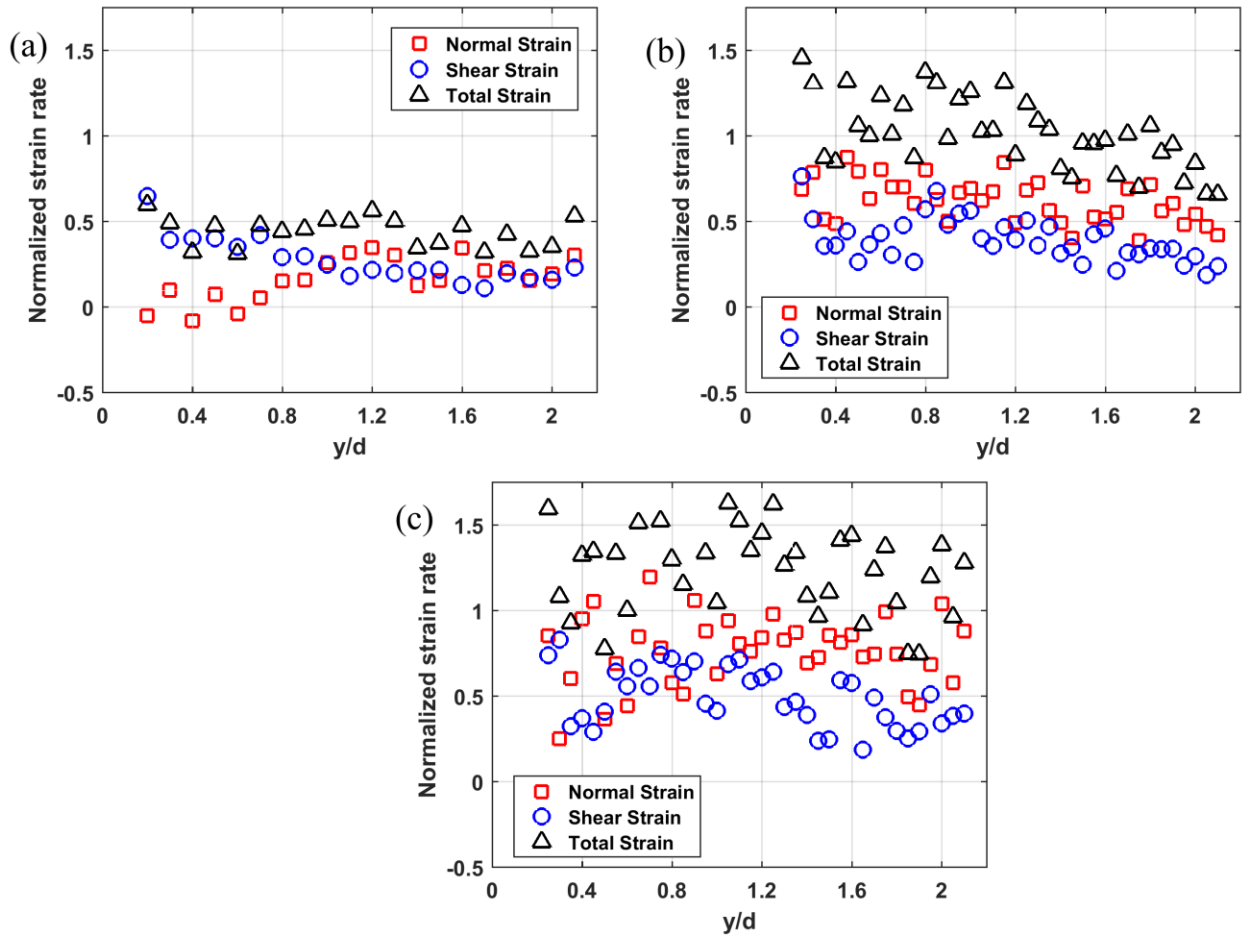

Fig. 5.16. Variation of mean strain rate for methane/air flames for T.I: 30% at (a) ϕ=0.85 (b) ϕ=0.65 and (c) ϕ=0.62

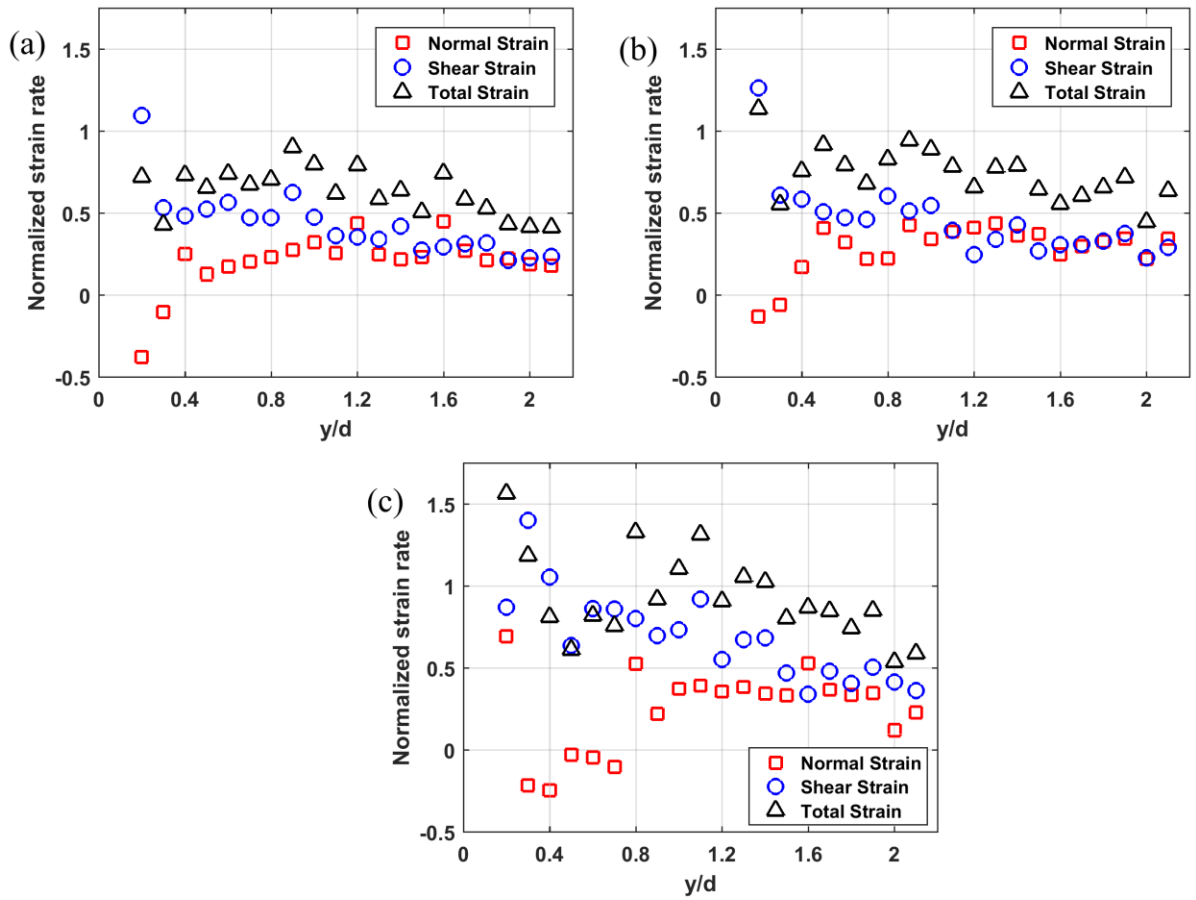

Fig. 5.17. Variation of mean strain rate for propane/air flames for T.I: 30% at (a) ϕ=0.85 (b) ϕ=0.81 and (c) ϕ=0.78

Comparing the condition of methane/-, propane/- and ethylene/air at ϕ= 0.85 (shown in Fig. 5.16 - Fig. 5.18a) clearly shows that the strain experienced by propane/air flames is much closer to its extinction strain rate relative to methane/- and ethylene/air flames. This can be attributed to the lower flame speed owing to the propane/air flames residing in close proximity to the higher vorticity regions of the shear layer. As the equivalence ratio is reduced to 0.78 strain rate experienced by the propane/air flame significantly increases relative to the corresponding extinction strain rate, as shown in Fig. 5.17c. For comparison, additional experiments were

performed for methane/- and ethylene/air flames at ϕ = 0.78 and the corresponding variation of mean strain rate is shown in Fig. 5.19. For both of these flames, the mean strain is observed to increase slightly relative to the stably burning condition at ϕ = 0.85 and this can be attributed to the decrease in turbulent flame speed which shifts the flame relatively closer to the shear layer. As the flame speed of methane/- and ethylene/air flames were much higher than propane/air flames, significant reduction in equivalence ratio causes these flames to overlap with the higher vorticity regions of the shear layer.

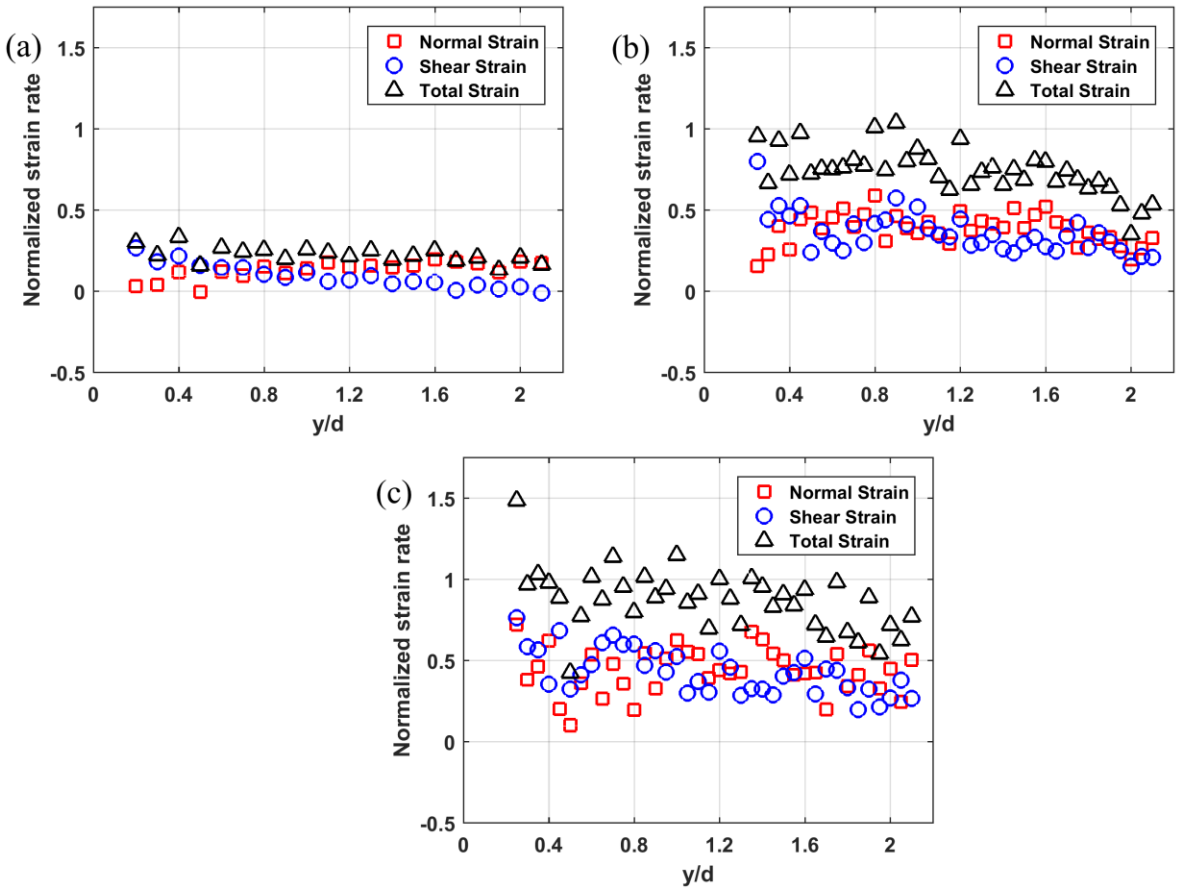

Fig. 5.18. Variation of mean strain rate for ethylene/air flames for T.I: 30% at (a) ϕ=0.85 (b) ϕ=0.63 and (c) ϕ=0.60

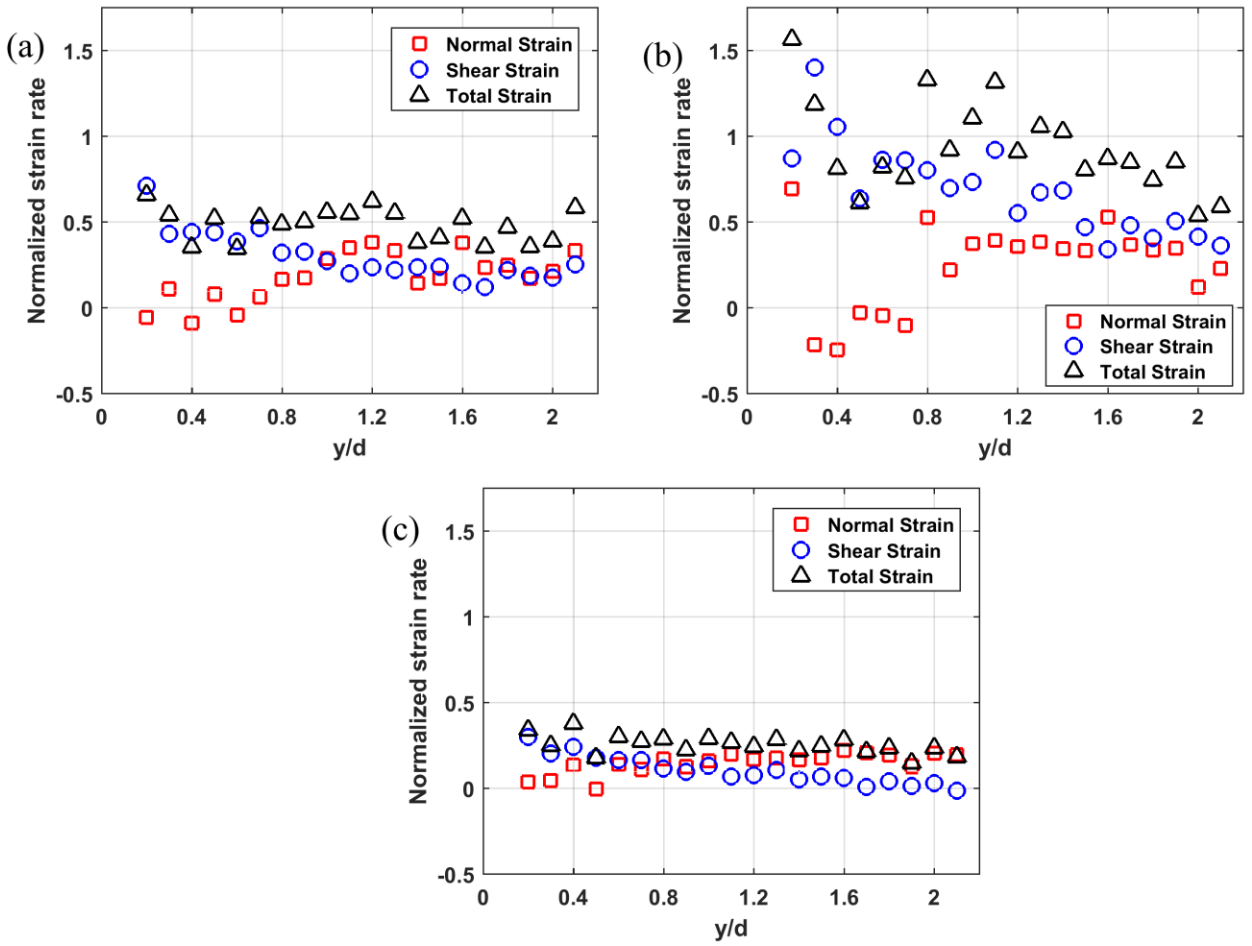

Fig. 5.19. Variation of mean strain rate for flames at T.I: 30% and ϕ=0.78 for (a) methane/air flames (b) propane/air flames and (c) ethylene/air flames

5.4 Concluding Remarks

In this chapter, the effect of fuel properties on the blowoff dynamics of a bluff body stabilized flame was presented. For both methane/- and ethylene/air flames, the blowoff equivalence ratio was observed to increase with increasing turbulence intensity. It was observed that these values were much lower than that obtained for propane/air flames at identical flow conditions. Detailed flame structure was investigated by simultaneous OH PLIF, CH_2O PLIF and PIV to determine the sequence of events leading to blowoff. Near blowoff, the flame front entangled with the high

vorticity region along the shear layer which exerted high local strain that exceed the corresponding extinction stretch rates, resulting in local flame holes. As blowoff was approached, significant increase in the frequency of holes was observed along the flame sheet for low and moderate turbulence conditions. For the higher turbulence conditions, fragmentation of the flame along with the presence of sinuous wakes was observed which aided in the penetration of reactants into the recirculation zone. Measurements of the burning fraction quantified the degree of local extinctions at conditions near to blowoff. Enhanced corrugations along with modification of the flame fronts resulted in broadening of the curvature pdfs. Qualitatively similar behavior is observed for methane/-, propane/- and ethylene/air flames at conditions near blowoff even though the blowoff equivalence ratios differed. The variation of the blowoff equivalence ratio has been attributed to turbulent flame speed and has been shown by estimates of mean strain at different conditions.

CHAPTER SIX

6. Conclusions & Future Work

A novel turbulence generating arrangement was developed to study the effect of different levels of free stream turbulence on lean premixed, bluff-body stabilized flames. The turbulence intensities in the approach flow were varied from 4 to 30%. The most interesting feature of this arrangement is that the turbulence intensity levels were independent of the mean velocity. The integral length scales of the flow at the intense turbulence conditions (24 and 30 %) were comparable to those present in practical combustors. Detailed characterization of the flow field was performed by using hot wire anemometry and high-speed particle image velocimetry. Simultaneous imaging of hydroxyl (OH) and formaldehyde (CH_2O) by planar laser induced fluorescence and particle image velocimetry (PIV) was used to study the interaction between the flame and the flow field. A summary of the key conclusions from the work that were presented in previous chapters are consolidated in the following sections. Finally, this chapter closes with suggestions for further research.

6.1 Summary

6.1.1. Stably burning flames

The flame front structure was observed to be strongly dependent on the free stream turbulence level of the incoming fuel/air mixture as well on the properties of the fuel/air mixture. To study the effect of fuel properties, lean premixed methane/-, propane/- and ethylene/flames were investigated. The low turbulence intensity flame front featured weak corrugations and mostly symmetric flame structures with continuous heat release regions. Pronounced formation of cusps and unburnt mixture fingers were observed as the turbulence intensity was increased from 4 to

14 % without discontinuities in the heat release front. At the intense turbulence condition, the effect of the properties of the fuel/air mixture was clearly discernible. For methane/- and ethylene/air (ϕ = 0.85), localized extinctions along the flame sheet and flamelet merging were observed which created isolated pockets of CH_2O within the flame envelope with heat release regions along their boundary. In addition to these features, significant disintegration of the flame into multiple fragments was observed for propane/- and ethylene/air (ϕ = 0.655) flames. The general shape of these flames was observed to change intermittently from symmetric to asymmetric mode with increasing levels of free stream turbulence. The strain rate pdfs showed that flames under highly turbulent conditions experienced larger strain rates which lead to localized extinction zones along the flame surface. Burning fraction estimates for the different flames showed that the degree of localized extinctions was highest for lean propane/air flames and least for ethylene/air flames at ϕ = 0.85. The mean strain calculations along the flame sheet supported this observation. Enhanced wrinkling along with strong distortion of the flame fronts resulted in broadening of the curvature pdfs. The brush thickness increased with increasing turbulence intensity but for methane/-, propane/- and ethylene/air (ϕ= 0.655) saturated beyond 24 % while the two-dimensional flame surface density decreased for all the investigated conditions. As turbulence intensity was increased, the mean flame surface area ratio was observed to grow and eventually result in a non-linear behavior owing to merging, extinction and fragmentation events. Turbulent flame speed was computed based on the mean flame structure and their correlation revealed the dependency on molecular diffusivity and flow straining.

6.1.2. Near blowoff flames

The blowoff equivalence ratio was determined for methane/-, propane/- and ethylene/air flames for mean velocities of 5, 10 and 15 m/s at the different free stream turbulence levels. Apart from

the propane/air flames at apporach velcoity of 5 m/s and a turbulence intensity of 30 %, increasing turbulence intensity was found to reduce the flame stability. As blowoff was approached, the flame front was observed to overlap with the shear layer vortices which exerted high local strain rates on the flame front that exceed the extinction strain rate. This resulted in significant breaks along the reaction zone. At conditions near blowoff, significant increase in the frequency of breaks along the reaction zone was observed for low and moderate turbulence conditions. For the higher turbulence conditions, fragmentation of the flame along with the presence of sinuous wakes was observed which aided in the penetration of reactants into the recirculation zone, leading to the presence of low temperature combustion processes inside the recirculation zone at conditions very close to lean extinction. Mean strain rates computed along the flame sheet supported the observation of increased localized quenching for the near blowoff flames. Velocity vectors near the flame holes indicate the penetration of the reactants into the recirculation zone, leading to the presence of low temperature combustion processes inside the recirculation zone at conditions very close to lean extinction. Mostly similar sequence of events were observed for methane/-, propane/- and ethylene/air flames near blowoff. However, the blowoff equivalence ratios were observed to be influenced by the fuel/air mixture. Based on the observation of the flame - flow interaction, turbulence flame speed was attributed to be the primary factor governing the blowoff equivalence ratio.

6.2 Future Work

- *Temperature Measurements*: Under the intense turbulence condition, the general shape of robustly burning propane/- and ethylene/air (ϕ= 0.655) flames was observed to intermittently switch from varicose to sinuous mode which had previously been observed only for near blowoff flames. Based on the past studies [61,62], this has been attributed to reduction in

density ratio between the flame and its surrounding. There is a large scatter in the critical values of the density ratio at which this phenomenon occurs. Direct measurements of temperature and velocity field by simultaneous two-line OH PLIF thermometry and particle image velocimetry can be more conclusive in testing this hypothesis. Also, at conditions near blowoff, the effect of entrained reactants on the thermal state of the recirculation zone can be better understood by temperature measurements of the gases in the recirculation zone.

- *Examining the behavior of practical fuels:* An experimental setup has been developed which can pre-vaporize liquid hydrocarbon fuels and create a premixed fuel/air mixture that can be fed into the burner. Using this arrangement, characteristics of practical liquid fuels under intense turbulence conditions can be studied. Large hydrocarbon transportation fuels exhibit strong low temperature chemistry behavior which can significantly modify the flame front structures as has been demonstrated in the recent work by Won *et al.* [83] for n-heptane/air flames stabilized in a slot burner. However, in this work of Won *et al.* [83], the turbulence intensity was limited to 14% and the integral length scales were varied up to 4 mm. Detailed studies of turbulent premixed flames of heavy hydrocarbon fuels under highly turbulent conditions are necessary as the presence of the low temperature chemistry behavior can strongly modify the characteristics of stably burning flames as well as the blowoff dynamics.

- *Effect of bluff body geometry:* The flow field associated with a two-dimensional bluff body is different compared to that of an axisymmetric bluff body which can modify the blowoff equivalence ratios and flame-flow interactions. Also, the blockage ratio of the bluff body has been shown to affect the sequence of events leading to flame blowoff. Detailed study of the planar flame front structure and comparison with the results of the present study would be useful.

References

[1] B. Bender, Lean Pre-mixed Combustion, NETL Gas Turbine Handb. (2006) 217–227. http://www.netl.doe.gov/technologies/coalpower/turbines/refshelf/handbook/TableofContents.html.

[2] J.F. Driscoll, Turbulent premixed combustion: Flamelet structure and its effect on turbulent burning velocities, Prog. Energy Combust. Sci. 34 (2008) 91–134. doi:10.1016/j.pecs.2007.04.002.

[3] P. Clavin, Dynamic behavior of premixed flame fronts in laminar and turbulent flows, Prog. Energy Combust. Sci. 11 (1985) 1–59. doi:10.1016/0360-1285(85)90012-7.

[4] A.N. Lipatnikov, J. Chomiak, Turbulent flame speed and thickness: Phenomenology, evaluation, and application in multi-dimensional simulations, Prog. Energy Combust. Sci. 28 (2002) 1–74. doi:10.1016/S0360-1285(01)00007-7.

[5] I.G. Shepherd, Flame surface density and burning rate in premixed turbulent flames, in: Symp. Combust., 1996: pp. 373–379.

[6] A. Buschmann, F. Dinkelacker, T. Schäfer, M. Schäfer, J. Wolfrum, Measurement of the instantaneous detailed flame structure in turbulent premixed combustion, Symp. Combust. 26 (1996) 437–445. doi:10.1016/S0082-0784(96)80246-3.

[7] Y.-C. Chen, R.W. Bilger, Experimental Investigation of Three-Dimensional Flame- Front Structure in Premixed Turbulent Combustion — I : Hydrocarbon / Air Bunsen Flames, Combust. Flame. 131 (2006) 400–435. doi:10.1016/S0010-2180(02)00418-2.

[8] M.J. Dunn, A.R. Masri, R.W. Bilger, R.S. Barlow, G.H. Wang, The compositional structure of highly turbulent piloted premixed flames issuing into a hot coflow, Proc. Combust. Inst. 32 II (2009) 1779–1786. doi:10.1016/j.proci.2008.08.007.

[9] J.E.G. Temme, T.M. Wabel, A.W. Skiba, J.F. Driscoll, Measurements of premixed turbulent combustion regimes of high Reynolds number flames, in: 53rd AIAA Aerosp. Sci. Meet. Kissimmee, FL, January, 2015.

[10] A.W. Skiba, T.M. Wabel, J. Temme, J.F. Driscoll, Experimental Assessment of Premixed Flames Subjected to Extreme Turbulence, AIAA Aerosp. Sci. Meet. 54 (2016) 1454. doi:10.2514/6.2016-1454.

[11] T.M. Wabel, A.W. Skiba, J.E. Temme, J.F. Driscoll, Measurements to determine the regimes of premixed flames in extreme turbulence, Proc. Combust. Inst. 0 (2016) 1–8. doi:10.1016/j.proci.2016.08.065.

[12] R. Borghi, On the structure and morphology of turbulent premixed flames, in: Recent Adv. Aerosp. Sci., Springer, 1985: pp. 117–138.

[13] A.W. Skiba, T.M. Wabel, C.D. Carter, S.D. Hammack, E. Jacob, J.F. Driscoll, The structure of turbulent premixed flames subjected to extreme turbulence and the

development of a new measured regime diagram, (2017) 5–10.

[14] S. Kheirkhah, O.L. Gülder, Turbulent premixed combustion in V-shaped flames: Characteristics of flame front, Phys. Fluids. 25 (2013). doi:10.1063/1.4807073.

[15] S. Kheirkhah, L. Gülder, Topology and brush thickness of turbulent premixed V-shaped flames, Flow, Turbul. Combust. 93 (2014) 439–459. doi:10.1007/s10494-014-9563-3.

[16] S. Kheirkhah, Ö.L. Gülder, Consumption speed and burning velocity in counter-gradient and gradient diffusion regimes of turbulent premixed combustion, Combust. Flame. 162 (2015) 1422–1439. doi:10.1016/j.combustflame.2014.11.009.

[17] P. Goix, P. Paranthoen, M. Trinite, A tomographic study of measurements in a V-shaped H2 air flame and a lagrangian interpretation of the turbulent flame brush evolution, Combust. Flame. 81 (1990) 229–241.

[18] H. Guo, B. Tayebi, C. Galizzi, D. Escudié, Burning rates and surface characteristics of hydrogen-enriched turbulent lean premixed methane-air flames, Int. J. Hydrogen Energy. 35 (2010) 11342–11348. doi:10.1016/j.ijhydene.2010.07.066.

[19] M. Namazian, I.G. Shepherd, L. Talbot, Characterization of the density fluctuations in turbulent V-shaped premixed flames, Combust. Flame. 64 (1986) 299–308. doi:10.1016/0010-2180(86)90147-1.

[20] D. Veynante, J. Piana, J.M. Duclos, C. Martel, Experimental analysis of flame surface density models for premixed turbulent combustion, Symp. Combust. 26 (1996) 413–420. doi:10.1016/S0082-0784(96)80243-8.

[21] T. Sponfeldner, N. Soulopoulos, F. Beyrau, Y. Hardalupas, A.M.K.P. Taylor, J.C. Vassilicos, The structure of turbulent flames in fractal- and regular-grid-generated turbulence, Combust. Flame. 162 (2015) 3379–3393. doi:10.1016/j.combustflame.2015.06.004.

[22] S.S. Sattler, D.A. Knaus, F.C. Gouldin, Determination of three-dimensional flamelet orientation distributions in turbulent V-flames from two-dimensional image data, Proc. Combust. Inst. 29 (2002) 1785–1792. doi:10.1016/S1540-7489(02)80216-4.

[23] E.E. Zukoski, F.E. Marble, The role of wake transition in the process of flame stabilization on bluff bodies, AGARD Combust. Res. Rev. (1955) 167–180.

[24] E.E. Zukoski, F.E. Marble, Experiments Concerning the Mechanism of Flame Blowoff From Bluff Bodies, Proc. Gas Dyn. Symp. Aerothermochemistry. (1956) 205–2010.

[25] G.C. Williams, H.C. Hottel, A.C. Scurlock, Flame stabilization and propagation in high velocity gas streams, in: Symp. Combust. Flame, Explos. Phenom., 1948: pp. 21–40.

[26] J.P. Longwell, Flame stabilization by bluff bodies and turbulent flames in ducts, in: Symp. Combust., 1953: pp. 90–97.

[27] S.L. Plee, A.M. Mellor, Characteristic time correlation for lean blowoff of bluff-body-

stabilized flames, Combust. Flame. 35 (1979) 61–80. doi:10.1016/0010-2180(79)90007-5.

[28] K.V.L. Rao, A.H. Lefebvre, Flame Blowoff Studies Using Large-Scale Flameholders, J. Eng. Power. 104 (1982) 853–857. http://dx.doi.org/10.1115/1.3227355.

[29] N.K. Rizk, A.H. Lefebvre, Influence of laminar flame speed on the blowoff velocity of bluff-body-stabilized flames, AIAA J. 22 (1984) 1444–1447.

[30] S.J. Shanbhogue, S. Husain, T. Lieuwen, Lean blowoff of bluff body stabilized flames: Scaling and dynamics, Prog. Energy Combust. Sci. 35 (2009) 98–120. doi:10.1016/j.pecs.2008.07.003.

[31] S. Yamaguchi, N. Ohiwa, T. Hasegawa, Structure and blow-off mechanism of rod-stabilized premixed flame, Combust. Flame. 62 (1985) 31–41. doi:10.1016/0010-2180(85)90091-4.

[32] B. Kiel, K. Garwick, J.R. Gord, J. Miller, A. Lynch, R. Hill, S. Phillips, A Detailed Investigation of Bluff Body Stabilized Flames, 45th AIAA Aerosp. Sci. Meet. Exhib. (2007) 0–9. doi:10.2514/6.2007-168.

[33] S. Nair, T. Lieuwen, Acoustic Detection of Blowout in Premixed Flames, J. Propuls. Power. 21 (2005) 32–39. doi:10.2514/1.5658.

[34] S. Nair, T.C. Lieuwen, Near-Blowoff Dynamics of a Bluff-Body Stabilized Flame, J. Propuls. Power. 23 (2007) 421–427. doi:10.2514/1.24650.

[35] S. Chaudhuri, S. Kostka, M.W. Renfro, B.M. Cetegen, Blowoff dynamics of bluff body stabilized turbulent premixed flames, Combust. Flame. 157 (2010) 790–802. doi:10.1016/j.combustflame.2009.10.020.

[36] S. Chaudhuri, S. Kostka, S.G. Tuttle, M.W. Renfro, B.M. Cetegen, Blowoff mechanism of two dimensional bluff-body stabilized turbulent premixed flames in a prototypical combustor, Combust. Flame. 158 (2011) 1358–1371. doi:10.1016/j.combustflame.2010.11.012.

[37] S.G. Tuttle, S. Chaudhuri, S. Kostka, K.M. Kopp-Vaughan, T.R. Jensen, B.M. Cetegen, M.W. Renfro, Time-resolved blowoff transition measurements for two-dimensional bluff body-stabilized flames in vitiated flow, Combust. Flame. 159 (2012) 291–305. doi:10.1016/j.combustflame.2011.06.001.

[38] S.G. Tuttle, S. Chaudhuri, K.M. Kopp-Vaughan, T.R. Jensen, B.M. Cetegen, M.W. Renfro, J.M. Cohen, Lean blowoff behavior of asymmetrically-fueled bluff body-stabilized flames, Combust. Flame. 160 (2013) 1677–1692. doi:10.1016/j.combustflame.2013.03.009.

[39] J.R. Dawson, R.L. Gordon, J. Kariuki, E. Mastorakos, A.R. Masri, M. Juddoo, Visualization of blow-off events in bluff-body stabilized turbulent premixed flames, Proc. Combust. Inst. 33 (2011) 1559–1566. doi:10.1016/j.proci.2010.05.044.

[40] J. Kariuki, J.R. Dawson, E. Mastorakos, Measurements in turbulent premixed bluff body

flames close to blow-off, Combust. Flame. 159 (2012) 2589–2607. doi:10.1016/j.combustflame.2012.01.005.

[41] J. Kariuki, A. Dowlut, R. Yuan, R. Balachandran, E. Mastorakos, Heat release imaging in turbulent premixed methane-air flames close to blow-off, Proc. Combust. Inst. 35 (2015) 1443–1450. doi:10.1016/j.proci.2014.05.144.

[42] J. Kariuki, A. Dowlut, R. Balachandran, E. Mastorakos, Heat Release Imaging in Turbulent Premixed Ethylene-Air Flames Near Blow-off, Flow, Turbul. Combust. 96 (2016) 1039–1051. doi:10.1007/s10494-016-9720-y.

[43] D.R. Ballal, A.H. Lefebvre, Weak Extinction Limits of Turbulent Flowing Mixtures, J. Eng. Power. 101 (1979) 343–348. doi:10.1115/1.3230272.

[44] B.C. Huelskamp, The Development of a Correlation to Predict the Lean Blowout of Bluff Body Stabilized Flames with a Focus on Relevant Timescales and Fuel Characteristics, University of Dayton, 2013.

[45] G. Coppola, A. Gomez, Experimental investigation on a turbulence generation system with high-blockage plates, Exp. Therm. Fluid Sci. 33 (2009) 1037–1048. doi:10.1016/j.expthermflusci.2009.06.001.

[46] R.W. Schaefer, A. V Oppenheim, Discrete-time signal processing, D Prentice-Hall. (1989).

[47] M.J. Barrett, D.K. Hollingsworth, On the calculation of length scales for turbulent heat transfer correlation, 1999.

[48] R.J. Kee, J.F. Grcar, M.D. Smooke, J.A. Miller, E. Meeks, PREMIX: a Fortran program for modeling steady laminar one-dimensional premixed flames, Sandia Natl. Lab. Rep. (1985).

[49] H. Wang, X. You, A. V Joshi, S.G. Davis, A. Laskin, F. Egolfopoulos, C.K. Law, USC Mech Version II. High-Temperature Combustion Reaction Model of H2/CO/C1-C4 Compounds, (2007).

[50] B. Zhou, C. Brackmann, Q. Li, Z. Wang, P. Petersson, Z. Li, M. Ald??n, X. song Bai, Distributed reactions in highly turbulent premixed methane/air flames. Part I. Flame structure characterization, Combust. Flame. 162 (2015) 2937–2953. doi:10.1016/j.combustflame.2014.12.021.

[51] C.K. Law, C.J. Sung, Structure, aerodynamics, and geometry of premixed flamelets, Prog. Energy Combust. Sci. 26 (2000) 459–505. doi:10.1016/S0360-1285(00)00018-6.

[52] S. Chaudhuri, B.M. Cetegen, Blowoff characteristics of bluff-body stabilized conical premixed flames with upstream spatial mixture gradients and velocity oscillations, Combust. Flame. 153 (2008) 616–633. doi:10.1016/j.combustflame.2007.12.008.

[53] J.L. Delfau, J. Biet, M. Idir, L. Pillier, C. Vovelle, Experimental and numerical study of premixed, lean ethylene flames, Proc. Combust. Inst. 31 I (2007) 357–365.

doi:10.1016/j.proci.2006.07.167.

[54] C.K. Westbrook, F.L. Dryer, K.P. Schug, A comprehensive mechanism for the pyrolysis and oxidation of ethylene, Symp. Combust. 19 (1982) 153–166. doi:10.1016/S0082-0784(82)80187-2.

[55] R.K. Cheng, I.G. Shepherd, B. Bédat, L. Talbot, Premixed turbulent flame structures in moderate and intense isotropic turbulence, 2002. doi:10.1080/713712911.

[56] I.G. Shepherd, R.K. Cheng, The burning rate of premixed flames in moderate and intense turbulence, Combust. Flame. 127 (2001) 2066–2075. doi:10.1016/S0010-2180(01)00309-1.

[57] Y.C. Chen, N. Peters, G.A. Schneemann, N. Wruck, U. Renz, M.S. Mansour, The detailed flame structure of highly stretched turbulent premixed methane-air flames, Combust. Flame. 107 (1996) 223–244. doi:10.1016/S0010-2180(96)00070-3.

[58] A.N. Lipatnikov, J. Chomiak, V.A. Sabelnikov, S. Nishiki, T. Hasegawa, Unburned mixture fingers in premixed turbulent flames, Proc. Combust. Inst. 35 (2015) 1401–1408. doi:10.1016/j.proci.2014.06.081.

[59] S.A. Filatyev, J.F. Driscoll, C.D. Carter, J.M. Donbar, Measured properties of turbulent premixed flames for model assessment, including burning velocities, stretch rates, and surface densities, Combust. Flame. 141 (2005) 1–21. doi:10.1016/j.combustflame.2004.07.010.

[60] J.R. Osborne, S.A. Ramji, C.D. Carter, S. Peltier, S. Hammack, T. Lee, A.M. Steinberg, Simultaneous 10 kHz TPIV, OH PLIF, and CH2O PLIF measurements of turbulent flame structure and dynamics, Exp. Fluids. 57 (2016). doi:10.1007/s00348-016-2151-7.

[61] P.G. Mehta, M.C. Soteriou, Combustion heat release effects on the dynamics of bluff body stabilized premixed reacting flows, in: 41st Aerosp. Sci. Meet. Exhib., 2003.

[62] B. Emerson, J. O'Connor, M. Juniper, T. Lieuwen, Density ratio effects on reacting bluff-body flow field characteristics, J. Fluid Mech. 706 (2012) 219–250. doi:10.1017/jfm.2012.248.

[63] H. Wang, E.R. Hawkes, J.H. Chen, B. Zhou, Z. Li, M. Aldén, Direct numerical simulations of a high Karlovitz number laboratory premixed jet flame – an analysis of flame stretch and flame thickening, J. Fluid Mech. 815 (2017) 511–536. doi:10.1017/jfm.2017.53.

[64] N. Peters, Turbulent Combustion, Meas. Sci. Technol. 12 (2001) 2022–2022. doi:10.1088/0957-0233/12/11/708.

[65] A.E. Lutz, R.J. Kee, J.F. Grcar, F.M. Rupley, OPPDIF: A Fortran program for computing opposed-flow diffusion flames, 1997.

[66] C. Meneveau, T. Poinsot, Stretching and quenching of flamelets in premixed turbulent combustion, Combust. Flame. 86 (1991) 311–332.

[67] A.M. Steinberg, J.F. Driscoll, Straining and wrinkling processes during turbulence-premixed flame interaction measured using temporally-resolved diagnostics, Combust. Flame. 156 (2009) 2285–2306. doi:10.1016/j.combustflame.2009.06.024.

[68] C.J. Rutland, A. Trouvé, Direct simulations of premixed turbulent flames with nonunity Lewis numbers, Combust. Flame. 94 (1993) 41–57. doi:10.1016/0010-2180(93)90018-X.

[69] J. Yuan, Y. Ju, C.K. Law, Effects of turbulence and flame instability on flame front evolution, Phys. Fluids. 18 (2006). doi:10.1063/1.2359744.

[70] M.Z. Haq, C.G.W. Sheppard, R. Woolley, D.A. Greenhalgh, R.D. Lockett, Wrinkling and curvature of laminar and turbulent premixed flames, Combust. Flame. 131 (2002) 1–15. doi:10.1016/S0010-2180(02)00383-8.

[71] J. Kariuki, J.R. Dawson, E. Mastorakos, Measurements in turbulent premixed bluff body flames close to blow-off, Combust. Flame. 159 (2012) 2589–2607. doi:10.1016/j.combustflame.2012.01.005.

[72] G. Damkohler, Jahrb. deut. Luftfahrtforsch, Z. Electrochem. 46 (1940) 113.

[73] R. Balachandran, B.O. Ayoola, C.F. Kaminski, a P. Dowling, E. Mastorakos, Experimental investigation of the non linear response of turbulent premixed flames to imposed inlet velocity oscillations, Combust. Flame. 143 (2005) 37–55. doi:10.1016/j.combustflame.2005.04.009.

[74] J.C. Pan, M.D. Vangsness, D.R. Ballal, Aerodynamics of bluff-body stabilised confined turbulent premixed flames, J. Eng. Gas Turb. Power. 114 (1992) 783–789.

[75] T. Poinsot, D. Veynante, Theoretical and Numerical Combustion (Flourtown, PA: RT Edwards), (2001).

[76] C.J. Sung, C.K. Law, Extinction mechanisms of near-limit premixed flames and extended limits of flammability, Symp. Combust. 26 (1996) 865–873. doi:10.1016/S0082-0784(96)80296-7.

[77] M.K. Geikie, K.A. Ahmed, Lagrangian mechanisms of flame extinction for lean turbulent premixed flames, Fuel. 194 (2017) 239–256.

[78] E. Mastorakos, A. Taylor, J.H. Whitelaw, Extinction of turbulent counterflow flames with reactants diluted by hot products, Combust. Flame. 102 (1995) 101–114.

[79] C.E. Smith, D. Nickolaus, T. Leach, B. Kiel, K. Garwick, LES blowout analysis of premixed flow past V-gutter flameholder, AIAA Pap. 170 (2007). doi:10.2514/6.2007-170.

[80] T. Lieuwen, S. Shanbhogue, Dynamics of Bluff Body Flames near Blowoff, 45th AIAA Aerosp. Sci. Meet. Exhib. (2007) 1–13.

[81] C.W. Foley, I. Chterev, J. Seitzman, T. Lieuwen, High Resolution Particle Image Velocimetry and CH-PLIF Measurements and Analysis of a Shear Layer Stabilized

Flame, J. Eng. Gas Turbines Power. 138 (2015) 31603. doi:10.1115/1.4031367.

[82] T.C. Lieuwen, Unsteady combustor physics, Cambridge University Press, 2012.

[83] S.H. Won, B. Windom, B. Jiang, Y. Ju, The role of low temperature fuel chemistry on turbulent flame propagation, Combust. Flame. 161 (2014) 475–483. doi:10.1016/j.combustflame.2013.08.027.